Function, Structure, and Gene Expression in Electroactive Bacteria

by

Ethan Howley

A Dissertation Presented in Partial Fulfillment
of the Requirements for the Degree
Doctor of Philosophy

Approved November 2022 by the
Graduate Supervisory Committee:

César Torres, Co-Chair
Rosa Krajmalnik-Brown, Co-Chair
Brent Nannenga

ARIZONA STATE UNIVERSITY

December 2022

ABSTRACT

Electroactive bacteria connect biology to electricity, acting as living electrochemical catalysts. In nature, these bacteria can respire insoluble compounds like iron oxides, and in the laboratory, they are able to respire an electrode and produce an electrical current. This document investigates two of these electroactive bacteria: *Geobacter sulfurreducens* and *Thermincola ferriacetica*. *G. sulfurreducens* is a Gram-negative iron-reducing soil bacterium, and *T. ferriacetica* is a thermophilic, Gram-positive bacterium that can reduce iron minerals and several other electron acceptors. Respiring insoluble electron acceptors like metal oxides presents challenges to a bacterium. The organism must extend its electron transport chain from the inner membrane outside the cell and across a significant distance to the surface of the electron acceptor. *G. sulfurreducen*s is one of the most-studied electroactive bacteria, and despite this there are many gaps in knowledge about its mechanisms for transporting electrons extracellularly. Research in this area is complicated by the presence of multiple pathways that may be concurrently expressed. I used cyclic voltammetry to determine which pathways are present in electroactive biofilms of *G. sulfurreducens* grown under different conditions and correlated this information with gene expression data from the same conditions. This correlation presented several genes that may be components of specific pathways not just at the inner membrane but along the entire respiratory pathway, and I propose an updated model of the pathways in this organism. I also characterized the composition of *G. sulfurreducens* and found that it has high iron and lipid content independent of growth condition, and the high iron content is explained by the large abundance of multiheme cytochrome expression that I observed. I used multiple

microscopy techniques to examine extracellular respiration in *G. sulfurreducens*, and in the process discovered a novel organelle: the intracytoplasmic membrane. I show 3D reconstructions of the organelle in *G. sulfurreducens* and discuss its implications for the cell's metabolism. Finally, I discuss gene expression in *T. ferriacetica* in RNA samples collected from an anode-respiring culture and highlight the most abundantly expressed genes related to anode-respiring metabolism.

ACKNOWLEDGEMENTS

I would like to acknowledge the contributions of the work of other researchers in several chapters in this document: Dongwon Ki's cell composition measurements in Ch. 3; Anna Mangus' confocal microscopy and Dewight Williams' cryotomography in Ch. 4. I also thank my advisors for their mentorship which contributed to every chapter of my dissertation.

TABLE OF CONTENTS

CHAPTER 1

INTRODUCTION

Life is inseparable from electrochemistry. Every living organism is constantly shuffling electrons in each cell, reducing and oxidizing molecules to conserve energy for cellular processes. For most organisms, the redox reactions that power metabolism occur within the boundaries of the cell membrane as both electron donor and electron acceptor can be easily transported into and out of the cell. Some organisms, however, utilize insoluble compounds that require part of the chain of redox reactions that make up the metabolism to happen external to the cell itself. I define electroactive organisms as any that have a metabolism requiring the transfer of electrons across the cell membrane in a way that can interact with an electrode. There are many examples of electroactive microorganisms, but this document focuses on one type: dissimilatory metal-reducing bacteria (DMRB). DMRB use insoluble metal compounds as terminal electron acceptors e.g. iron oxides. My dissertation concerns the study of electroactive DMRB with a focus on the bacterium *Geobacter sulfurreducens*. *G. sulfurreducens* is a model organism for electroactive DMRB because of its ubiquity and metabolism. In nature, *G. sulfurreducens* is found in iron-rich soils and sediments. Its metabolism involves the oxidation of acetate, hydrogen, or formate and the reduction of a wide variety of metallic minerals, most commonly iron (III) compounds. In an engineered system, *G. sulfurreducens* will respire an electrode, and this behavior makes it an excellent laboratory organism. The system I use to grow electroactive bacteria (EAB) is a microbial electrochemical cell (MEC), and *G. sulfurreducens* functions as a living catalyst by converting a chemical electron donor into an electrical current that I can measure (Figure 1.1). The direct relationship between

bacterial metabolism and electrical signal makes possible many of the experiments in my dissertation.

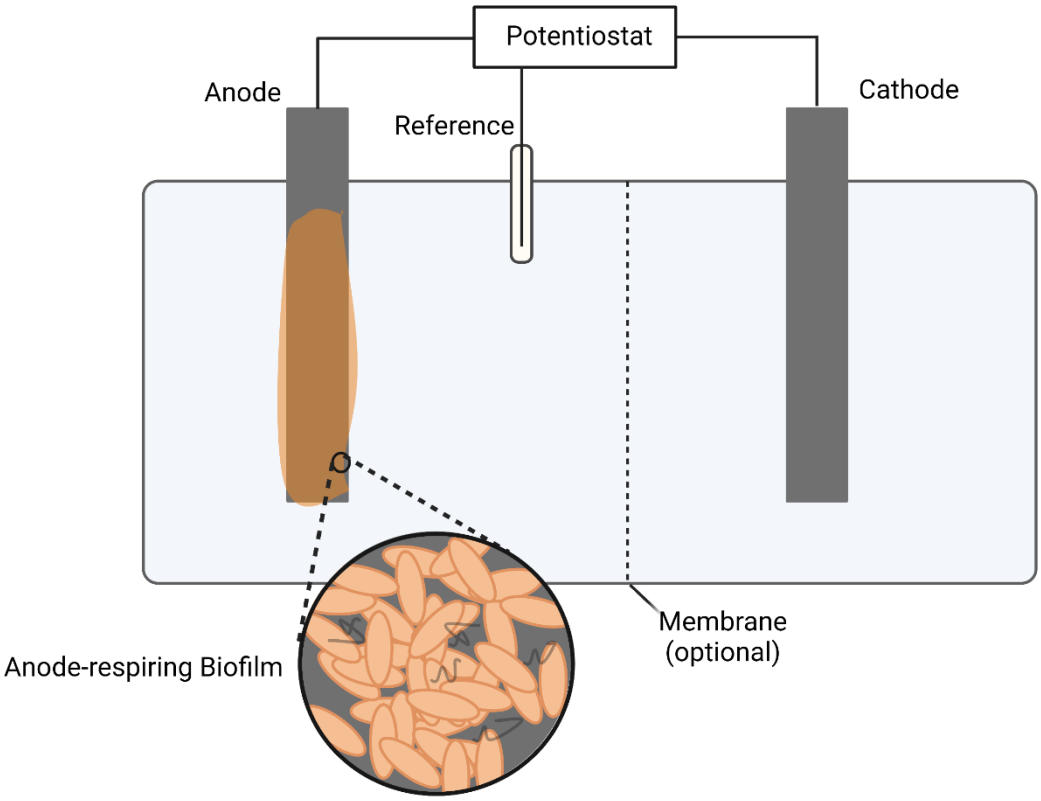

Figure 1.1 Schematic of a generic microbial electrochemical cell.

Metallic minerals in nature are a heterogeneous electron acceptor for DMRB. Iron (III), for example, forms several compounds with different crystal structures or number of oxy(hydroxide) ligands, and each unique mineral has a different electrochemical potential. In addition, as DMRB reduce electron acceptors, the effective potential of the remaining acceptor may change. To be broadly successful at reducing metallic minerals, *G. sulfurreducens* must be able to utilize electron acceptors in a wide range of redox potentials.

Bacterial metabolisms consist of a series of controlled chemical reactions. Electrons move through electroactive proteins and other molecules where energy is conserved by the creation of a proton motive force. Each individual component of the electron transfer chain performs a specific reaction at a specific redox potential. If the terminal electron acceptor or initial electron donor changes potential, the entire electron transfer chain needs to adapt, or the organism will not be able to respire efficiently. *G. sulfurreducens* has evolved a complex network of metabolic components to deal with this challenge. Electrochemical and mutation studies have identified three distinct electron transport chains in *G. sulfurreducens*. Each cell may express one or more of the pathways depending on growth conditions, and each pathway has a range of electron acceptor potential where it is required for respiration.

Although we know that *G. sulfurreducens* has three pathways for respiration, there are gaps in knowledge when it comes to the components and mechanism of each. Only one protein from each pathway has been positively identified by gene knockout experiments. The proteins ImcH, CbcL, and CbcAB are required to complete the "high," "medium," and "low" pathways, respectively. All three of these are c-type cytochromes located in the inner membrane of *G. sulfurreducens*. There is a lack of knowledge when it comes to the other components of each pathway. Undoubtedly, electrons must be transported through the periplasm, across the outer membrane, and over a significant distance away from the cell to the solid terminal electron acceptor. This is called extracellular electron transport (EET). To maintain efficiency, it seems likely that there would be different proteins between different pathways at multiple points in the electron flow between inner membrane and electron acceptor.

In many cases, biologists learn more about the function of an organism by examining its structure. While there is an extensive body of genetic research on *G. sulfurreducens*, its cellular structure had not been studied to the level of detail that modern technology allows. Previous work has used light microscopy or thin-section transmission electron microscopy (TEM) to image *G. sulfurreducens*. Light microscopy is good for imaging large eukaryotic cells or multicellular bacterial biofilms, but it does not have sufficient resolution to identify subcellular structure in small bacteria. Conventional thin-section TEM allows extremely high resolution, down to the imaging of individual proteins, but the sectioning requires a biological sample to be dehydrated by solvent substitution and then embedded in resin for slicing (Murray & Watson, 1965). This sample preparation procedure causes significant damage to membrane structures, and it can be difficult to differentiate real observations from destroyed areas. Recent technological advancements have led to a new way of imaging biological samples. Electron cryotomography uses high speed freezing and cryogenic tilt series imaging to create 3D volumes of samples without any preparation artifacts (Bouchet-Marquis & Hoenger, 2011). With this technique, it's possible to image cells with their membrane structure intact.

In this document, I use several research methods to address knowledge gaps in the understanding of *G. sulfurreducens*. In Chapter 2, I investigate the differential expression of electroactive proteins, and I correlate differentially expressed proteins with specific electron transfer pathways that I identified using electrochemistry. I show that *G. sulfurreducens* changes expression of multiheme cytochromes not only at the inner membrane, but also in the periplasm, outer membrane, and extracellular space, and that some of these differentially expressed proteins can be assigned to one of the three

electron transfer pathways. In Chapter 3, I used electron cryotomography and confocal microscopy to study the cellular structure of *G. sulfurreducens*, and I identify a type of bacterial organelle called the intracytoplasmic membrane which has not been observed in *Geobacter* or any close relatives. This novel organelle is more frequently observed under certain growth conditions, and I show that this differential expression is likely related to the organelle's contribution to respiration in energy-limited conditions. Chapter 4 continues my characterization of *G. sulfurreducens* with a thorough analysis of the cell composition. I show that cultures of *G. sulfurreducens*, regardless of electron acceptor, show a remarkably high lipid and iron content relative to other Gram-negative bacteria, and I discuss how this knowledge fits into the broader understanding of the organism. Chapter 5 is an analysis of gene expression data from a culture of *Thermincola ferriacetica*, a thermophilic EAB that has a metabolism quite different from *G. sulfurreducens*.

Taken as a whole, my dissertation is a significant contribution to the field of electroactive bacteriology, and especially to the understanding of *G. sulfurreducens*. The discovery of intracytoplasmic membranes in *G. sulfurreducens* may explain the high lipid content, and the gene expression data I present provides more information about the complicated metabolic network in *G. sulfurreducens*. This knowledge will be used by microbiologists who study EAB, as well as those who study intracytoplasmic membranes in other organisms. Biotechnologists will also benefit from a refined idea of the nutrient requirements in *Geobacter* species.

CHAPTER 2

CYTOCHROME EXPRESSION IN *G. SULFURREDUCENS* FOR EFFICIENT RESPIRATION

Geobacter sulfurreducens is an anaerobic, gram negative, dissimilatory metal reducing bacterium (DMRB) that is important in natural systems as an iron reducer as well as in engineered microbial electrochemical systems as an anode-respiring bacterium (ARB) (Bond & Lovley, 2003; Caccavo et al., 1994). It can efficiently reduce various metal oxides with a wide range of redox potentials (Levar et al., 2017; Pat-Espadas et al., 2013; Shelobolina et al., 2007), and this flexibility extends to respiring to an anode where *G. sulfurreducens* is capable of adapting to a range of poised anode potentials (Gao et al., 2018; Yoho et al., 2014).

The genome of *G. sulfurreducens* contains genes for over 100 putative c-type cytochromes, with more than 70 of those containing multiple heme-binding motifs (Ding et al., 2008). These multiheme cytochromes have been the target of many studies into electron transfer in *G. sulfurreducens*, but only a few have been definitively linked to a precisely explained function (Salgueiro et al., 2022). Even well-characterized cytochromes, such as the periplasmic cytochrome PpcA (Pessanha et al., 2006) or the outer membrane complex OmcB (Liu et al., 2015), are often known to participate in certain respiratory conditions, but their specific electron donor/acceptor are unknown. As such, the specific electron transport chain pathway for *G. sulfurreducens* has been extensively speculated but not well elucidated (Bonanni et al., 2013; Santos et al., 2015).

Early transcriptomic and proteomic studies on *G. sulfurreducens* focused on comparing growth with different electron acceptors, particularly between soluble (e.g., fumarate, iron citrate) and solid ones (e.g. anodes, iron oxides). Through these studies, several cytochromes have been confirmed to be important in extracellular respiration. For example, OmcB, OmcS, OmcZ, and other cytochromes were implicated in extracellular electron transfer because their gene transcripts were more abundant in conditions using a solid terminal electron acceptor relative to an insoluble one (Holmes et al., 2006; Nevin et al., 2009). It has been hypothesized that long-range electron transfer in *G. sulfurreducens* was due to some combination of pili and associated cytochromes like OmcZ (Malvankar et al., 2011; Nevin et al., 2009). Recent cryo-electron microscopy studies have shown that the nanowires that *G. sulfurreducens* produce are actually composed of repeating subunits of OmcS or OmcZ, and differences in strain and electron acceptor can alter which protein is dominantly expressed (F. Wang et al., 2019; Yalcin et al., 2020).

More recently, researchers have discovered three elements at the inner membrane that are required for *G. sulfurreducens* to respire at certain potentials, independent of the electron acceptor used. Deleting the inner membrane cytochrome CbcL prevents *G. sulfurreducens* from respiring at electrode potentials below -0.1 V vs. SHE, and deleting the inner membrane cytochrome ImcH prevents *G. sulfurreducens* from respiring at potential above -0.1 V vs. SHE (Levar et al. 2017; Levar, Chan, and Mehta-kolte 2014; Zacharoff, Chan, and Bond 2016). Recently, the protein complex CbcAB has been shown to facilitate respiration at potentials below -0.21 V vs. SHE (Joshi et al., 2021). At the moment, it is unknown how pathway switching occurs, and what other proteins are

involved in each pathway. Nonetheless, these studies have shifted the perspective on how pathways are used in *G. sulfurreducens*, where instead of the type of electron acceptor, the potential of such acceptor plays a major role in pathway utilization. By using an anode as the electron acceptor, I can closely control potential and directly measure respiration in real time.

Previous work has also investigated how *G. sulfurreducens* adapts to electron acceptors with different potentials through the use of electrochemical signals (Peng & Zhang, 2017; Richter et al., 2009; Zhu et al., 2012). Our group used electrochemical techniques to identify and characterize two distinct electrochemical responses dependent on anode potential and hypothesized that *G. sulfurreducens* is using different electron transfer pathways to efficiently adapt to different potentials (Yoho et al., 2014). These distinct signals were later associated to the pathways in which ImcH and CbcL are present (Levar et al., 2017; Levar, Chan, Mehta-kolte, et al., 2014). The relative magnitude of the signals associated to these pathways would shift within an hour of a potential shift, suggesting a dynamic and complex optimization of respiratory pathways by *G. sulfurreducens*. Anode-respiring biofilms of *G. sulfurreducens* exhibit different electrochemical responses during cyclic voltammetry based on the anode potential they have been acclimated to, providing an additional tool to differentiate between biofilms grown at different potentials.

In order for *G. sulfurreducens* to efficiently reduce solid electron acceptors at a wide range of redox potentials while conserving energy, it must have a mechanism to change its electron transport chain. Each cytochrome has its own distinct redox potential due to heme orientation and ligands within the overall protein (Pessanha et al., 2006; Pokkuluri

et al., 2011), and therefore has an optimal potential (or range of potentials) under which it will accept and donate electrons in a pathway. If the terminal electron acceptor changes potential significantly, the terminal electron transfer protein may no longer be able to donate electrons and a different terminal electron acceptor will be required to continue respiration. Thus, I hypothesized that a shift in the potential of the electron acceptor would not only require shifts in inner-membrane cytochromes, but throughout the whole respiratory pathway. I designed this study to attempt to find periplasmic, outer membrane, and/or extracellular proteins that are associated with *G. sulfurreducens* respiration at different redox potentials.

I studied wild type *Geobacter sulfurreducens PCA* grown on anodes using electrochemistry and mRNA expression to identify genes that are likely involved in different electron transfer pathways. With cyclic voltammetry (CV) on *G. sulfurreducens* biofilms, I can identify if different pathway signals are present in biofilms grown at different anode potentials, and what typical anode potentials each pathway is associated with. I associated these CV signals with mRNA-Seq transcriptomics to correlate gene expression with the electrochemical data and find genes that may be associated with adaptation to different electron acceptor potentials. Since previous studies have identified the inner membrane elements associated with each pathway, I closely examined the periplasmic, outer membrane, and extracellular electron-transfer proteins that might shift expression as a function of anode potential.

Results and Discussion

When studying ARB, I can directly measure respiration via chronoamperometry while varying anode potential to create different respiratory conditions. Anode biofilm cyclic voltammograms (CV) on biofilms of *G. sulfurreducens* can be modeled with the Nernst-Monod expression (C. I. Torres et al., 2008, 2010) which assumes a single enzymatic step is rate limiting. Additionally, in cases where multiple pathways are being utilized, multiple Nernst-Monod functions have been used (Yoho et al., 2014).

Knockout studies have shown that *G. sulfurreducens* has at least three different electron transfer pathways that are each active in only a certain electron acceptor range, and the switch between pathways is likely facilitated by inner membrane cytochromes (Levar et al., 2017). The pathway containing the inner membrane cytochrome ImcH is used at potentials higher than -0.1 V vs. SHE, while the pathway containing the cytochrome CbcL is active at potentials lower than -0.1 V vs. SHE (Levar et al., 2017; Levar, Chan, Mehta-kolte, et al., 2014). Recently, a third pathway was discovered that contains the *bc*-type cytochrome CbcBA which is required for respiration at potentials below -0.21 V vs. SHE (Joshi et al., 2021). I chose the anode potentials in this experiment (-0.17 V, -0.07 V, -0.01 V vs. SHE) in an attempt to create conditions that would require different known pathways in *G. sulfurreducens*, and our modeling approach assumes three distinct electrochemical signals in attempt to represent these pathways.

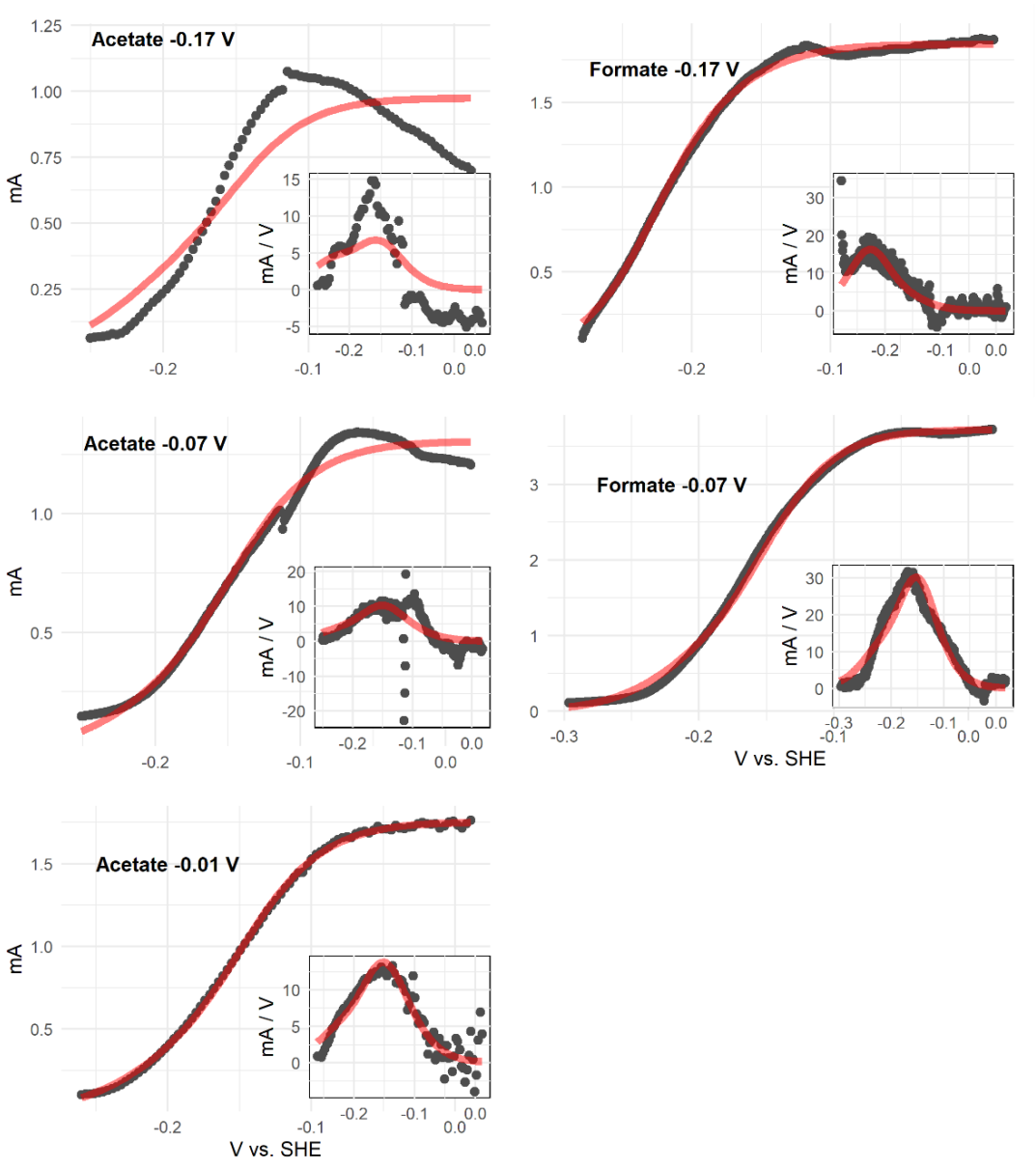

Figure 2.1 One representative cyclic voltammogram from each condition with its respective Nernst-Monod model fitting. The experimental data is plotted as gray points, and the model fitting is the red line. Labels on each plot describe the electron donor used (acetate or formate) and the fixed anode potential grown at (−0.17 V, −0.07 V, or −0.01 V vs SHE). Inset in each plot is the differentiation of the CV data (slope) plotted in gray and the derivative of the model fit function as a red line. Cyclic voltammograms were

collected at a scan rate of 5 mV/s at a biofilm current density between 1-2 A/m^2 during exponential current increase in order to capture a thin biofilm at a fast enough scan rate to prevent transcriptional adaptation to the shifting potential.

Multiple pathway signals fit to a Nernst-Monod model.

I were able to approximately fit CVs of the anode biofilm conditions used in this study by adding Nernst-Monod signals with three midpoint potentials: -0.10, -0.15, and -0.227 V vs. SHE; which were selected based on preliminary nonlinear fitting where midpoint was optimized in different conditions (Figure 2.1). I call these signals High for -0.10 V vs. SHE, Medium for -0.15 V vs. SHE, and Low for -0.227 V vs. SHE. The additive approach to the fitting assumes the signals are utilized simultaneously within the biofilm and cells are not changing expression significantly during the scan. This assumption should be valid with the fast-scan CVs (5 mV/s) I used for fitting, while slower scans are shown to result in pathway shifts within the scan itself (Yoho et al., 2014). With nonlinear fitting, I minimized the error in each fitting by varying the j_{max} coefficient for each E_{KA}. In some cases, such as the Acetate -0.17 V growth condition, fitting had a higher error due to a peak in current density that cannot be estimated by the steady-state assumption of the Nernst-Monod (C. I. Torres et al., 2008, 2010). I averaged the fractional contribution of each of the coefficients from biological replicates of the same condition to estimate the contribution of each pathway in that condition (Table 2.1). Fittings were tested in CVs and the derivative of the CV, having similar outcomes for the fitting.

Table 2.1 Average fractional contribution of each Nernst-Monod function to the overall CV fit in each condition. A larger fraction represents a stronger contribution of a certain pathway to the overall signal, while a fraction close to zero suggests that a certain pathway does not contribute to the overall signal in its respective growth condition. Calculated as $j_{max,i}/\Sigma j_{max,n}$ for each cyclic voltammogram. Numbers in parentheses under each value are the sample standard deviations of each parameter from the number of replicates listed in the 'n' column. The "High", "Medium", and "Low" E_{KA} values represent the midpoint potentials (vs. SHE) of each Nernst-Monod expression that add up to best fit the experimental data.

	Fraction of signal from each E_{KA}			
Electron donor,	***Low***	***Medium***	***High***	n
Anode potential	**-0.227 V**	**-0.15 V**	**-0.10 V**	
Acetate, -0.17 V	0.59	0.41	0.00	3
	(0.28)	(0.29)	(0.01)	
Acetate, -0.07 V	0.29	0.60	0.11	4
	(0.22)	(0.21)	(0.04)	
Acetate, -0.01 V	0.11	0.75	0.14	3
	(0.08)	(0.19)	(0.15)	
Formate, -0.17 V	0.85	0.10	0.05	2
	(0.08)	(0.01)	(0.07)	
Formate, -0.07 V	0.45	0.40	0.14	3
	(0.27)	(0.40)	(0.17)	

Our cyclic voltammetry fitting with the Nernst-Monod expression indicates that there is an observable difference in which pathways are contributing most to the overall biofilm CV signal (Table 2.1). The acetate -0.07 V, acetate -0.17 V, and formate -0.07 V conditions had contributions from the Low and Medium signals with little to no contribution from the High pathway. On the other hand, the CVs from the formate -0.17 V condition were overwhelmingly influenced by the Low signal, and CVs from the acetate -0.01 V condition were mainly fitted with the Medium signal. Even though two of the conditions had an anode potential above -0.1 V, none of the CVs had a major contribution from the High signal (Table 2.1) although higher growth potentials should have a higher contribution of this pathway. The small contributions of the High signal that I observed may be due to the anode potentials I used being lower than the switch point that would trigger expression of the High pathway. Using the information from this model fitting of our CV data, I can discuss differential expression of electron pathway genes in the context of what pathway they may be more strongly associated with.

Growth conditions affect the overall transcriptome.

The main drivers of differential gene expression were the different electron donors and electron acceptors used. The fumarate biofilm and the planktonic fumarate samples are highly differentiated from the anode samples, and among the anode samples there is a clear differentiation between formate and acetate conditions but for acetate there was no clear differentiation based on different anode potentials. All three of the anode biofilms grown on acetate cluster closely together, although there are still some significantly differentially expressed genes. A multi-tab .xlsx file with significantly different genes for all pairwise comparisons is included in the SI. The different anode potentials I used had a

small effect on the overall transcriptome of *G. sulfurreducens* grown using acetate, but there is clear separation between the two conditions using formate as the electron donor.

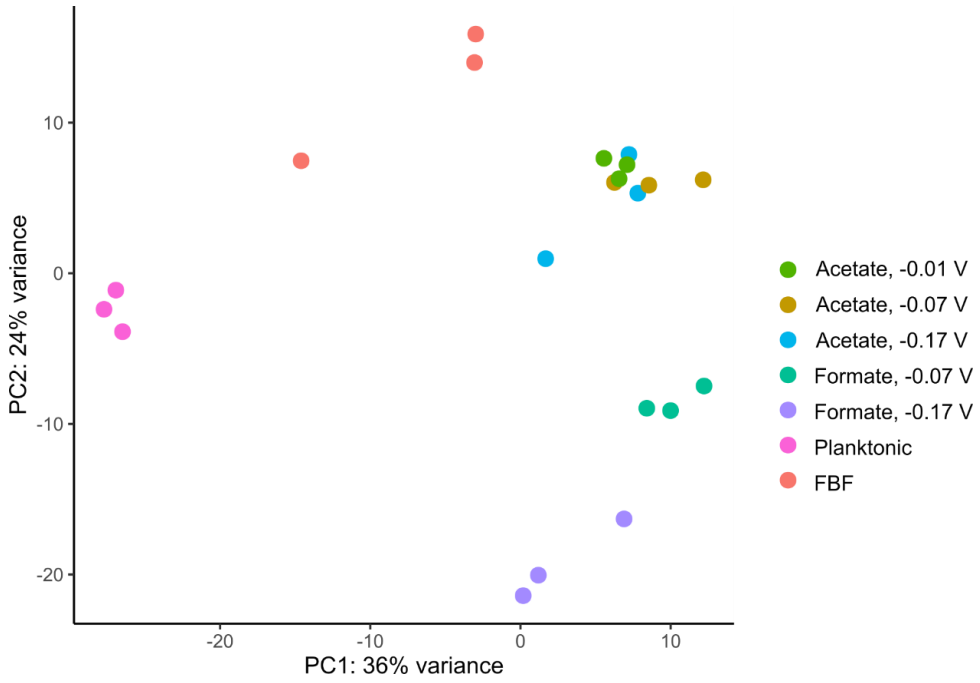

Figure 2.2 PCA plot of variance in expression between triplicate samples grown under seven different electron donor and acceptor conditions. FBF is a fumarate biofilm condition that was grown on an unconnected graphite rod with fumarate as the electron acceptor.

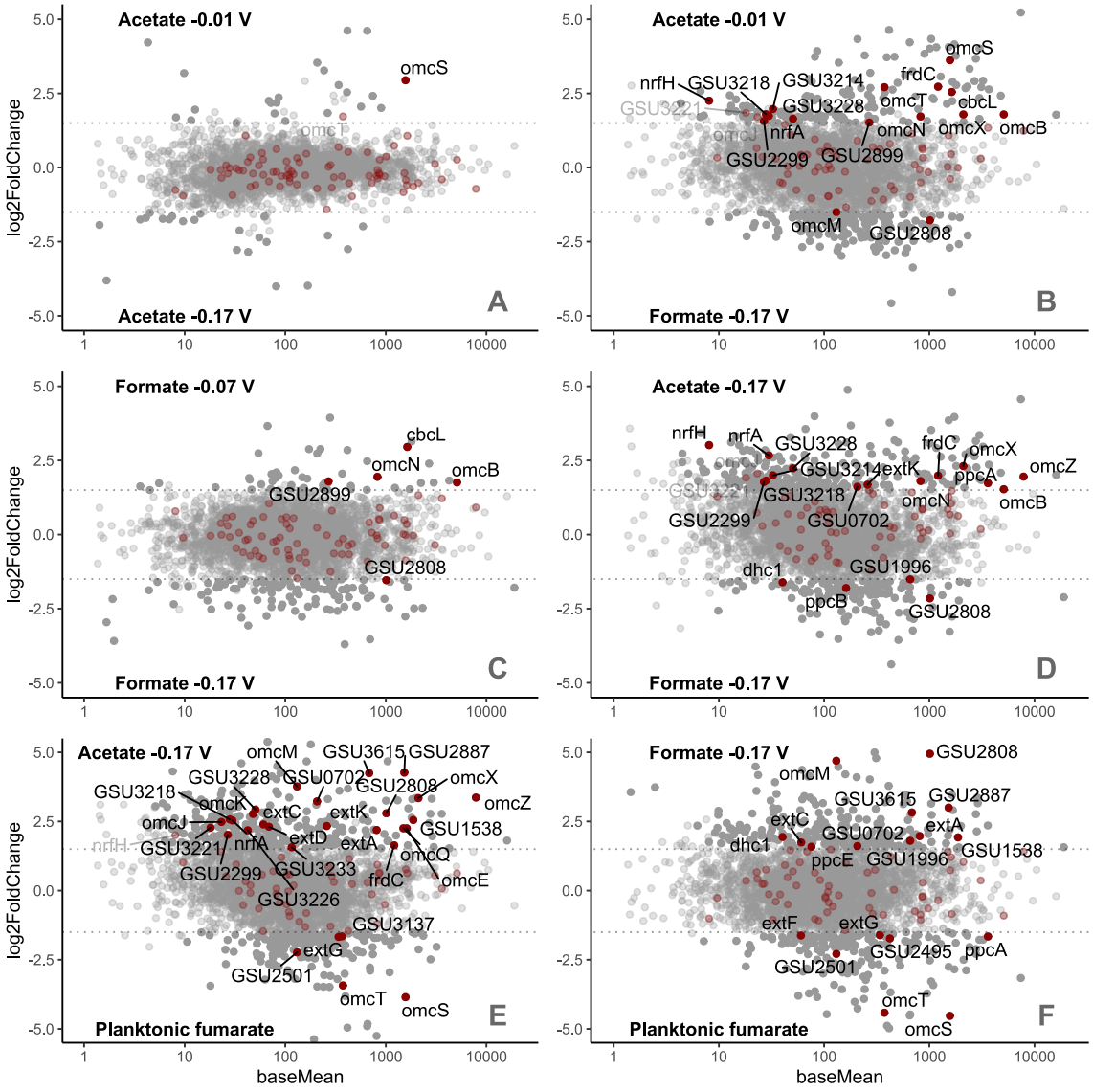

Figure 2.3 MA plots highlighting interesting pairwise comparisons of differential gene expression with multiheme cytochromes highlighted in red. Labels at top and bottom indicate conditions plotted for comparison. Dotted lines are at ±1.5 $\log_2$ fold change, and all clearly labeled genes meet an adjusted p-value <0.05. Base mean is calculated using Deseq2's method for normalizing counts across samples and p values were corrected by the Benjamini Hochberg method. Table A.1 lists all the highlighted genes and the associated pathways and cellular locations.

EET pathways in *G. sulfurreducens* are populated with multiheme cytochromes – some known and some unknown. By synthesizing the modeling outputs from our CV data (Table 2.1) and the differential gene expression of multiheme cytochromes in important pairwise comparisons (Figure 2.3), I can create associations between cytochromes and electrochemical pathways (Table A.1).

Membrane cytochromes can be associated to a specific pathway.

Four clusters of outer membrane genes have been shown to be required for EET in *G. sulfurreducens* under certain conditions: ExtABCD, ExtEFG, ExtHIJK, and OmcBC; deleting all four clusters prevents EET respiration (Otero et al., 2018). Our differential expression data suggests that these clusters may be associated with different electron acceptor potentials. In our data, *extJ* and *extK* were downregulated in the formate -0.17 V biofilm versus the acetate -0.17 V biofilm ($log_2FC=2.6$, $p_{adj}=0.016$, $log_2FC=1.7$, $p_{adj}=0.016$). The formate -0.17 V biofilm was predominantly represented by the Low pathway in our electrochemical data whereas the acetate -0.17 V biofilm had a strong signal from the Medium pathway. From this, I can infer that the ExtHIJK proteins may contribute to the Medium pathway signal. SHE. Likewise, I infer that ExtEFG may be associated with respiration at the highest potentials due to the downregulation of *extF* and *ExtG* in the formate condition grown at an electrode potential of -0.17 V when compared to the expression in planktonic fumarate sample which I assume represents expression of the pathway associated with the highest potential. The fumarate/succinate redox couple has a standard potential of 0.03 V at pH 7, making it more positive than any other acceptor used in this study.

The expression of the gene *omcB* is downregulated in the formate -0.17 V biofilm relative to the acetate anode biofilms at all three potentials and the formate -0.07 V biofilm, indicating that it may be associated with the Medium pathway. OmcB forms part of a conduit that transfers electrons through the outer membrane and is involved in reduction of Fe(III) citrate and ferrihydrite (Liu et al., 2015). I observed differential expression of *omcB* but not *omcC* – two paralogs with 65% amino acid similarity. *GSU2808* is another outer membrane cytochrome with the opposite expression pattern to *omcB*. *GSU2808* was significantly upregulated in the formate -0.17 V biofilm relative to all other anode biofilm conditions indicating an association with the Low pathway. *GSU2808* is a 5 heme cytochrome that has been linked to palladium reduction with acetate as the electron donor (Hernández-Eligio et al., 2020).

I expected to see upregulation of *imcH*. ImcH is the inner membrane cytochrome required for EET at anode potentials above -0.1 V vs. SHE, but there was no significant change among any anode potentials. Yet, *imcH* was a highly expressed cytochrome gene in all conditions, with a base mean of 869 which is in the 94th percentile among all genes. Given the anode potentials I chose, it is possible that our experimental design did not capture the differential expression of *ImcH*. Based on our electrochemical modeling and the differential expression data, none of the conditions I studied were primarily using the High pathway associated to *ImcH* (Table 2.1). CbcL, the inner membrane cytochrome required for potentials below -0.1 V vs. SHE, was significantly downregulated in the formate -0.17 vs. SHE samples compared to the formate -0.07 V samples (log2FC = 3.0, adjusted p = 1.8E-5) but not significantly different between any of the acetate anode biofilm potentials. This observation fits well with the CV data where all conditions

except for the -0.17 V formate biofilm had a signal from the Medium pathway. Recent work has identified CbcAB as a crucial protein complex for *G. sulfurreducens* to respire at potentials below -0.2 V vs. SHE (Joshi et al preprint 2021), but I did not detect any differential expression in *cbcA* or *cbcB*, although each gene had a base mean of counts in the 97th and 95th percentile, respectively. Apart from these known inter membrane proteins, *dhc1* was differentially expressed with an association to the Low potential condition (Table A.1). This gene encodes for a unique diheme cytochrome of unknown function with a predicted inner membrane localization.

Extracellular cytochromes network adapts to redox conditions.

Filaments made of OmcS or OmcZ units have been implicated as a critical component of long distance EET (F. Wang et al., 2019; Yalcin et al., 2020). I observed that *omcS* was significantly upregulated in the fumarate conditions relative to all anode biofilms except for the acetate -0.07 V vs. SHE condition. *G. sulfurreducens* may use OmcS for EET only at higher anode potentials, above ~ (−0.1) V vs. SHE. Fumarate, with a standard reduction potential of 0.03 V vs. SHE, appears to be stimulating the expression of the High pathway. To our knowledge, previous studies on OmcS filaments have all used either fumarate or an electrode poised above 0 V vs. SHE as the electron acceptor. Of the "*omc*" genes, the most likely candidate for replacing the function of OmcS at lower potentials based on our data is *omcZ*. The OmcZ protein was recently shown to form nanowires with a high conductivity in *G. sulfurreducens* (Yalcin et al., 2020) and has been shown to be preferentially expressed at low potentials (Peng & Zhang, 2017). Our data supports that the differential expression of *omcS* vs. *omcZ* appears to be at least partially controlled by electron acceptor potential with *omcZ* being important when the

Medium pathway is detected. Interestingly, I did not observe an upregulation of *omcZ* in the Formate -0.17 V condition relative to planktonic fumarate despite the down regulation of *omcS* (Figure 2.3B and 2.3F), suggesting that there may be more than just *omcS* and *omcZ* responsible for the pathway-dependent switch in the extracellular part of the pathway. Other cytochromes with predicted extracellular localization (GSU2887, GSU3615) were more abundantly expressed under the Low Pathway conditions, but the function of these cytochromes is yet to be elucidated (Kim et al., 2005; Leang et al., 2005; Peng et al., 2016)

Differential expression of Ppc proteins may maximize respiratory efficiency. Five periplasmic triheme cytochromes (PpcA-E) have been identified and characterized in *G. sulfurreducens* (Lloyd et al., 2003). PpcA was first characterized and shown that its deletion affects Fe(III) and U(VI) reduction, but not fumarate reduction. PpcB-D were initially identified due to their high similarity to PpcA (75-100%), while predictions confirmed their periplasmic location (Shelobolina et al., 2007). Most studies have suggested the role of these cytochromes is to transfer electrons collected at the inner membrane to outer-membrane cytochromes (Lloyd et al., 2003; Morgado et al., 2010; Shelobolina et al., 2007). Interestingly, further studies have confirmed that PpcA and PpcD perform a proton-coupled electron transfer; which leads to the possibility that these periplasmic cytochromes are associated to ATP production (Morgado et al., 2010). It has also been confirmed that electron transfer by PpcB and PpcE are not proton coupled, suggesting a different cellular function compared to PpcA/PpcD (Silva et al., 2021).

Our observed gene expression for Formate at -0.17 V vs SHE, which has primarily the Low pathway evident, shows an increased expression of PpcB (Fig. 3D) and PpcE (Fig.

3F) over PpcA compared to conditions where the Medium pathway is active. Our study associates the use of PpcB and PpcE to the Low pathway. On the other hand, *ppcA* seems to be highly expressed in all other samples, this suggests its utilization for the Medium and/or High pathways. Given that the lower potential pathway is associated with lower electron-transfer energy available in *G. sulfurreducens* metabolism, there is limited energy for proton pumping and ATP production. The use of PpcB/PpcE could be an approach to decrease ATP production when the energy gradient is limiting, while PpcA is used when more energy is available. Thus, our results are consistent with the hypotheses that PpcA/PpcD are associated with ATP production (Morgado et al., 2010; Silva et al., 2021). Analyses of these periplasmic cytochromes have also discussed differences in working potentials, which could indicate different electron acceptors (Morgado et al., 2010). The PpcA-E proteins function as periplasmic electron carriers in *G. sulfurreducens'* EET, so a change in the distribution of the different Ppc proteins could allow *G. sulfurreducens* to maintain efficiency as external redox conditions change. I also observed differential expression of several large cytochromes, each with at least a dozen hemes. *GSU3218* (15 hemes), *GSU0702* (35 hemes), and *omcN* (34 hemes) are upregulated in the acetate -0.17 V condition relative to the formate -0.17 V condition, and therefore I associate them with the Medium pathway (Table A.1). *GSU0702* has been previously associated with respiration of electrodes at lower potentials as it was upregulated in *G. sulfurreducens* grown at -0.25 V vs. SHE compared to +0.2 V (Peng et al., 2016). Deleting *omcN* does not impact the reduction of soluble or insoluble electron acceptors in one study (Aklujkar et al., 2013). The 27-heme cytochrome gene *GSU2887* is associated with the Low pathway. The proteins encoded by *GSU2887* and *GSU0702*

are both predicted to be extracellular by PSORTb 3.0, but it is not clear what the function of such large cytochromes would be outside the cell.

Formate metabolism suppresses the TCA cycle.

When acetate is available, *Geobacter* uses NADH generated from the TCA cycle to pump protons across the membrane using NADH dehydrogenase for energy conservation. When formate is the only electron donor available, *Geobacter* suppresses the TCA cycle and shifts to an alternate metabolism. There were 80 genes differentially expressed between *G. sulfurreducens* anode biofilms grown with the same -0.07 V vs. SHE potential with either acetate or formate as the electron acceptor. Ten genes encoding for subunits of the NADH dehydrogenase complex were significantly downregulated in the formate condition. Every gene encoding for an enzyme in the TCA cycle except for *sucA*, 2-oxoglutarate dehydrogenase, was downregulated in the formate samples. In the formate condition, I observed the upregulation of 15 genes including *fdhD* (formate dehydrogenase) (Supplemental spreadsheet). The downregulation of NADH dehydrogenase (*nuo* genes) and the upregulation of formate dehydrogenase that I observe in formate biofilms indicate that formate dehydrogenase is replacing NADH dehydrogenase as the primary electron carrier in the membrane electron transfer chain. There is no evidence that *Geobacter*'s formate dehydrogenase can pump protons in the same way as NADH dehydrogenase.

Formate may stimulate a similar response as hydrogen in *Geobacter*. *hgtR*, the hydrogen-dependent growth transcriptional regulator, is a critical protein for shifting metabolism to use hydrogen as the electron donor (Ueki & Lovley, 2009). Joshi, Chan, and Bond 2021 also found that *hgtR* is upregulated in a mutant *G. sulfurreducens* where an upstream

regulator of CbcAB is deleted (Δ*bccR*), potentially because of thermodynamic limitations on respiration. I observed upregulation of *hgtR* in both formate biofilms relative to all acetate conditions except for the acetate -0.01 V biofilm. Although I did observe downregulation of the TCA cycle in formate conditions, the fact that *hgtR* was also relatively highly expressed in the -0.01 V acetate biofilm suggests that it is not solely related to hydrogen/formate metabolism, but instead a thermodynamic response in *G. sulfurreducens.* It is also possible that small amounts of hydrogen were produced in our single-chamber reactors, and this activated *hgtR*, but in that case I would not expect to see differential expression as a function of potential or electron donor.

I initially chose to study conditions where fumarate was the electron acceptor to capture the transcriptome of cells that did not need to use EET. Instead, I observed the expression of many of the EET-associated proteins in the fumarate conditions. Our data support other work that has shown that *G. sulfurreducens* is not optimized to grow with fumarate. OmcS nanowires have been isolated from fumarate cultures of *G. sulfurreducens* (F. Wang et al., 2019), indicating that fumarate cultures produce the machinery of the High potential EET pathway. *G. sulfurreducens* also prefers Fe(III) as an electron acceptor when both Fe(III) and fumarate are available despite fumarate providing more energy (Esteve-Núñez et al., 2004). *G. sulfurreducens* uses a reversible enzyme complex, FrdCAB for both fumarate reduction during fumarate respiration and succinate dehydrogenation as part of the TCA cycle (Butler et al., 2006). In our data *frdC* was differentially expressed, although it was not correlated with fumarate utilization. Rather, fumarate reductase was regulated along with the other elements of the TCA cycle. *frdC* was downregulated in the formate conditions relative to the acetate biofilms which is

consistent with the downregulation of the other TCA cycle enzymes. I did, however, observe an increased expression of *dcuB* in fumarate conditions. DcuB is the fumarate transporter in *G. sulfurreducens* (Butler et al., 2006).

Conclusion

Due to its complicated electron pathways, fully understanding EET in *G. sulfurreducens* will require synthesizing data from many techniques, and a large body of literature. In this study, I combined electrochemical CV fittings using Nernst-Monod modeling and RNASeq to identify electrochemical conditions that change the expression of genes associated with different pathways. I have identified at least eight genes that show an association to different respiratory pathways in *G. sulfurreducens*, and this technique could be expanded in further studies to answer more unresolved questions about the metabolism of *G. sulfurreducens* and other electroactive organisms.

Over decades of research in *G. sulfurreducens*, expression studies have often assumed an anode, often poised at high potentials, as a fixed condition for growth; only recently have studies started to recognize the importance of shifting anode potentials in its expression and electrochemical behavior (Levar et al., 2017; Peng et al., 2016). Our results suggest that a small shift in the anode potential (100-160 mV in our study) cause significant changes in the respiratory pathway of *G. sulfurreducens*. While this is a small potential change, it constitutes a significant increase (87-139%) in available energy for growth using acetate as electron donor ($E^{0'} = -285$ mV vs SHE). It seems that changes along the full electron path, from the inner membrane to the extracellular matrix, occur because of a change in potential. In Figure 2.4, I hypothesize an updated model of EET in *G. sulfurreducens*. Trifurcation of electrons occurs at the inner membrane as previously

reported (Joshi et al., 2021; Levar et al., 2017). In order to maintain efficient energy conservation, many redox proteins along the EET pathway should change to create a cascading potential gradient from the inner membrane to the anode. Based on our data, I propose in Figure 2.4 some of the electron carriers in each of the three pathways, with changes at the periplasmic, outer membrane, and extracellular portions of the electron transfer chain. I anticipate that future studies will associate more electron carriers with each pathway and complete the model.

Since the respiratory pathways in *G. sulfurreducens* involve a complex network of cytochromes extending to the extracellular space, changing this pathway due to a shift in electron acceptor conditions (e.g., change in anode or metal oxide potential) would require a significant energy investment. Thus, my results imply some limitations in respiratory efficiencies as redox conditions change and add more context to the complicated story of *G. sulfurreducens*.

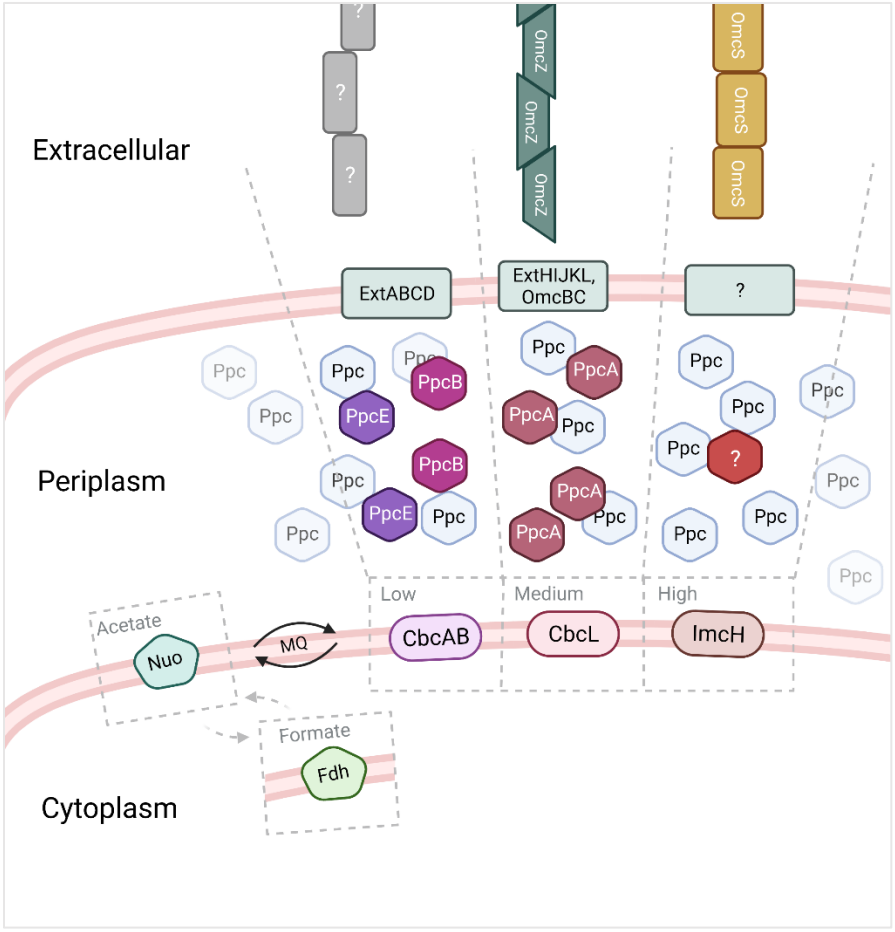

Figure 2.4 My hypothesized schematic of the EET process in *G. sulfurreducens* and how it is differentiated based on electron acceptor potential. At the inner membrane NADH dehydrogenase (Nuo) reduces menaquinone (MQ), or in the case of formate metabolism Nuo is downregulated and formate dehydrogenase (Fdh) initializes the inner membrane electron transfer chain. At the inner membrane, electrons enter one of three EET pathways. In the Low pathway, CbcAB (Joshi et al., 2021) oxidizes menaquinol, the periplasmic electron transfer favors PpcB and PpcE, and the ExtABCD complex is involved at the outer membrane. In the Medium pathway, CbcL transfers electrons to PpcA in the periplasm and then to ExtHIJKL and OmcBC and OmcZ at the outer membrane. Our study did not capture the High pathway well, but I do know it uses ImcH

(Levar et al., 2017) at the inner membrane and OmcS as an extracellular electron carrier. This diagram is not a complete explanation of all the EET pathways in *G. sulfurreducens* but rather a way to highlight some of the associations I have discovered. Created with BioRender.com.

Methods

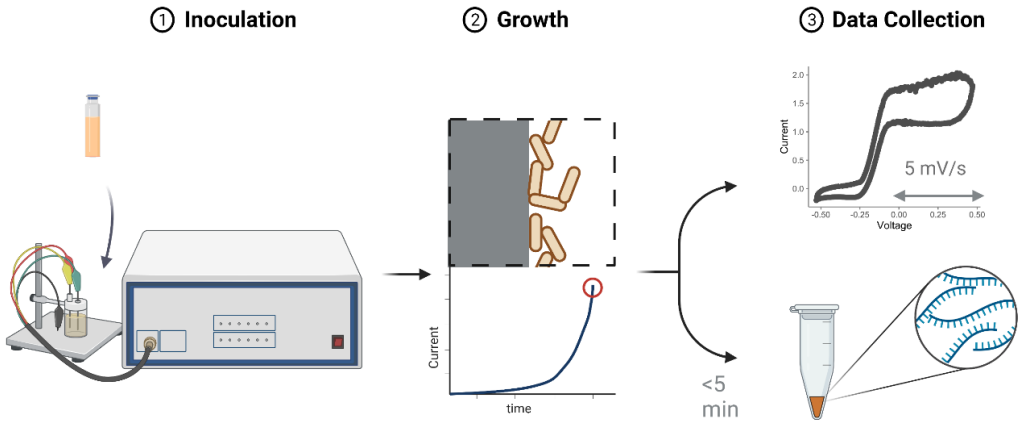

Figure 2.5 1) *G. sulfurreducens* is inoculated into a microbial electrochemical cell with a graphite electrode acting as the electron acceptor for growth using a potentiostat to apply a potential. 2) Growth is monitored via chronoamperrometry until the bacteria produce 1-2 A/m^2 during exponential growth, indicating a thin and active biofilm. 3) At this stage, I perform cyclic voltammetry on the biofilm, or the biofilm is collected, and RNA is extracted for transcriptomics. Created with BioRender.com.

Growth.

Geobacter sulfurreducens PCA was grown under 7 different conditions. “Planktonic” samples used ATCC 1957 medium in sealed anaerobic test tubes and extracted 48 hours after inoculation. Anode biofilm samples used a modified ATCC 1957 medium without sodium fumarate in a single chamber microbial electrochemical cell with a graphite rod electrode (600-800mm^2) serving as an anode. The reactor volume was 100mL with an Ag/AgCl reference electrode (BASi, Indiana USA) and a stainless-steel wire as cathode. Acetate anode biofilms were poised at three different potentials, -0.07 V vs. SHE, -0.17 V vs. SHE, and -0.01 V vs. SHE. Formate anode biofilms were poised at two potentials – -0.07 V vs. SHE, and -0.17 V vs. SHE. I used a conversion of -0.27 V vs. Ag/AgCl is 0 V vs. SHE. Anode biofilm growth was monitored with a BioLogic VMP3 potentiostat (Tennessee, USA) and samples were collected during exponential current growth phase in the range of 1-3 A/m^2 to capture a thin biofilm. Fumarate biofilm samples used ATCC 1957 medium in a continuously mixed flow-through reactor identical to the anode biofilm reactor with a hydraulic retention time less than the reported doubling time for *G. sulfurreducens* and with the cell in open circuit. Planktonic samples were collected by centrifugation, and biofilms were collected by scraping. Seven conditions were sampled in biological triplicate for a total of twenty-one samples.

RNA processing.

RNA was extracted from all samples with a QIAGEN PowerMicrobiome RNA extraction kit (Germany). The extraction process began within 5 minutes of disturbing each culture. RNA quality and quantity were assessed with a Nanodrop spectrophotometer and an Agilent Bioanalyzer 2100. Ribosomal RNA contamination was reduced with the

MICROBExpress Bacterial mRNA enrichment kit (ThermoFisher, Massachusetts USA). Illumina (California USA) sequencing libraries were prepared with KAPA Biosystems Hyperprep RNA (Massachusetts USA) before pooling and sequencing on an Illumina Nextseq 500 2x150 module. Sequencing was performed at the OKED Genomics Core at Arizona State University.

Differential Expression.

Sequence quality was assessed with FastQC (Andrews, 2010). After demultiplexing, reads were trimmed with trimmomatic (Bolger et al., 2014) to remove low quality read segments. The majority of ribosomal reads were removed by alignment to reference sequences in Bowtie2 Filtered reads were aligned to the *G. sulfurreducens* PCA RefSeq genome using Bowtie2 (Langmead & Salzberg, 2012), and only paired alignments were kept. Alignment files were transformed for analysis in R with samtools (Li et al., 2009). In R, aligned reads were mapped to the NCBI RefSeq assembly for *G. sulfurreducens*. Ribosomal RNA-mapped reads were removed before differential expression analysis. Differential gene expression was analyzed with the R package DESeq2 (Love et al., 2014). Ribosomal protein genes are removed from data presented here. Transcriptomic data and metadata are hosted in the NCBI Gene Expression Omnibus database under accession number GSE200066.

Electrochemistry.

Anode biofilms used for cyclic voltammetry were grown under similar conditions to the samples used for RNA extraction. I used a Bio-Logic VMP3 potentiostat for all chronoamperometry and cyclic voltammetry. Cyclic voltammograms were recorded with a scan rate of 5 mV/s from −0.5 V vs. SHE to +0.5 V vs SHE. A total of 3 consecutive

scans were performed for each biofilm and the second scan was used for fittings. Fitting to Nernst-Monod curves to the data by optimizing each j_{max} was performed in using the nl2sol non-linear least squares regression from the R package stats (R 3.6.3, 2021).

$$j = j_{1_{max}}\left(\frac{1}{1+\exp\left(-\frac{F}{RT}(E-E_{KA_1})\right)}\right) + j_{2_{max}}\left(\frac{1}{1+\exp\left(-\frac{F}{RT}(E-E_{KA_2})\right)}\right) + j_{3_{max}}\left(\frac{1}{1+\exp\left(-\frac{F}{RT}(E-E_{KA_3})\right)}\right)$$

Equation 1: Three-part Nernst-Monod expression to model the *G. sulfurreducens* biofilm cyclic voltammograms. F is Faraday's constant (96,485 C/mol), R is ideal gas law constant (−8.314 J/mol K, T is temperature (K), and E is the anode potential (V) as measured by the potentiostat. j is current density (A/m^2). In the model, each $j_{i,max}$ was a fitting parameter.

Acknowledgements.

The funding for this work was provided by the Office of Naval Research (ONR awards N0014-15-1-2702 and N0014-20-1-2269).

CHAPTER 3

G. SULFURREDUCENS' HIGH IRON AND LIPID CONTENT

The following chapter is adapted from a publication in Microbiology Spectrum (Appendix B).

Anode-respiring electroactive bacteria , such as *Geobacter sulfurreducens*, have been studied for almost two decades for their capability to produce electrical current from metabolic respiration of organic compounds while in multi-layered biofilms (Bond et al., 2012; Reguera et al., 2006; C. I. Torres, 2014) . A unique feature of these biofilms is the extracellular matrix that allows the transport of electrons over tens of micrometers (Chadwick et al., 2019; Geobacter Protein Nanowires, 2019; F. Wang et al., 2017). As part of this extracellular matrix, several components have been proposed to be crucial in achieving extracellular electron transport (EET). The transport of electrons starts at the inner membrane, and travels across the periplasm and outer membrane before it reaches the extracellular environment. Cytochromes at these locations are known to play an important role in delivering electrons outside the cell (Levar et al., 2017; Otero et al., 2018; Pessanha et al., 2006; Zacharoff et al., 2016). Microbial nanowires, now also identified as cytochrome polymers (Geobacter Protein Nanowires, 2019; F. Wang et al., 2017), are the main path by which electrons are thought to be conducted in the extracellular environment, reaching a solid electron acceptor. Extracellular polymeric substances (EPS) have also been proposed to play a role in EET in *G. sulfurreducens* as well (Bond et al., 2012; Rollefson et al., 2011). On the other hand, *Shewanella oneidensis* MR-1 has been shown to produce outer membrane and periplasmic extensions, which are lipid bilayers and contain extracellular cytochromes (Pirbadian et al., 2014; Subramanian

et al., 2018). In both cases, it is clear that the EET mechanism creates an extra metabolic burden to electroactive organisms and that it can alter their cell composition and nutrient requirements when compared against microorganisms performing respiration of soluble electron acceptors. These nutrient requirements, however, have not been assessed in a systematic way.

Transcriptomic and proteomic studies in *G. sulfurreducens* have highlighted the importance of respiratory and EET proteins for their growth on anodes and metal oxides. Extracellular and outer membrane proteins, including pili, outer membrane channels, and c-type membrane cytochromes, are essential to the metabolism of *G. sulfurreducens* (Aklujkar et al., 2013; Estevez-Canales et al., 2015; Jiménez Otero et al., 2021; Joshi et al., 2021; Kim et al., 2005; Leang et al., 2005; Levar, Chan, Mehta-Kolte, et al., 2014; Liu et al., 2015; Lloyd et al., 2003; Mehta et al., 2005; Nevin et al., 2009; Peng & Zhang, 2017; Shelobolina et al., 2007; Zacharoff et al., 2016). The high abundance of these proteins and other possible extracellular components may result in a unique cellular composition. For example, each cytochrome contains one or more iron-containing heme complexes which can influence the iron content of the cell. An analysis of cell composition can provide insights into the composition of the extracellular matrix and EET-related components.

Several studies have provided insights into the cellular composition of *G. sulfurreducens*. For example, the lipid fraction of *Geobacter sulfurreducens* was reported 15% wt/wt by Mahadevan et al., 2006, where an additional 4% lipopolysaccharides fraction was assumed (Mahadevan et al., 2006). In comparison, the lipid in *Escherichia coli* has been reported to be 9.1% wt (Neidhart et al., 1990) while cyanobacterium *Synechocystis* sp.

PCC6803, known to produce thylakoid membranes, has been reported to be as high as 14% wt(Cuellar-Bermudez et al., 2015) and the lipid-rich microalgae *Schizochytrium* sp. can contain up to 30% lipid (Byreddy et al., 2016). The high lipid content of *G. sulfurreducens* has potential implications for biotechnology applications.

To our knowledge, few studies have performed a metallomic analysis in *G. sulfurreducens*, and the existing literature has conflicting results. Previous research showed that *G. sulfurreducens*, when grown on fumarate as electron acceptor, has similar metal content to that of *E. coli*. On the other hand, the closely related organism *Geobacter metallireducens* grown on iron citrate showed an order of magnitude higher iron content; but the possible formation of inorganic precipitates was reported to be a possible hindrance to the measurement (Budhraja et al., 2019). Another study found that *G. sulfurreducens* had a per cell iron content an order of magnitude higher than *E. coli*, and that limiting growth medium iron content inhibited EET in *G. sulfurreducens* (Estevez-Canales et al., 2015).

In this study, I hypothesized that *G. sulfurreducens* has a significantly different cellular composition compared to other cells performing soluble respiratory metabolisms. The differences that stem out of the EET requirements can help explain how EET develops. Understanding these characteristics can lead to a better growth and maintenance of this microorganisms in laboratory and applied systems. I performed a metallomic analysis on *G. sulfurreducens* grown on an anode versus fumarate as electron acceptors and compared it to *E. coli* K12. The use of an anode allows us to study EET and eliminates the interference of possible iron oxides reported by Budhraja et al. (Budhraja et al., 2019). I also performed an elemental analysis (C, H, O, N, ash content) and a fraction

analysis (protein, carbohydrates, and proteins) to obtain a comprehensive cell composition and determine if the previously observed lipid fractions measured in fumarate samples are also observed during anodic respiration. The results are complemented with a transcriptomic analysis of *G. sulfurreducens* grown under similar conditions.

Methods

Bacterial strain and culture media.

We subcultured *Geobacter sulfurreducens* PCA (ATCC) and *Escherichia coli* K-12 from commercially available stocks. Medium compositions are listed in detail in Table A.2 for four different cases: 1. *G. sulfurreducens* grown in microbial electrochemical cell (electrode), 2. *G. sulfurreducens* grown in sodium fumarate-containing serum bottle (fumarate), 3. *E. coli* grown in *Geobacter* medium, and 4. *E. coli* grown in M9 medium. In brief, *Geobacter* medium contained sodium acetate (50 mM), $NaHCO_3$ (30 mM), NH_4Cl (20 mM), NaH_2PO_4 (4 mM), KCl (1 mM), vitamin mix (10 mL), and trace minerals (10 mL). Trace minerals contained Nitrilotriacetic acid, trisodium salt (5.5 mM), $MgSO_4 \cdot 7H_2O$ (12 mM), $MnSO_4 \cdot H_2O$ (2.9 mM), NaCl (17 mM), $FeSO_4 \cdot 7H_2O$ (0.36 mM), $CaCl_2 \cdot 2H_2O$ (0.68 mM), $CoCl_2 \cdot 6H_2O$ (0.42 mM), $ZnCl_2$ (0.95 mM), $CuSO_4 \cdot 5H_2O$ (0.4 mM), $AlK(SO_4)_2 \cdot 12H_2O$ (0.2 mM), H_3BO_4 (0.16 mM), $Na_2MoO_4 \cdot H_2O$ (0.01 mM), $NiCl_2 \cdot 6H_2O$ (0.01 mM), and $Na_2WO_4 \cdot 2H_2O$ (8.5 μM). We provided higher concentration of acetate (50 mM) than the previous studies(Snider et al., 2012; Strycharz-Glaven et al., 2011; Yates et al., 2016) (10 mM), as we used a higher electrode surface area requiring more reduced electron donor. For *G. sulfurreducens* grown in serum bottles, sodium fumarate (100 mM) was added in the medium. We bubbled the media with N_2/CO_2 (80:20 v/v) to remove oxygen before autoclaving. After autoclaving, $FeCl_2 \cdot 4H_2O$ (20 μM), $Na_2S \cdot 9H_2O$ (54 μM), sodium bicarbonate, and vitamins were added in anaerobic glove box. *E. coli* medium (ATCC Medium 2511 - M9 Minimal Broth) contained glucose (44 mM), Na_2HPO_4 (180 mM), KH_2PO_4 (44 mM), NaCl (17 mM), NH_4Cl (37 mM), $MgSO_4 \cdot 7H_2O$ (0.2 mM), CaCl2 (10 μM), and thiamin (24 μM). Media for *E. coli* (M9

and *Geobacter* medium) were autoclaved without any gas sparging. *Geobacter* medium for *E. coli* contained the same ingredients of *G. sulfurreducens* for microbial electrochemical cells except electron donor; the same concentration of glucose as M9 (44 mM) were used instead of acetate.

Electrochemical setup and operation.

Single-chamber microbial electrochemical cells were constructed in 500 mL bottles with rubber stoppers located on top having PTFE tubing for gas inflow and outflow, carbon anode as working electrode, nickel wire cathode as counter electrode, and reference electrode. We used two square graphite electrodes to grow biofilms of *G. sulfurreducens* with a surface area of ~20.9 cm^2, and an Ag/AgCl reference electrode (BASi, West Lafayette, IN). We mixed the chambers with magnetic stirrer bars at 180 rpm and flushed humidified N_2/CO_2 gas (80:20 v/v) continuously. Before filling up the media in the anaerobic glove box, electrochemical cells were autoclaved for sterilization. We set -0.3 V vs Ag/AgCl (-0.03 V vs. SHE) as fixed anode potential using a VMP3 digital potentiostat (Bio-Logic USA, Knoxville, TN). This is at the lower end of the range of electrode potentials that *G. sulfurreducens* can respire. Fumarate-grown *G. sulfurreducens* reactors were set up in 250 mL serum bottles. Both electrochemical cells and serum bottles were in a temperature-controlled room at 30 °C. Also, the media filling along with inoculation was performed in the anaerobic glove box. We used 250 mL flasks for *E. coli* cultivation with M9 and *Geobacter* media. *Geobacter* medium (G medium) for *E. coli* was used to compare the cell composition with *G. sulfurreducens*. After filling the media and inoculation for *E. coli*, we placed the flasks in an incubator with shaking at 180 rpm and temperature at 37 °C.

Sample preparation.

For the determination of carbohydrate, protein, lipid, metal, and element per dried cell, we collected the *G. sulfurreducens* grown on anodes in the microbial electrochemical cells and in serum bottle reactors and the *E. coli* grown in flasks. *G. sulfurreducens* biofilms grown on the anodes were scraped off with a needle in an anaerobic glove box. Grown cells of *G. sulfurreducens* and *E. coli* from the serum bottles and flasks were separated by centrifugation (Eppendorf Centrifuge 5810 R, USA) at 4000 rpm in microcentrifuge tubes. Cells were washed once with a Ringer's solution (25% strength) and centrifuged again (Table A.2). The cells dried overnight at 105 °C in plastic tubes and the cool pellets were then broken up with a sterile stainless-steel spatula.

Analytical methods.

We measured proteins by bicinchoninic acid (BCA) protein assay (Brown et al., 1989). In brief, dried cell biomass (2-3 mg) treated with 0.1 N NaOH at 90 °C for 30 min, re-suspended and centrifuged the lysate, and used 0.1 mL of supernatant for the assay. Carbohydrates were measured by a colorimetric method (DuBois et al., 1956). In brief, dried cell biomass (2-3 mg) was acidified in sulfuric acid with sonication for 2 hours, and dissolved samples (0.5 mL) added in the test tubes with distilled water (0.5 mL), phenol (50 μL), and sulfuric acid (5 mL) for overnight reaction. Concentrations of proteins and carbohydrates were determined using calibration curve with bovine serum albumin and glucose with the absorbance at wavelengths of 485 and 562 nm, respectively. Crude lipids were extracted from the dried cell biomass using the Folch method (Folch et al., 1957). The dried biomass (~15 mg) was sonicated for 1 hour and vortexed for 1 hour with Folch solution (chloroform-methanol, 2:1, v/v) at room temperature. Solvent

extracts were obtained after removing the biomass by centrifugation at 4000 rpm. The crude lipid weight was determined by evaporating in the water bath (60 °C) and weighing the tube before and after the evaporation of lipid. For metal extraction, we added dried cell biomass (3-5 mg) to glass vials along with hydrochloric acid (12 M) and sonicated at 60 °C for 2 hours. The dissolved metals in acid were analyzed by inductively coupled plasma - optical emission spectrometer (ICP-OES, Thermo iCAP6300). Carbon, hydrogen, and nitrogen in the dried cell biomass (~2 mg) were measured using CHN Elemental Analyzer (PE2400). Instrumentation for ICP-OES and CHN Elemental Analyzer was done in Goldwater Environmental Laboratory at Arizona State University. For oxygen estimation, we measured ash content of the dried cell biomass (~10 mg) following the previous method (Sluiter et al., 2008), burning the biomass at 600 °C in an alumina crucible. Then we subtracted the fraction of C, H, N, and ash content from the dried cell biomass (100%) for O estimation. Based on the elemental analysis data (%C, %H, %O, and %N), we obtained the empirical biomass formula followed by Equation 1 below (McCarty & Rittmann, 2001),

$$C_N H_a O_b N_c + \left(\frac{2n+0.5a-1.5c-b}{2}\right) O_2 \longrightarrow nCO_2 + cNH_3 + \frac{a-3c}{2} H_2O$$

(Eq. 1)

where, n = $\frac{\%C}{12T}$, a = $\frac{\%H}{T}$, b = $\frac{\%O}{16T}$, and c = $\frac{\%N}{14T}$,

and, $T = \frac{\%C}{12T} + \frac{\%H}{T} + \frac{\%O}{16T} + \frac{\%N}{14T}$.

Transcriptomic analysis.

I sequenced reverse transcribed RNA from *G. sulfurreducens* grown in a single chamber microbial electrochemical cell as an anode biofilm with an anode poised at -0.28 V vs.

Ag/AgCl as the electron acceptor, and in anaerobic test tubes with fumarate as the electron acceptor. Both conditions were collected in biological triplicate. I extracted RNA with the Qiagen/MOBIO PowerMicrobiome RNA extraction kit and used the ThermoFisher MicrobExpress bacterial mRNA enrichment kit to reduce the fraction of rRNA following manufacturer's recommendations. RNA library preparation and sequencing were performed by the genomics core facility at ASU. I mapped the reads to the RefSeq assembly for *G. sulfurreducens PCA* and used DESeq2 in R for differential expression analysis. The cutoff determination for differential expression was set as a $\log_2$ fold change of at least 1.5 and a multiple comparison adjusted *p*-value of less than 0.05. The sequencing data I used here is a subset of data analyzed in Chapter 2, and raw sequence data is available from NCBI under accession number GSE200066 (Howley, Krajmalnik-Brown, et al., 2022).

Results and Discussion

Elemental analysis.

I analyzed the trace metals and macronutrients of dried *G. sulfurreducens* and *E. coli* grown in the lab with different environments (Table A.3, Table 3.3, Figure 3.1). I found significant differences between the two species in the mass fraction of several trace metals (Figure 3.1, Table A.3, Figure A.1). Media compositions were different in each growth condition, matching each organism's requirements (Table A.3). There were few differences between anode-grown and fumarate grown *G. sulfurreducens*. Significant differences in Mn and Fe content were observed in *E. coli* when growing in M9 medium versus *Geobacter* medium. Given the low abundance of nutrients in M9's minimal

medium, significant increases in Cu, Fe, Mn, and Se were observed when *E. coli* was grown in *Geobacter* medium. I use this latter condition as point of reference when comparing *G. sulfurreducens* and *E. coli*.

Several metals were present at higher concentrations in anode- and fumarate-grown *G. sulfurreducens* when compared to *E. coli*, but only a subset of them had statistically significant differences between the organisms (Table A.3, Figure 3.1).

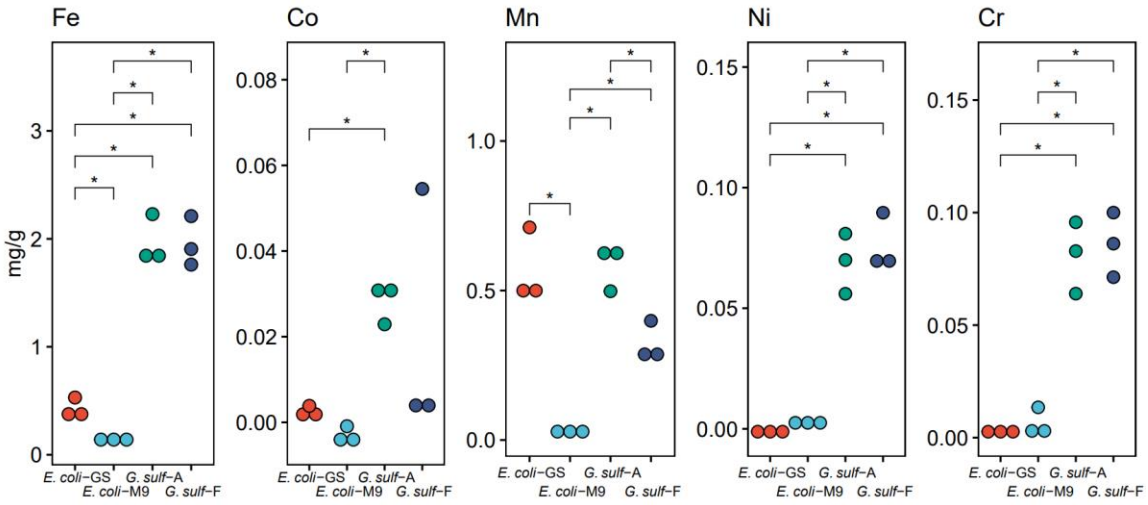

Figure 3.1. Relevant differences in metal concentrations between *E. coli*-GS (Geobacter medium), *E. coli*-M9 (M9 medium), *G. sulf*-A (biofilm grown on an electrode), and *G. sulf*-F (planktonic cells using fumarate as the electron acceptor). See Figure A.1 for more comparisons. *(p<0.05), pairwise t-test with multiple comparison correction performed with the Benjamini-Hochberg method. I chose to omit alkali metals from this figure, but Lithium did have significant differences as well (Table A.3).

Metals used as cofactors.

Fe is a required trace metal for cellular respiration in many organisms as the cofactor in cytochromes. In both growth conditions for *G. sulfurreducens*, Fe was much higher than in *E. coli*, which suggest a much higher abundance of Fe-containing metalloproteins and other iron-containing biomolecules (Figure 3.1).

In previous studies, listed in Table 1, anaerobic bacteria are reported to have more iron per cell biomass than aerobic bacteria. Phototrophic bacteria (*Rhodospirillum*, *Rhodopseudomonas*, *Chromatium*) and facultative bacteria (*Escherichia*, *Enterobacter*) have 150-500 μg/gdw Fe. *Desulfovibrio vulgaris*, an anaerobic Deltaproteobacterium like *G. sulfurreducens*, has over 900 μg/gdw. Not included in our analysis are iron oxidizing bacteria, whose Fe precipitates can lead to Fe concentrations over 2% by dry mass (Rouf, 1964). To our knowledge, *G. sulfurreducens* has the highest Fe content among bacteria studied, with almost twice the content of *D. vulgaris*. This is consistent with their production of heme-containing cytochromes in much higher abundance than other microorganisms, leading to not only cytoplasmic and membrane metalloproteins, but also an extensive abundance of extracellular cytochromes. Growing *G. sulfurreducens* on the anode versus fumarate did not change the total Fe amount, suggesting similar abundance of Fe metalloproteins. OmcS nanowires have been isolated from fumarate culture (F. Wang et al., 2017), indicating that *G. sulfurreducens* does not necessarily downregulate its EET metabolism when it is not needed. Our gene expression data also shows a high expression of cytochromes associated with EET in fumarate and anode biofilm culture (Figure 3.2).

Table 3.1: Amount of iron in different prokaryotic species

Bacterial species	Iron (ug Fe/gdw)	References
Rhodospirillum rubrum	Light - 202 (± 13) Dark - 198 (± 10)	Kassner & Kamen, 1968* (Kassner & Kamen, 1968)
Rhodopseudomonas spheroides	Light - 163 (± 21) Dark - 230 (± 24)	
Chromatium	Light - 456 (± 76)	
Desulfovibrio vulgaris	952	Lancaster et al., 2014** (Lancaster et al., 2014)
Enterobacter cloacae	154	
Escherichia coli	223	Hartmann and Braun, 1981 (Hartmann & Braun, 1981)
	280	Abdul-Tehrani et al., 1999 (Abdul-Tehrani et al., 1999)
	300	
Micrococcus roseus	200	Rouf, 1964 (Rouf, 1964)
Bacillus cercus	300~400	
Pseudomonas aeruginosa	0.1	Ma et al.,1999 (J. F. Ma et al., 1999)
Shewanella oneidensis	147§	Daly et al., 2004 (Daly et al., 2004)
Escherichia coli	G medium - 430 (± 90) M9 medium - 130 (± 50)	This study
Geobacter sulfurreducens	Electrode - 1970 (± 226) Fumarate - 1960 (± 229)	

* Photosynthetic bacteria were grown in different growth conditions with and without light exposure. ** Iron in *D. vulgaris* and *E. cloacae* were estimated with the measured iron per total protein of the cells; I used a conversion factor of 0.55 to convert from protein to volatile solids (Neidhart et al., 1990). § *S. oneidensis* iron content was converted from nmol Fe/ mg protein to µg Fe/gdw using 52.8% protein content as measured previously (Pinchuk et al., 2010).

Fe may be a limiting trace mineral in commonly used *G. sulfurreducens* media. Estevez-Canales et al. found that a medium concentration of 2 μM Fe limits biomass culture in a chemostat growing *G. sulfurreducens* led to a culture with 1.9 x 10^{-6} ng of Fe per cell (Estevez-Canales et al., 2015). If I assume the average cell dry weight of *G. sulfurreducens* is between 100 and 1000 femtograms, as has been shown in *E. coli* (Loferer-Krößbacher et al., 1998), our results would give an iron content of 2 x 10^{-7} ng to 2 x 10^{-6} ng Fe per cell in *G. sulfurreducens*.

Nickel, cobalt, and chrome content were significantly higher in both *G. sulfurreducens* conditions relative to *E. coli* (Table A.3, Figure 3.1). Nickel is a cofactor in Ni-Fe hydrogenases, and the genome of *G. sulfurreducens* encodes for several (Coppi, 2005; Tremblay & Lovley, 2012). *G. sulfurreducens* is able to assimilate cobalt through its cobamide-synthesis pathways (Yan et al., 2012), but it may also be precipitated on the cell surface as a defense mechanism against cobalt toxicity (Dulay et al., 2020).

Precipitating metals.

There are some metals that may be overrepresented in our *G. sulfurreducens* samples due to precipitation. *G. sulfurreducens* requires at least two multicopper proteins, OmpC and OmpB, to respire Fe (III) oxide (Holmes et al., 2008), and while these and other metalloproteins are a likely reservoir of Cu in our samples, *G. sulfurreducens* is capable of reducing Cu(II) to Cu_2S nanoparticles that associate with cells (Kimber et al., 2020). This phenomenon makes it difficult to estimate how much copper was required for metalloproteins, and how much may have been trapped as inorganic precipitates. *G. sulfurreducens* can also immobilize copper through dissimilatory reduction (Gong et al.,

2018). In our data, the *G. sulfurreducens* samples were enriched in Cr compared to *E. coli* (Figure 3.1), while differences in Cu were not statistically significant. Manganese was significantly lower in the *E. coli* grown with M9 medium compared to all other conditions including *E. coli* grown with the *G. sulfurreducens* medium recipe because M9 medium does not contain manganese (Figure 3.1, Table A.3).

Based on the metal content of the *G. sulfurreducens* cells collected, I can estimate a maximum cell density from the available mineral content in the common Geobacter medium (ATCC 1957). Table A.4 shows the estimated growth cell assuming cells require the observed metal concentrations and only have the medium as a source. As expected, Fe is the most limiting metal in the medium, allowing for only 0.10 g cells/L. Cu and Zn are also close to this limitation and could lead to a multi-nutrient limitation when growing *G. sulfurreducens* at ~0.1 g/L. This nutrient limitation can either limit cell density in cell suspensions or limit current generation in microbial electrochemical technologies when operated in batch mode. Assuming a current production of ~0.28 A/g protein (Otero et al., 2021) or 0.6 A/g cell (based on Table A.1), one liter of *Geobacter* medium can support enough *G. sulfurreducens* cells to produce 60 mA, an amount of current that is enough for most experimental setups but might be limiting in electrochemical cells with a high specific surface area.

Cell composition of G. sulfurreducens is different to an average bacterium.

I also studied the cell composition and elemental analysis (C, H, O, N, Ash) of *G. sulfurreducens*. Interestingly, the *G. sulfurreducens* cell showed a high abundance of lipids in both growth conditions (Table 3). The values of ~32% lipid content were much higher than previously reported and similar to lipid-accumulating algal cultures (C. Ma et al., 2017; Piligaev et al., 2018; Wahidin et al., 2013). It is not clear why *G. sulfurreducens* requires such a high lipid content. Their smaller diameter (~ 0.5 mm) and distinct morphology (Caccavo et al., 1994) compared to other rod-shape bacteria certainly plays a role in the increased lipid content. *Shewanella oneidensis*, another electrogenic organism, is known to produce outer membrane extensions for electron transfer (Pirbadian et al., 2014). While it is likely that our analysis captured some extracellular polymeric substances, the extracellular matrix of *G. sulfurreducens* has not been found to have a significant lipid component (Stöckl et al., 2019). Most microorganisms exhibiting this high lipid fraction have either lipid accumulation, as in the case of certain algal species (C. Ma et al., 2017; Piligaev et al., 2018; Wahidin et al., 2013) or have internal lipid structures that increase its relative fraction as in the case of thylakoid membranes and intracytoplasmic membranes (Davies & Whittenbury, 1970; Greening & Lithgow, 2020; Murray & Watson, 1965). The lipid fraction in *E. coli* was lower than *G. sulfurreducens* and higher than has been previously reported at 24.3 ± 3.6%. However, there is a high variance in reported *E. coli* lipid content with values ranging from 9 to 19% by dry weight (Damoglou & Dawes, 1968; Lee et al., 2011). Because of the higher lipid content, *G. sulfurreducens* cells show a significantly lower protein content when compared to other microorganisms (~22-26%, Table 3). Fumarate-

grown cells had a larger protein fraction than in anode-grown cells. On the other hand, total carbohydrates were ~2 times higher in anode-grown cell; exopolysaccharide (EPS) excreted from *G. sulfurreducens* to form a biofilm on the electrode probably increases the carbohydrate content in this growth condition.

Our elemental analysis of *G. sulfurreducens* cells is consistent with the low protein, high lipid content measured. Following Eq. 1, empirical cell biomass formulas of *G. sulfurreducens*, normalized to N, were calculated as $C_{5.77}H_{10.61}O_{2.43}N$ for electrode-grown and $C_{6.58}H_{12.48}O_{3.02}N$ for fumarate-grown cells. Compared with general formulas for bacterial biomass, such as $C_5H_7O_2N$ (McCarty & Rittmann, 2001), *G. sulfurreducens* has a higher C:N ratio typical of a low protein content. It also has a higher hydrogen content, due to the higher lipid content that has approximately a 1:2 for fumarate-grown cells.

Table 3.2 Cell compositions of *G. sulfurreducens* and *E. coli* in different growth conditions. Error is the sample standard deviation.

Growth condition		*G. sulf.* electrode	*G. sulf.* fumarate	*E. coli* M9 medium
Proteins (mg BSA/gdw)		215 (± 7)	262 (± 56)	284 (± 15)
Crude Lipids (mg/gdw)		323 (± 45)	321 (± 35)	243 (± 36)
Carbohydrates (mg glucose/gdw)		193 (± 11)	87 (± 24)	68 (± 19)
Elements	C (%)	47.0 (± 1.1)	46.8 (± 1.8)	46.9 (± 0.7)
	H (%)	7.2 (± 0.6)	7.4 (± 0.1)	7.4 (± 1.0)
	N (%)	9.5 (± 0.2)	8.3 (± 0.3)	12.5 (± 0.0)
	O (%)	26.4 (± 3.3)	28.6 (± 3.9)	24.8 (± 2.0)
	Ash (%)	9.9 (± 3.0)	9.0 (± 3.3)	8.4 (± 1.3)

I compared our cellular composition of *G. sulfurreducens* to that reported in Mahadevan et al. 2006 (Mahadevan et al., 2006). The main differences between the fraction distributions reported here and those reported in Mahadevan et al. is the higher lipid content at the expense of a lower protein content. I do not know the reason for the discrepancy, but in both cases the lipid content is significantly higher than *E. coli* and other bacterial cells.

Iron-containing genes are highly expressed.

Our analysis identified 434 genes that were differentially expressed between the anode biofilm samples and the planktonic fumarate cells out of 3434 annotated genes detected at quantifiable levels. 205 genes were more highly expressed in the anode biofilm, and 229 genes were more highly expressed in the planktonic samples. In Figure 3.2, MA plots visualize the differential expression and highlight several types of iron-containing protein-coding genes. While a greater number of cytochromes were significantly upregulated in the anode biofilm than the number upregulated in the planktonic samples, most cytochromes were not differentially expressed. Ferritin domain containing protein- and nonheme Fe-S domain protein-coding genes were also present among the differentially expressed genes. Our data show that iron-containing protein-coding genes are expressed in both planktonic fumarate cultures and anode biofilms, but that there are specific iron-related genes whose expression depends on growth conditions. The abundance of expression of Fe-containing proteins is consistent with the high Fe abundance in both conditions. I also investigated the expression of lipid synthesis pathway genes and found that many of them were present in the transcriptome but not

differentially expressed, although a few lipid-associated genes showed significant differences (Figure A.2).

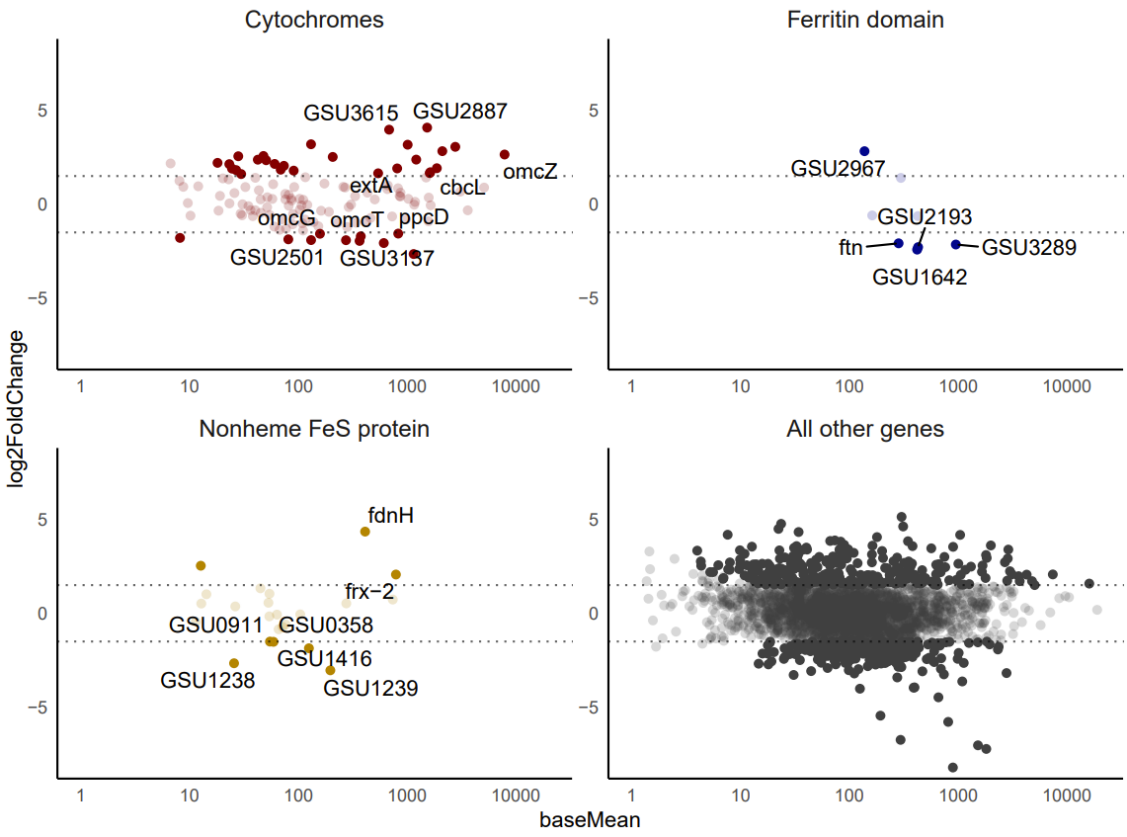

Figure 3. 2 MA plots of mRNA gene expression data comparing planktonic cells and anode biofilms. Positive log2 fold change indicates higher expression in the anode biofilm condition. Solid points indicate a log2 fold change greater than 1.5 and an adjusted *p*-value below 0.05.

Conclusions

G. sulfurreducens is a bacterium with a complex system of electroactive proteins, and those electroactive proteins largely require iron. This may be a factor in the high iron concentration I measured in *G. sulfurreducens* relative to non-electroactive Gram-negative *E. coli* and values reported in literature for other bacteria. Our analysis complements previous work showing that restricting iron limits EET in *G. sulfurreducens* (Estevez-Canales et al., 2015). This study estimates what the nutrient limitations might be for *G. sulfurreducens*, and this information is valuable for biotechnologists developing applications using this and similar organisms. The nearly identical composition between anode-grown and fumarate-grown cells supports the hypothesis that *G. sulfurreducens* is not adapted to efficiently grow on fumarate – it makes electron carriers for EET regardless of the electron acceptor if the nutrients are available. The lipid content measured in *G. sulfurreducens* was higher than what has been reported before, and relatively high for a bacterium without lipidic storage. While all samples were taken from active biofilms or suspended cultures, I did not have a mechanism to separate dead cells from active cells, and it is probable that the composition of an individual cell may differ from the composition of the bulk samples analyzed. When compared to similar studies on other bacteria and the *E. coli* in our study, I have shown that *G. sulfurreducens* has a unique composition to support its complex metabolism.

The funding for this work was provided by Office of Naval Research (ONR awards N0014-15-1-2702 and N0014-20-1-2269). I also thank Roy Erickson and Adam Smith for assistance of ICP-OES and elemental analysis (Goldwater Environmental Laboratory at ASU) and the Genomics Core at ASU for sequencing.

CHAPTER 4

INTRACYTOPLASMIC MEMBRANES DEVELOP IN *G. SULFURREDUCENS*

While biologists classically differentiate prokaryotes from eukaryotes by a difference in organelle compartmentalization of the cytoplasm, reality is more complicated. Prokaryotes with a diverse variety of metabolisms and ecological niches express various well-defined intracellular organelles (Chowdhury et al., 2014; Greening & Lithgow, 2020; Shively, 2006). Most of the organelles that have been characterized in prokaryotes fall into one of two categories. The first are isolated compartments where specialized conditions are maintained to perform chemical processes not possible in the cytoplasmic space e.g. the anammoxosome (Strous et al., 1999), the carboxysome (Shively et al., 1973), and the acidocalcisome (Seufferheld et al., 2003). The second category of prokaryotic organelles consists of densely packed membrane structures that facilitate higher throughput for membrane-dependent metabolic processes by increasing the available surface area in a cell e.g. the thylakoid, the chlorosome (Staehelin et al., 1980), and membranous structures in methane, nitrite, and ammonia oxidizers (Davies & Whittenbury, 1970; Fassel et al., 1992; Fiencke & Bock, 2006; Watson, 1971). I use the general term ‘intracytoplasmic membrane’ (ICM) to describe all these lipidic structures in prokaryotes as it includes organelles with membranous structures with unknown functions. For organisms operating with thin thermodynamic margins or performing slow chemical reactions, the rate of enzyme activity, e.g., ATP production, should be proportional to the membrane surface area available for those enzymes. In methane-oxidizing bacteria, for example, two essential membrane-associated metabolic enzymes – methane monooxygenase and methanol dehydrogenase – are localized in the ICM,

providing higher throughput for a potentially rate-limiting reaction (Brantner et al., 2002; Fassel et al., 1992), and the same has been observed with ammonia monooxygenase in ammonia-oxidizing bacteria (Fiencke & Bock, 2006). Interestingly, the relationship between membrane proteins and ICMs goes both ways, as modifying a bacterium to overexpress a membrane-bound enzyme can spur ICM-like structures in a bacterium that normally lacks any organelles (von Meyenburg et al., 1984; Weiner & Lemire, 1984). *Geobacter sulfurreducens* is a gram-negative Thermodesulfobacterium (previously classified as a d-proteobacterium) that reduces iron and other metals in anaerobic environments (Caccavo et al., 1994). As an organism adapted to respire insoluble metal oxides in nature, *G. sulfurreducens* is capable of respiring man-made solid electron acceptors as well (Bond & Lovley, 2003). In an engineered system, I can take advantage of this extracellular electron transfer (EET) to produce a measurable electrical current. Amplicon sequencing of electroactive biofilms typically finds *Geobacter* species to be the most abundant organism, regardless of the source of inoculum (Yates et al., 2012). *G. sulfurreducens* reduces electron acceptors with a wide range of estimated redox potentials (Levar et al., 2017; Pat-Espadas et al., 2013) (−0.17 [goethite] to +0.98 V vs. SHE [palladium]), produces a relatively high current density in engineered systems (as high as 10 $A \cdot m^{-2}$)(C. I. C. I. Torres et al., 2008), and has a complex network of electron carriers (Bonanni et al., 2012; Howley, Krajmalnik-Brown, et al., 2022; Joshi et al., 2021; Levar et al., 2017). In order to adapt as the redox potential of its electron acceptor changes, *G. sulfurreducens* expresses at least three different electron transfer pathways that each have an optimal growth condition and distinct electrochemical signal (Joshi et al., 2021; Levar

et al., 2017; Levar, Chan, Mehta-Kolte, et al., 2014). For these reasons, *G. sulfurreducens* is considered a model electroactive organism (Lovley et al., 2011).

Metal-reducing bacteria like *G. sulfurreducens* can operate in a relatively energy-limited niche. *G. sulfurreducens* oxidizing acetate and reducing natural iron (III) minerals can have as little as 0.12 Volts of redox differential in the case of goethite (Orsetti et al., 2013), versus ~1.1 V for aerobic acetate oxidation. In electroactive biofilms, *G. sulfurreducens* experiences a gradient of redox potential since cells in the outer region of the biofilm will have a lower effective potential due to impedance in the biofilm matrix (C. I. Torres et al., 2010). *G. sulfurreducens'* ability to adapt to varying redox conditions depends on a complex network of electron carriers. This flexible metabolism is strictly dependent on membrane processes; the inner membrane electron transport chain in *G. sulfurreducens* requires different electron carrier proteins dependent on the amount of energy available to the cell i.e., the redox potential of the terminal electron acceptor (Joshi et al., 2021; Levar et al., 2017; Levar, Chan, Mehta-kolte, et al., 2014; Yoho et al., 2014). When energy-limited by electron acceptors with low redox potentials, *G. sulfurreducens*' growth could be limited by both a lower rate of respiration according to Nernstian kinetics (Kato Marcus et al., 2007; C. I. Torres et al., 2010) and by a lower yield of ATP generation per electron respired. The effect is a membrane-limited respiratory metabolism. This limitation results in a decreased growth and respiratory rate for *G. sulfurreducens* growing on low redox potential electron acceptors (Levar, Chan, Mehta-kolte, et al., 2014; Wei et al., 2010).

In this work, I have discovered ICM structures in *G. sulfurreducens*. I used confocal microscopy, plastic embedded thin-section transmission electron microscopy (TEM), and

cryogenic electron tomography (CryoET), to identify ICM structures in *G. sulfurreducens* that are localized in specific subcellular regions. By observing cells in different redox conditions, I can test the hypothesis that ICM in *G. sulfurreducens* is associated with thermodynamic conditions where cells must respire at low potential. These observations have significant implications for the holistic understanding of respiration under energy-limited conditions.

Results and Discussion

Morphology of ICM in *G. sulfurreducens* through TEM imaging. In thin plastic sections prepared via freeze substitution of plunge-frozen cells, I observed ICM structures in *G. sulfurreducens* cells collected from a biofilm that was grown on an anode at -0.07 V vs. SHE. The ICMs mostly appear as parallel bands of membrane in the cytoplasm and are localized to a fraction of the cell's entire volume (Figure 4.1). In some cases, the ICMs were also observed as curved or circular structures. In most cases, when the TEM section showed the full length of the cell, ICMs mostly appeared towards one of the tips of the cell (Figure 4.1B, D). I did not find cells with ICM in more than one area of the cytoplasm, and not every cell in our plastic sections had evidence of the structure. I repeated the plastic sectioning procedure with cells grown using fumarate, a soluble electron acceptor with a higher redox potential (E'_0 = 0.03 V vs SHE), and I did not find evidence of ICM in the resulting micrographs (Figure A.3-A.6).

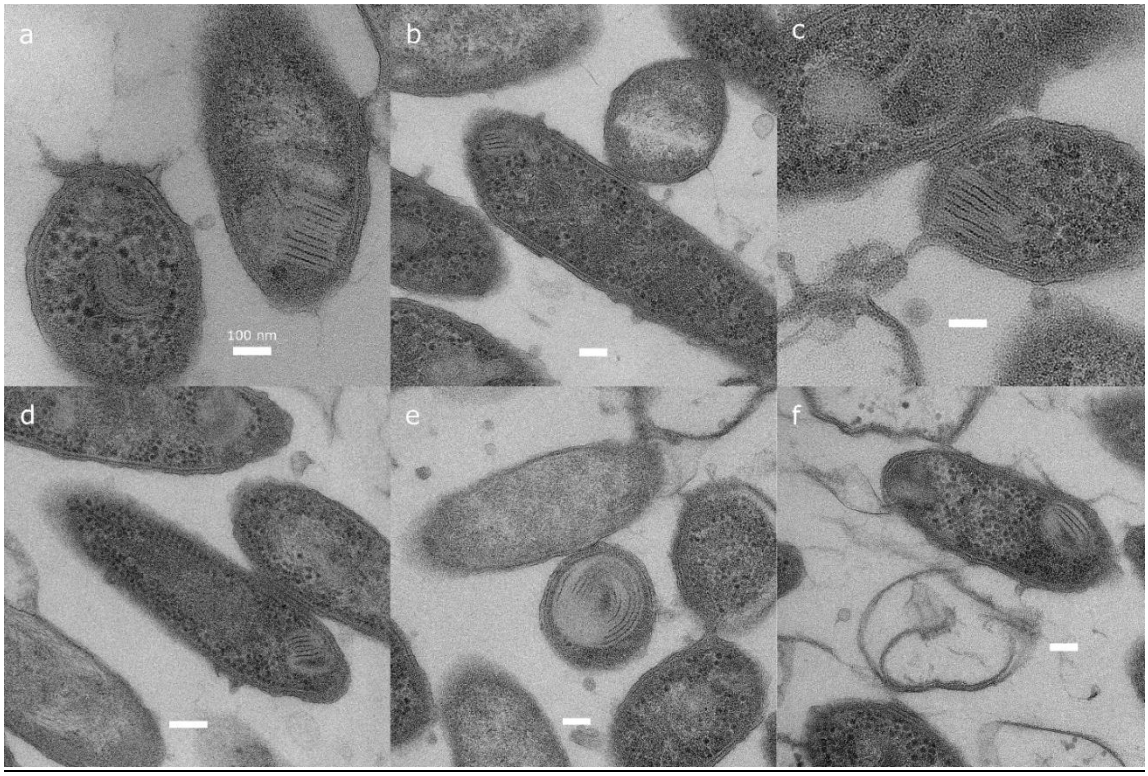

Figure 4.1 Plunge frozen, freeze substituted plastic embedded TEM micrographs of *G. sulfurreducens* collected from an anode biofilm poised at -0.07 V vs. SHE. ICM structures present as parallel bands in one area of a cell. 3A, 3C, and 3E show ICM in cells sliced perpendicular to the major axis, while 3B, 3D, and 3F show ICM in cells sliced parallel to the major axis where the ICM is located near the tip of the cell. Micrographs were collected on an FEI TF20. Scale bars: 100 nm.

Conventional plastic embedded TEM has been used to characterize bacterial ICMs for over 50 years(Murray & Watson, 1965). The ICM of *G. sulfurreducens* shares some morphological characteristics with previously described structures in other bacteria. Ammonia-oxidizing bacteria (AOB) can produce ICMs with one continuous membrane folded tightly into parallel bands localized to one area of the cell, although the ICM in

AOB appears to occupy a larger fraction of the cell volume compared to what I observed in *G. sulfurreducens* (Murray & Watson, 1965). The ICM in AOB forms from invagination of the inner membrane (Murray & Watson, 1965). In the AOB *Nitrosomonas eutropha*, ICM development is stimulated by ammonia-oxidizing conditions, but ICM is not developed during anoxic denitrification (Schmidt et al., 2001). Similarly, I observed the production of ICM in *G. sulfurreducens* in response to certain environmental redox conditions. In *G. sulfurreducens*, I have not yet determined the signal mechanism that activates ICM expression or if there are cytoskeletal-like proteins involved in their organization.

3D structure of ICM- Using CryoET of whole cells, I observed ICM without the artifacts and membrane damage commonly introduced by dehydration (Bouchet-Marquis & Hoenger, 2011). I grew *G. sulfurreducens* directly attached on TEM grids with the grid itself serving as the anode in an electrochemical cell followed by immediate vitrification. Reconstructions of *G. sulfurreducens* cells display ICM that are not as tightly packed and regular as what I observed with plastic section TEM (Figure 4.2, Figure 4.3). The difference in ICM appearance between CryoET and plastic embedded thin-section TEM could be related to artifacts from the dehydration process prior to embedding, or due to a difference in the growth stage of the biofilm. CryoET revealed that the ICM in *G. sulfurreducens* has significant variance in morphology. In some cells, the ICM is a loosely organized mass of membrane structures (Figure 4.3), but in others it is more regular and composed of smaller units (Figure 4.2). This variance may represent different stages of development of the structure, since cryotomography samples were taken only after 24 hours of introducing an EM grid into the electrochemical cell, while plastic-

section TEM images capture cells that were collected from a fully developed biofilm. ICMs as observed in cryotomograms were closely associated to the inner membrane in most cases, and typically near the tip of the cell (Figure 4.2).

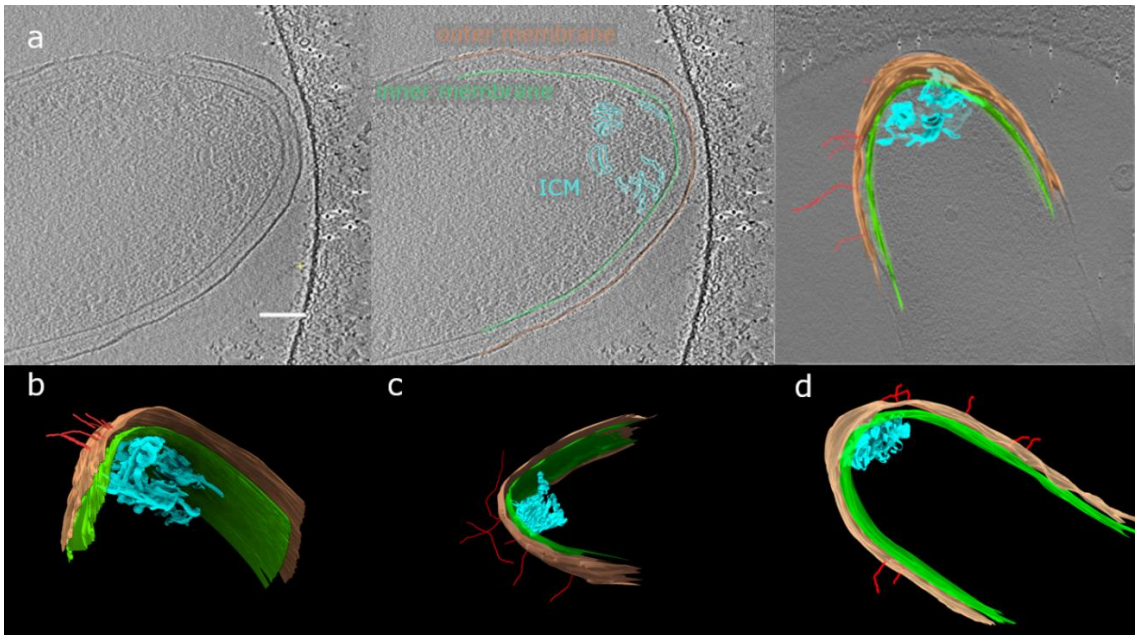

Figure 4.2 (A) Tomogram slices illustrating how 3D models were created via tomogram segmentation of ICM located in the tip of a *G. sulfurreducens* cell with the inner membrane, outer membrane, ICM, and several nanowires modeled from the tomogram. The scale bar is 100 nm. (B, C, D) 3D models of three separate cells displaying ICM near the tip of each cell. These cells were grown at -0.07 V vs. SHE directly on a grid.

Protein nanowires are important to the respiration of *G. sulfurreducens* (Peng & Zhang, 2017; F. Wang et al., 2019). I observed extracellular protein nanowires in most of the cryotomograms that I collected, but it is unclear if there is a direct relationship between nanowires and ICMs (Figure 4.2). Some nanowires intersect the outer membrane near the ICM locations, but others do not. As the ICM is expected to be an area of high metabolic

activity, the location of nanowires for extracellular electron transfer might be preferentially localized near this area.

In a sample grown with a lower potential anode (−0.17 vs. SHE), I can observe a putative earlier ICM development stage (Figure 4.3). The ICM is clearly shown to be formed by invagination of the inner membrane, which is consistent with ICM formation in other bacteria (e.g, *Rhodobacter sphaeroides*) (Tucker et al., 2010; Woronowicz et al., 2013). While a complex ICM network is evident, close inspection shows all sections to be interconnected with cytoplasmic space within them. Thus, it is a continuous inner membrane invagination. Most importantly, the periplasmic space is continuous, providing a path to the outer membrane from all regions of the ICM. This continuous periplasmic space is most crucial for *G. sulfurreducens'* metabolism of extracellular respiration, where electrons from the inner membrane must be transported extracellularly, passing through periplasmic cytochromes along the way (Aklujkar et al., 2013; Lloyd et al., 2003).

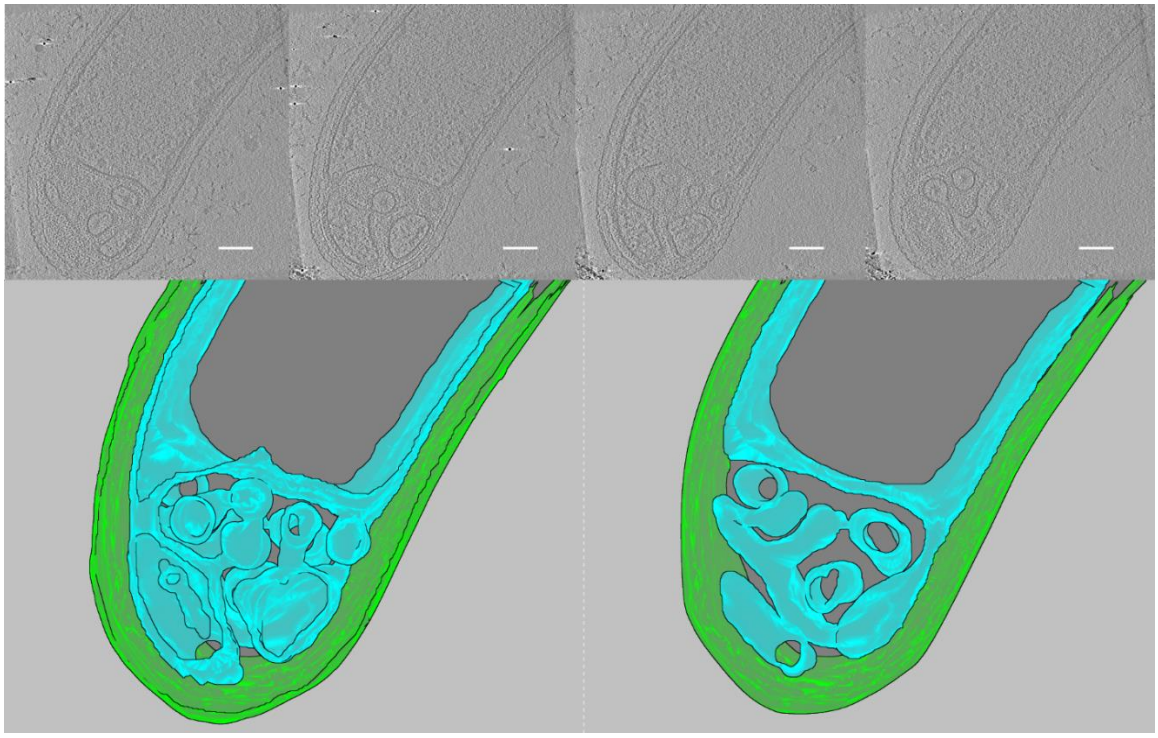

Figure 4.3 Cryotomograph slices and 3D model of a *G. sulfurreducens* cell grown at –0.17 V vs SHE on a holey-carbon/gold cryo-EM grid as anode for 24 hrs. Cryotomogram shows how ICM seems to form by invagination of the inner membrane. Top – selected tomogram slices in the z axis displaying sections of the invagination. Bottom – 3D model of the inner membrane and outer membrane through (bottom left) the entire thickness of the modeled volume and (bottom right) the model sliced approximately in half in the z axis to show the ICM profile at a different depth. Scale bar: 100 nm.

ICM abundance differences

I can also identify the presence of ICM in *G. sulfurreducens* with confocal microscopy. A similar technique has been used to identify ICM in methanotrophs (Whiddon et al., 2019). I took confocal images of fixed *G. sulfurreducens* biofilm cells grown at different anode potentials, or from cell suspensions grown with fumarate as electron acceptor, and

each image had numerous individual cells (Table A.5). The ICM is a localized bright area within a cell when it is stained with Nile red, a lipid-selective fluorescent dye (Greenspan et al., 1985) . Some cells have a single ICM, while others have multiple distinct ICM regions (Figure 4.1b). Generally, the ICM are located near the tips of cells, but I also observed ICM in locations throughout the length of a cell. By using the ImageJ plugin MicrobeJ (Ducret et al., 2016), I can detect cell boundaries and the local maxima within them that I have identified as ICM. The ICM area as a fraction of total cell area had a median value of 5.7% in the electrode biofilm grown at -0.07 V and 4.2% in the fumarate cells, but there is a high variance in fractional area with some cells having over 30% of the area occupied by ICM (Figure A.6 and Figure A.7). This is lower than the cell area occupied by ICMs in methanotrophs (Whiddon et al., 2019). By applying identical image analysis (ICM counting) to cells collected from different conditions, I found that a change in electron acceptor significantly affects the frequency of *G. sulfurreducens* cells displaying ICM (Figure 4a). In biofilms grown on anodes at higher potentials I observed a relatively lower fraction of cells with ICM (41 ± 4% at -0.03 V vs. SHE vs. 58 ± 8% at -0.17 V vs. SHE). Cells grown with fumarate had the lowest incidence of ICM (14 ± 10%) despite the fumarate/succinate redox couple having a potential around +0.03 vs. SHE, similar in redox potential to our highest anode potential studied. In a biofilm, however, there will be a redox potential gradient because of ohmic losses and diffusion limitations (Bond et al., 2012; Popat & Torres, 2016; C. I. C. I. Torres et al., 2008), so I anticipate that cells grown with fumarate will experience a higher redox potential on average than anode biofilm cells on an electrode at a similar potential. Since lower anode potentials provide less potential energy for growth, the higher abundance of ICM may be

an adaptation to energy limitation. Our image analysis used conservative parameters for identifying ICM within cells, so the absolute frequency of ICM is likely higher.

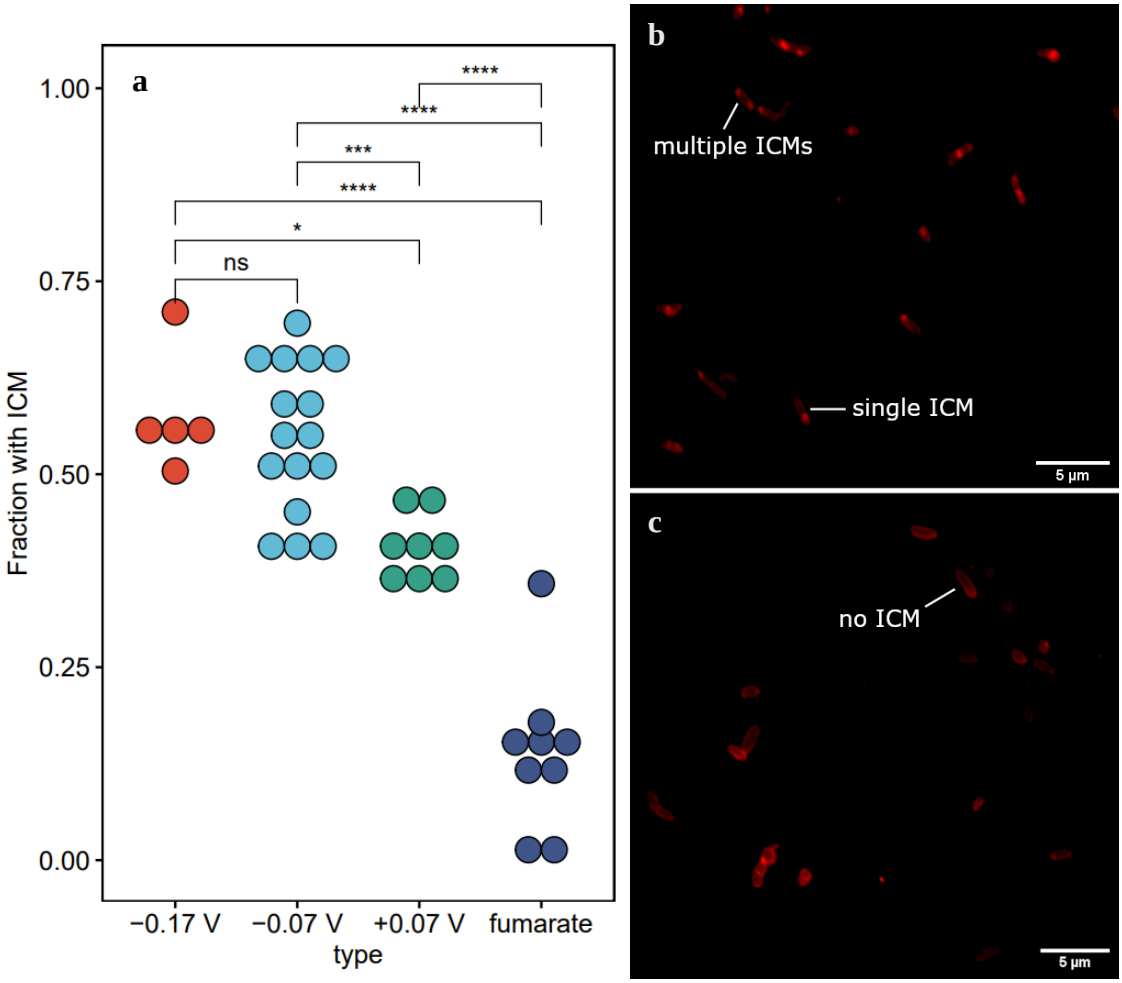

Figure 4.4 **a:** Fraction of cells with an ICM in *G. sulfurreducens* under different growth conditions. Each dot represents a unique image with an average of 113 cells, see Table A.5 for raw counts. The three potentials – -0.17, -0.07, and +0.07 – represent cells collected from anodes poised at the respective potentials vs. SHE. The 'fumarate' condition cells were grown planktonically with fumarate as the electron acceptor. Statistical testing consisted of a two-tailed t-test with Hochberg multiple comparison correction. *($\rho<0.05$), ***($\rho\leq0.001$), ****($\rho\leq0.0001$). **b:** Sum projection of confocal z-stacks of *G. sulfurreducens* cells grown on an electrode at -0.07 V vs. SHE with examples of ICM annotated. **c:** Sum projection of cells grown with fumarate as an

electron acceptor exemplifying typical cell morphology when ICM is not present. Both cell images were cropped from larger images taken at 100X magnification using Nile red as a phospholipid-selective fluorophore.

Significance

G. sulfurreducens has a complex and efficient respiratory metabolism. At the inner membrane, electrons are trifurcated into different respiration pathways depending on the redox potential of the terminal electron acceptor (Joshi et al., 2021; Levar et al., 2017; Levar, Chan, Mehta-Kolte, et al., 2014). Being an invagination of the inner membrane, the ICM must contain the critical inner membrane cytochromes for respiration. In ammonia- and methane-oxidizing bacteria, the rate-limiting respiratory enzymes – ammonia monooxygenase and methane monooxygenase, respectively – are present within the ICM (Brantner et al., 2002; Fiencke & Bock, 2006). For organisms with slim thermodynamic margins, an ICM could allow a higher respiration rate by increasing membrane surface area and the total number of respiratory proteins. Producing an ICM must be a significant energy investment for a cell, and the structural organization of the ICM in *G. sulfurreducens* suggests a specialized function outside of lipid storage. The production of ICMs explains why *G. sulfurreducens* is higher in lipid content than other gram negative bacteria (Howley, Ki, et al., 2022), as the production of ICM in other bacteria causes elevated lipid fractions (Patt & Hanson, 1978; Whiddon et al., 2019).
In our study I found higher incidence of ICM in cells growing with less thermodynamically favorable conditions (Figure 4.4a), consistent with the use of an ICM to increase respiratory rates in limiting conditions. A respiratory ICM in *G.*

sulfurreducens would require a mechanism to pass electrons to the rest of the extracellular electron transfer network, and if there is an open connection with the periplasm, as shown in Figure 4.3, electrons could transfer by diffusion of periplasmic cytochromes (e.g., PpcA, GSU1996) (Lloyd et al., 2003; Pokkuluri et al., 2011). Yet, transport of these cytochromes from ICMs to the outer membrane would be a much larger distance than the typical periplasmic space, since ICMs seem to span the whole cell thickness and have regions that are up to 200 nm from the outer membrane.

While *G. sulfurreducens* is not the only bacterium with an ICM, nothing like the ICM has been found in any closely related organisms. To our knowledge, it is the first organism from the phylum Thermodesulfobacteriota identified to produce an ICM, the first metal oxide reducer that does so, and the first documentation of ICMs formed in biofilms. The ICM in *G. sulfurreducens* provides a good opportunity to study ICM formation in general, because researchers can easily control its expression by changing the redox potential of the electron acceptor, and the polar localization of the ICM in the tip presents an opportunity to study intracellular organization in bacteria. The varying production of ICMs in *G. sulfurreducens* suggests that this structure is naturally formed to increase respiratory rates in thermodynamically and kinetically limiting conditions, a hypothesis that has been proposed before for other microorganisms (Greening & Lithgow, 2020). Unlike other bacteria that produce ICMs, *G. sulfurreducens* cannot complete its entire respiratory pathway within the ICM. Electrons from the ICM in *G. sulfurreducens* must travel to the outer membrane for extracellular respiration, and those electrons may have to travel microns through a biofilm before reaching the terminal electron acceptor

G. sulfurreducens has various approaches to optimize energy conservation under limiting and varying redox conditions. Three characterized pathways seem to be expressed concomitantly within an electrogenic biofilm to maximize energy conservation (He et al., 2021). The generation of ICMs at energy-limiting conditions seem to be an additional tool to maximize energy production within the cell. Nernstian models that are used to predict rates of respiration in *G. sulfurreducens* would predict a slow respiration rate at lower potentials (Kato Marcus et al., 2007; Richter et al., 2009; C. I. Torres et al., 2010) The slower respiration rate is the consequence of a rate-limiting electron transfer protein, proposed to be at the inner membrane (Lusk et al., 2018; C. I. Torres et al., 2010) . If *G. sulfurreducens* can increase the amount of this rate-limiting protein by increasing the amount of inner membrane present, the apparent limitation is alleviated, and higher respiratory rates can be achieved. Thus, knowledge of how ICMs are used and under which conditions they are produced will be important to predict rates of electrical current generation by *G. sulfurreducens.* Future *G. sulfurreducens* ICM studies will likely take advantage of the genetic tools that have been developed for the organism as well as creative imaging techniques.

Methods

G. sulfurreducens growth.

G. sulfurreducens PCA (ATCC, Virginia USA) was grown from glycerol freezer stocks using fumarate or an electrode as the electron acceptor as described in Chapter 2. Fumarate cells were grown in sealed anaerobic culture tubes with ATCC 1957 medium.

Electrode cells were grown in 100 mL single chamber microbial electrochemical cells on 6-8 cm^2 graphite electrodes (Graphitestore, Illinois USA) poised at either -0.17, -0.07, or +0.07 V vs. SHE and electrical current was monitored with a VMP3 potentiostat (BioLogic, Tennessee USA). Each reactor had an Ag/AgCl reference electrode (BASi, Indiana USA).

TEM.

G. sulfurreducens cells from a mature biofilm (~30 days of growth) were fixed in phosphate buffer containing 4% paraformaldehyde, 2% glutaraldehyde (v/v) and then plunge frozen in liquid propane before dehydration via freeze substitution in 2% osmium tetroxide dissolved in acetone on dry ice at -80° C. Cells were slowly returned to room temperature for embedding in Araldite 502 resin (Ted Pella, Inc.). These sections were cut at 70 nm thickness and secondary stained with lead acetate to improve contrast All thin section imaging was performed on a Tecnai TF-20 (FEI) or a Phillips CM12.

CryoET.

To grow electrode biofilm cells for cryoET, I designed a holder for fenestrated carbon TEM grids to insert into bioelectrochemical cells with actively growing cultures. The grids in the holder are held against a titanium plate that functions as an anode and electron acceptor for the bacteria. 6 nm BSA conjugated gold nanoparticle fiducials were dried then baked at 60° C to fix the gold fiducials onto the grids before introduction to the bioreactor. The TEM grids in the holder were removed after 24 hours and immediately plunge frozen into liquid nitrogen cooled ethane using an in house designed manual plunge freezer to capture the cells in their active state (Figure A.8 and A.9). For the

fumarate condition, a suspension of cells grown for 7-10 days was pipetted onto each grid, blotted to remove excess liquid, and frozen with the FEI Vitrobot Mark IV.
The frozen hydrated cells were imaged on a Krios G2 (FEI, Oregon USA) at tilts from −65° to +65˚ in 2.0˚ angular steps using a dose symmetric collection scheme(Hagen et al., 2017) in regions where individual cells could be observed over fenestrations in the carbon. Images were collected at a nominal magnification of 6500x giving a 1.8 Å pixel size in super-resolution mode on the K2 summit camera with a dose rate of 0.5 electron per $Å^2$ * second for three seconds with a frame rate of 0.2 frames per second (total dose of 100 electrons per $Å^2$). Individual movie frames were gain corrected, aligned with MotionCor2 (Zheng et al., 2017), and sum images were binned by 2 resulting in an image with a 3.6 Å/pixel scale. Summed images were restacked, then tomographic reconstruction in eTOMO (Mastronarde & Held, 2017) was performed. Slices from each tomogram were output from IMOD using the ZAP window saving feature which saves at the native resolution of the monitor. 3D modeling was performed in IMOD and visualized in ChimeraX (Pettersen et al., 2021).

Data Availability.

The tomograms used to create figures for this chapter can be accessed in the EMDB-EBI repository under accession numbers EMD-27710, EMD-27729, EMD-27748, and EMD-27747.

Confocal microscopy sample preparation and acquisition properties.

G. sulfurreducens anode biofilm cells were resuspended, fixed, and imaged between 12-20 days after current began growing exponentially and was at least 2 A/m^2. *G.*

sulfurreducens biofilm cells were removed from the electrode by gently vortexing in phosphate buffer, pelleted at 4000 RPM for 5 minutes, resuspended in 4% paraformaldehyde for 1 hour, then rinsed and stored in phosphate buffer at 7 ˚C. Live *G. sulfurreducens* cells grown under fumarate conditions were imaged 5-7 days after inoculation. Cells under both anode and fumarate conditions were diluted with 50 mM phosphate buffer and Nile red (ThermoFisher/Invitrogen, red, excitation: 561 nm) for lipid staining to a final concentration of 2 µg/mL. Samples were allowed to incubate for at least 15 minutes at room temperature in the dark. Stained cells were imaged on a standard glass slide, or 2% poly-L-lysine coated glass slide with a 1 ½ cover slip sealed with nail polish.

Fluorescence images were acquired with a Nikon C2+ confocal microscope equipped with a 100X Plan Apo λ (NA 1.45) oil objective using the adjacent NIS Elements software, operated inside an anaerobic glovebox. Nile red was excited with a 561 nm laser and filtered with a 525/50 561 LP filter cube.

Fluorescence image analysis.

Z stacks were processed into sum projections and a Gaussian blur (σ=1) filter applied for smoothing in ImageJ. The ImageJ MicrobeJ plug-in (Ducret et al., 2016) was used for bacterial and ICM detection of *G. sulfurreducens* cells under both anode and fumarate conditions with summary output in Table A.5. Statistical analysis was performed using the Student's t-Test corrected for multiple comparisons using the Benjamini-Hochberg method.

Acknowledgements.

The funding for this work was provided by the Office of Naval Research (ONR award N0014-20-1-2269). Confocal microscopy was performed in a Nikon C2+ obtained through an ONR DURIP grant #N00014-19-1-2531. All electron microscopy was performed at ASU's electron microscopy core facilities.

3D model manipulation was partially performed with UCSF ChimeraX, developed by the Resource for Biocomputing, Visualization, and Informatics at the University of California, San Francisco, with support from National Institutes of Health R01-GM129325 and the Office of Cyber Infrastructure and Computational Biology, National Institute of Allergy and Infectious Diseases.

CHAPTER 5

GENE EXPRESSION IN *T. FERRIACETICA*

Thermincola ferriacetica is a Gram-positive thermophilic bacterium that was isolated from a hot spring in Russia (Zavarzina et al., 2007). It is an extremophile with a diverse metabolism; *T. ferriacetica* can respire using hydrogen or acetate as an electron donor, and a variety of electron acceptors including iron III (hydr)oxides, electrodes, humic acids, and thiosulfate. It is mixotrophic; it is able to grow chemotrophically with an organic carbon source, or lithoautotrophically with only CO_2 as a carbon source. *T. ferriacetica* is not only thermophilic, having an optimum growth temperature of 57-60 C, but is also halotolerant and can survive and even grow under 100% CO headspace by fermenting it to H_2 and CO_2 (Zavarzina et al., 2007). Like many other iron-reducing bacteria, *T. ferriacetica* respires by extracellular electron transfer and therefore can grow using an electrode in a bioelectrochemical system as its electron acceptor (Wrighton et al., 2011).

Despite its unique metabolic capabilities, there is limited research on *T. ferriacetica* grown on electrochemical systems. Kinetic studies show the organism follows a Nernst-Monod kinetic correlation to anode potential (Parameswaran et al., 2013). Given the capacity of *T. ferriacetica* to grow at pH down to 5.2, this organism was also used to confirm that electrochemical responses are proton-coupled, suggesting an association of the electrochemical signal to an inner-membrane protein that pumps protons for energy generation (Lusk et al., 2018).

Organisms that perform extracellular electron transfer for respiration are widely studied for their unique metabolisms and potential biotechnological applications, but the

organisms that have been studied so far are almost exclusively Gram-negative, mesophilic bacteria. We assume that the extracellular electron transfer pathway in *T. ferriacetica* looks significantly different than the pathways that have been elucidated in organisms like *Geobacter sp.* and *Shewanella*. Gram-positive bacteria like *T. ferriacetica* have a thick cell wall and a smaller periplasmic space than Gram-negative bacteria. We know that in *G. sulfurreducens*, electrons leave the outer membrane and travel away from the cell via conductive nanowires. The presence of a thick layer of peptidoglycan surrounding the outer membrane may complicate the secretion of nanowires in *T. ferriacetica*. In the closely related *T. potens*, a study found cytochromes associated with the surface of the peptidoglycan cell wall which is unusual for Gram-positive bacteria (Carlson et al., 2012). The specific proteins in *T. ferriacetica* that compose the electron transfer chain at the inner membrane, periplasm, and outer membrane remain unresolved. The genome of *T. ferriacetica* contains at least 18 multi-heme cytochromes. Only a few have been purified or characterized. Among these, CwcA has been proposed as a homolog to the *G. sulfurreducens* protein OmcS because of a predicted ability to polymerize and produce cytochrome nanowires (Faustino et al., 2021). The multiheme cytochromes PdcA and ImdcA were electrochemically characterized and displayed electrochemical activity through a wide range of redox potentials due to the different organization of hemes within the proteins, as has been shown in *G. sulfurreducens* multiheme cytochromes (Faustino et al., 2021; Pokkuluri et al., 2011). These similarities suggest similarities in the way electroactive bacteria respire despite their significant differences in physiology.

Methods

I grew *T. ferriacetica* from a DSMZ stock culture. The inoculation culture was grown in a sealed test tube containing medium as described in Zavarzina et al. 2007 (Zavarzina et al., 2007), with 8 g/L anthraquinone-2-6 disulfonate as the electron acceptor and: [g/L] NH_4Cl, 0.33; KH_2PO4, 0.33; $MgCl_2$* $6H_2O$, 0.33; $CaCl_2$*$6H_2O$, 0.33; KCl, 0.33; yeast extract (Sigma), 0.05; NaHCO3, 0.7; sodium acetate, 20 mM; Wolin's mineral solution, 10 ml L^{-1}; Wolin's vitamin solution , 10 ml L^{-1} (WOLIN et al., 1963). I sparged the test tubes of culture medium with 20% CO_2, 80% N_2 and sealed before autoclaving. I inoculated the AQDS culture tubes with *T. ferriacetica* and incubated it at 57 C. When I observed a color change in the medium from yellow to black due to AQDS reduction, the culture was ready to be used to inoculate an MXC.

For this experiment, the MXC was a dual chamber microbial electrochemical cell with an anion exchange membrane separating the anode and cathode chambers. The anode and cathode were both graphite carbon rods, and the reference was an RE-5B Ag/AgCl reference (BASi). Using a VMP3 potentiostat (Bio-Logic), I poised the anode at −0.3 V vs. Ag/AgCl. The cathode chamber was filled with a solution containing 90 mM NaCl and 10 mM NaOH. The anode chamber was inoculated with *T. ferriacetica* via syringe, and I constantly bubbled 20% CO_2, 80% N_2 through the anode chamber for the entire experiment.

I collected the *T. ferriacetica* biofilms by scraping the graphite anode when the current density produced by the cells reached 1-2 A/m^2. As in Chapter 2, I immediately extracted total RNA from the scraped cells using the QIAGEN PowerMicrobiome RNA extraction kit with an on-column DNAse I digestion to remove genomic DNA. The RNA was

further cleaned with the Thermofisher MicrobEXPRESS bacterial mRNA enrichment kit which removes a large fraction of ribosomal RNA. Cleaned RNA was reverse transcribed into cDNA for sequencing library prep, and the sequences were processed on an Illumina NextSeq at ASU's Genomics Core.

Results and Discussion

I sequenced RNA transcripts from biological triplicates of *T. ferriacetica* biofilms grown on a graphite anode. I then aligned the sequencing reads to the scaffold reference genome to get counts of sequence hits per gene. My aligned data contained over 3 million reads per sample. While the reference genome for *T. ferriacetica* is only an assembly made up of individual contigs and not a complete circular chromosome, I was still able to measure the expression of more than three thousand predicted protein-coding genes. By quantifying and normalizing the transcript counts, I can find the most abundantly expressed transcripts. Table B1 (Appendix B) contains the top 30 annotated genes by basemean. Basemean is a normalized average of transcript counts as calculated by DESeq2, and it is a measure of a gene's expression relative to other genes.

Cytochrome expression in *T. ferriacetica.*

There are several respiratory genes of interest in the highly expressed group. The most highly expressed gene is *Tfer_3268*, an S-layer homology domain-containing protein. In Gram-positive bacteria, S-layer proteins form two-dimensional sheets on the cell surface to facilitate a number of biological functions (Fagan & Fairweather, 2014). *Tfer_3268* does not share a strong sequence similarity to any well-known S-layer proteins, so its function in *T. ferriacetica* is unknown. Genes *Tfer_2153*, *Tfer_0075*, and *Tfer_0077* are all predicted to encode for multiheme cytochromes, and their expression levels are in the

top five out of the over 3000 genes quantified. Tfer_2153 is a 7-heme cytochrome with a signal peptide indicating that it is located outside of the cytoplasm. Tfer_0075 is a 6-heme cytochrome that is predicted to be embedded in the cell wall, and it may be able to form conductive wires as OmcS does in *G. sulfurreducens* (Faustino et al., 2021). The most interesting of the three is the massive Tfer_0077, a large multiheme cytochrome with 54 heme-binding sites and a predicted interaction with the cell membrane. There is one other multiheme cytochrome represented in the most abundant transcripts, and that is *Tfer_1887* which encodes for a 10-heme cytochrome with a signal peptide for transport across the cell membrane, and has been putatively assigned to a periplasmic role in the electron transfer chain (Faustino et al., 2021).

In electroactive bacteria, multiheme cytochromes are critical for electron transport. Since I extracted this RNA from *T. ferriacetica* that was respiring an electrode, I assume that the most abundantly expressed cytochromes are related to that function. This assumption is supported by the data in Chapter 2, where I found cytochromes known to be used in extracellular respiration in *G. sulfurreducens* among the most abundantly expressed. My data suggests that Tfer_2153, Tfer_0075, Tfer_1887, and Tfer_0077 are likely important cytochromes for EET in *T. ferriacetica*. The first three of these are similar in size and heme content to membrane and extracellular cytochromes in other EAB, but Tfer_0077 is quite unique. Containing over 2100 amino acids and 54 heme-binding sites, Tfer_0077 would be a remarkably large cytochrome. The fact that it is predicted to be embedded in the cell membrane presents the possibility that it is part of the pathway for transporting electrons across the periplasm or outside of the cell. Several cytochromes from *T. ferriacetica* have been purified and characterized, and a putative EET pathway has been

proposed (Faustino et al., 2021). That work resolved a 3D structure of Tfer_0075 and proposed that it would be capable of forming a nanowire of repeating units, like OmcZ in *G. sulfurreducens* but perhaps transiting the cell wall instead of the extracellular space. The same publication also identified Tfer_1887 as an important component of the electron transfer pathway, but the exact order and location of each of these proteins remains to be determined. The gene expression data I present here confirms the importance of these proteins and suggests a few additional cytochromes to study in the future.

Carbon metabolism.

I grew *T. ferriacetica* using acetate as the electron donor, so I expected that it would use acetate in the tricarboxylic acid (TCA) cycle to drive metabolism and produce building blocks for cell growth. The gene expression data tells a different story. *T. ferriacetica* is capable of lithoautotrophic growth. It can fix inorganic carbon from CO or CO_2 to create organic carbon molecules for growth. I observed several components of this carbon fixation metabolism highly represented in the transcriptome (Table B1) including CO dehydrogenase, CO-methylating acetyl-CoA, and methyltransferase enzymes. These enzymes are the major components of the Wood-Ljungdahl pathway for CO_2 fixation (Ragsdale & Pierce, 2008). I did detect transcripts from the enzymes of the TCA cycle as well, but their abundance was small in comparison. It seems counterintuitive, it seems that *T. ferriacetica* is not using acetate in the direct way that a bacterium like *G. sulfurreducens* does. One possibility is that *T. ferriacetica* is using the Wood-Ljungdahl pathway in reverse to oxidize acetate and coupling it to reduction of its electron acceptor, as is seen in sulfate-reducing bacteria (Can et al., 2014). The abundant expression of a

reversible Wood-Ljungdahl pathway explains the extremely high tolerance to CO toxicity seen in *T. ferriacetica* (Zavarzina et al., 2007).

Extracellular structures.

For bacteria that respire extracellular electron acceptors, there must be a mechanism for transporting electrons to those acceptors. *T. ferriacetica* is known to form dense biofilms with multiple layers of cells (Parameswaran et al., 2013). If cells on the outer edge of the biofilm respire, they would need to transfer electrons over microns of distance. Based on what is known from other EAB, *T. ferriacetica* may produce a network of nanowires from cytochromes as discussed above, or it may have an EET mechanism that is completely different. In my gene expression data, the flagellin protein is among the most highly expressed. The limited microscopy of *T. ferriacetica* that I have found in literature does not give any idea of how this flagellin is expressed on the cell, but it is predicted by PSORTb that the flagellin proteins will be extracellular. I also observed the expression of flagellin motor proteins and associated proteins for flagellin control. This suggests that *T. ferriacetica* either has motility or expresses a flagellin for some other purpose. Due to the challenges of growing the organism, no live cell imaging of *T. ferriacetica* exists to observe potential cell movement.

Proposing a pathway

Based on my gene expression data, and the information available from previous studies on *T. ferriacetica* and *T. potens*, I can put together a putative electron transfer pathway in *T. ferriacetica* grown on an anode (Figure 5.1). I included only cytochromes in Figure 5.1 for simplicity. In reality, I expect NADH dehydrogenase to be embedded in the inner membrane, and I expect electrons to travel from NADH dehydrogenase to a quinone and

then to a cytochrome. I placed Tfer_0077 in the cellular membrane due to its predicted position. Because of its large size, I hypothesized that it may span the entire periplasm. Tfer_2153 was difficult to predict a location for. I placed it in the inner membrane, but it could just as likely be periplasmic or even in the cell wall. Tfer_2153 was the most abundantly expressed protein, so it could even be extracellular. Tfer_1887 I placed in the periplasm based on a previous study (Faustino et al., 2021), and Tfer_0075 I placed as a cell wall or extracellular nanowire because of its morphological characteristics that were modeled in that same study. My proposed model is oversimplified and likely incomplete, but it provides a hypothetical model that may be refined with more research.

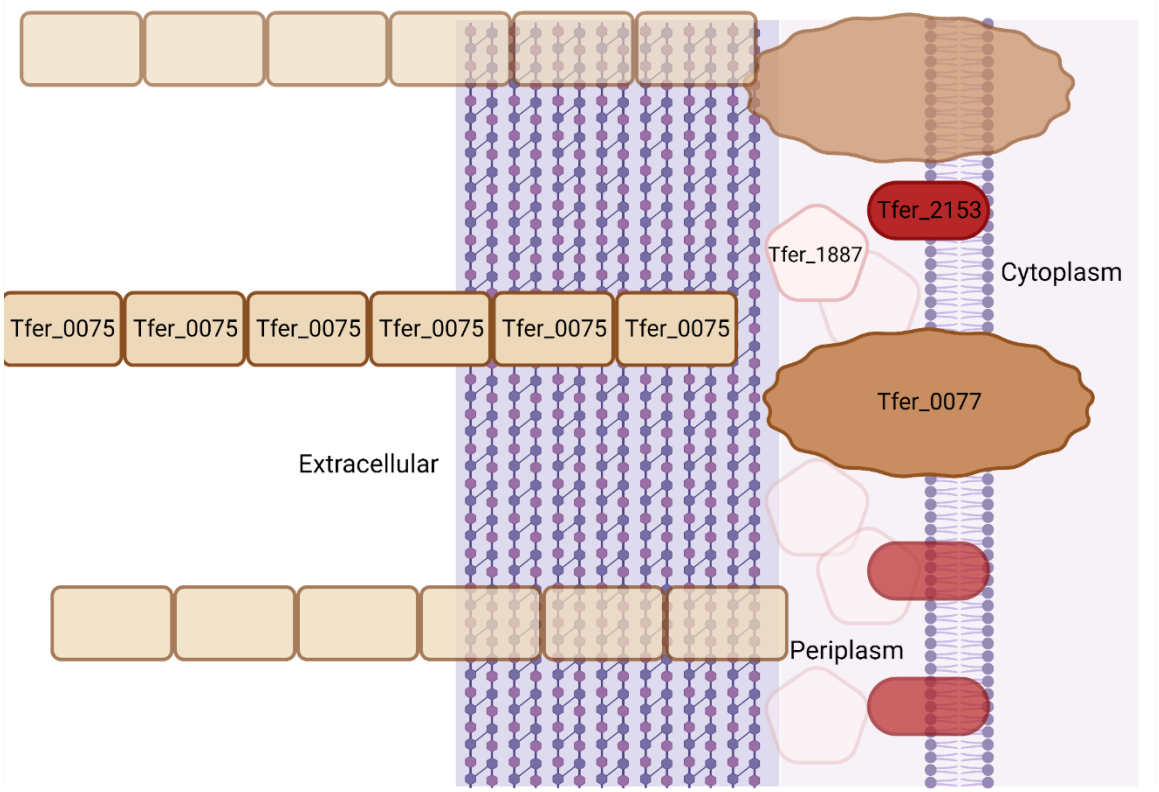

Figure 5.1 Proposed EET pathway cytochrome organization in *T. ferriacetica*. Created with Biorender.com

Summary

My gene expression study reveals new information about *T. ferriacetica* and its metabolism. It also provides possibilities for future investigation. It may be possible to separate and characterize nanowires as has been performed for *G. sulfurreducens*. Isolating and characterizing the protein Tfer_0077 may also be a good opportunity to study an unusually large electron transfer protein. In designing this experiment, I had intended to collect samples from other conditions to do comparisons, but my RNA yields were too small for sequencing. I believe that developing methods for consistent growth of large numbers of *T. ferriacetica* cells is a prerequisite for additional research with this organism.

CHAPTER 6

CONCLUSION

I believe my dissertation tells a fascinating story about the workings of *G. sulfurreducens* that has not been put together before. I have shown that *G. sulfurreducens* changes the expression of certain cytochromes depending on the potential of its electron acceptor. Therefore, it has evolved mechanisms to adapt to changing energetic conditions. One of these evolved mechanisms may be the ICM which is expressed only when less energy is available to the cells. Tying it all together is my chapter on cell composition because I suspect that the presence of ICM could contribute to the high lipid content that I observed in Chapter 3, and the abundant cytochrome expression influences the high iron content. These observations will guide the assumptions of future researchers, as the presence of additional cell surface area under some conditions might be an important parameter for those modeling this organism. I anticipate that ICM will be discovered in additional organisms now that the technology we used to find it is more widespread, and I would expect that the most likely candidates are other bacteria with narrow thermodynamic margins for metabolism.

The method I adapted for preparing electroactive bacteria for cryotomography will undoubtedly be used for many other organisms. By growing cells directly on a grid that can be poised at a certain potential, it is possible to freeze the cells as they are when respiring and image them on the actual electron acceptor without any disturbance. For electroactive organisms, the extracellular structures are often the most interesting research targets, and cryotomography allows the least disturbance to those structures.

Previous work has identified that there are different proteins at the inner membrane involved with each of the different electron transport pathways, and I have expanded that to show that there are changes in the periplasm, outer membrane, and extracellular proteins that can be linked to shifts in pathways. I anticipate that our model of respiration of *G. sulfurreducens* will continue to improve with additional research.

Future Work

Researchers building upon my work could tackle many different ideas, but there are certainly some questions I would like to know the answers to. While we know how many different EET pathways *G. sulfurreducens* can express and how to make it use each one, the question remains: How does *G. sulfurreducens* sense the change in potential and respond? The mechanisms have evolved to not only match the condition to the right pathway, but to prevent a thermodynamically possible but less efficient pathway to be used. Identifying how these functions may provide additional tools to synthetic biologists developing biosensors. Another question that my dissertation provokes is: What exactly is happening in ICM? I speculate based on evidence I present that it is metabolically active, but I am far from providing details on how the ICM interacts with the rest of the EET pathway. It seems that having a connection to the periplasm might allow diffusion of electron carriers, but that will require additional experimentation to determine.

My work has identified more respiratory proteins that may be associated with a specific pathway, but I know that there are still unknown details. If researchers can identify an entire electron transport chain from the quinone pool to the terminal electron acceptor and determine how it is assembled, it would be possible for synthetic biologists to import

an electroactive respiratory pathway into other organisms. This has been done with the EET pathway from *Shewanella oneidensis* and the non-electroactive *E. coli* (Q. Wang et al., 2019), but there are still knowledge gaps preventing the same from being done with *G. sulfurreducens*.

Lastly, I would like to see the experimental protocols for growing *T. ferriacetica* revisited. I struggled with growing this organism, despite following the published method to the letter. I wonder if a better, more reproducible growth method could be developed to make future experiments less burdensome on the researcher. I believe that the mysterious growth characteristics of *T. ferriacetica* have stymied research into the workings of an electroactive bacterium quite different than the ones that are commonly studied.

REFERENCES

Abdul-Tehrani, H., Hudson, A. J., Chang, Y. S., Timms, A. R., Hawkins, C., Williams, J. M., Harrison, P. M., Guest, J. R., & Andrews, S. C. (1999). Ferritin mutants of Escherichia coli are iron deficient and growth impaired, and fur mutants are iron deficient. *Journal of Bacteriology*, *181*(5), 1415–1428. https://doi.org/10.1128/jb.181.5.1415-1428.1999

Aklujkar, M., Coppi, M. V., Leang, C., Kim, B. C., Chavan, M. A., Perpetua, L. A., Giloteaux, L., Liu, A., & Holmes, D. E. (2013). Proteins involved in electron transfer to Fe(III) and Mn(IV) oxides by Geobacter sulfurreducens and Geobacter uraniireducens. *Microbiology (United Kingdom)*, *159*(PART3), 515–535. https://doi.org/10.1099/mic.0.064089-0

Andrews, S. (2010). *FastQC: A Quality Control Tool for High Throughput Sequence Data [Online]*. http://www.bioinformatics.babraham.ac.uk/projects/fastqc/

Bolger, A. M., Lohse, M., & Usadel, B. (2014). Trimmomatic: A flexible trimmer for Illumina sequence data. *Bioinformatics*, *30*(15), 2114–2120. https://doi.org/10.1093/bioinformatics/btu170

Bonanni, P. S., Massazza, D., & Busalmen, J. P. (2013). Stepping stones in the electron transport from cells to electrodes in Geobacter sulfurreducens biofilms. *Physical Chemistry Chemical Physics*, *15*(25), 10300–10306. https://doi.org/10.1039/c3cp50411e

Bonanni, P. S., Schrott, G. D., & Busalmen, J. P. (2012). A long way to the electrode: how do Geobacter cells transport their electrons? *Biochemical Society Transactions*, *40*(6), 1274–1279. https://doi.org/10.1042/BST20120046

Bond, D. R., & Lovley, D. R. (2003). Electricity Production by Geobacter sulfurreducens Attached to Electrodes. *AEM*, *69*(3), 1548–1555. https://doi.org/10.1128/AEM.69.3.1548

Bond, D. R., Strycharz-Glaven, S. M., Tender, L. M., & Torres, I. C. I. (2012). On Electron Transport through Geobacter Biofilms. *ChemSusChem*, *5*(6), 1099–1105. https://doi.org/10.1002/cssc.201100748

Bouchet-Marquis, C., & Hoenger, A. (2011). Cryo-electron tomography on vitrified sections: A critical analysis of benefits and limitations for structural cell biology. *Micron*, *42*(2), 152–162. https://doi.org/10.1016/j.micron.2010.07.003

Brantner, C. A., Remsen, C. C., Owen, H. A., Buchholz, L. A., & Collins, M. (2002). Intracellular localization of the particulate methane monooxygenase and methanol dehydrogenase in Methylomicrobium album BG8. *Archives of Microbiology*, *178*(1), 59–64. https://doi.org/10.1007/s00203-002-0426-2

Brown, R. E., Jarvis, K. L., & Hyland, K. J. (1989). Protein measurement using bicinchoninic acid: elimination of interfering substances. *Analytical Biochemistry*, *180*(1), 136–139. https://doi.org/10.1016/0003-2697(89)90101-2

Budhraja, R., Ding, C., Walter, P., Wagner, S., Reemtsma, T., Gary Sawers, R., & Adrian, L. (2019). The impact of species, respiration type, growth phase and genetic inventory on absolute metal content of intact bacterial cells. *Metallomics*, *11*(5), 925–935. https://doi.org/10.1039/c9mt00009g

Butler, J. E., Glaven, R. H., Esteve-nu, A., Shelobolina, E. S., Bond, D. R., & Lovley, D. R. (2006). *Genetic Characterization of a Single Bifunctional Enzyme for Fumarate Reduction and Succinate Oxidation in Geobacter sulfurreducens and Engineering of Fumarate Reduction in Geobacter metallireducens*. *188*(2), 450–455. https://doi.org/10.1128/JB.188.2.450

Byreddy, A. R., Barrow, C. J., & Puri, M. (2016). Bead milling for lipid recovery from thraustochytrid cells and selective hydrolysis of Schizochytrium DT3 oil using lipase. *Bioresource Technology*, *200*, 464–469. https://doi.org/10.1016/j.biortech.2015.10.019

Caccavo, F., Lonergan, D. J., Lovley, D. R., Davis, M., Stolz, J. F., & McInerney, M. J. (1994). Geobacter sulfurreducens sp. nov., a Hydrogen- and Acetate-Oxidizing Dissimilatory Metal-Reducing Microorganism. *Applied and Environmental Microbiology*, *60*(10), 3752–3759.

Can, M., Armstrong, F. A., & Ragsdale, S. W. (2014). Structure, function, and mechanism of the nickel metalloenzymes, CO dehydrogenase, and acetyl-CoA synthase. *Chemical Reviews*, *114*(8), 4149–4174. https://doi.org/10.1021/cr400461p

Carlson, H. K., Iavarone, a. T., Gorur, a., Yeo, B. S., Tran, R., Melnyk, R. a., Mathies, R. a., Auer, M., & Coates, J. D. (2012). Surface multiheme c-type cytochromes from Thermincola potens and implications for respiratory metal reduction by Gram-positive bacteria. *Proceedings of the National Academy of Sciences*, *109*(5), 1702–1707. https://doi.org/10.1073/pnas.1112905109

Chadwick, G. L., Jiménez, F., Gralnick, J. A., Bond, D. R., & Orphan, V. J. (2019). NanoSIMS imaging reveals metabolic stratification within current-producing biofilms. *Proceedings of the National Academy of Sciences*, *116*(41), 20716–20724. https://doi.org/10.1073/pnas.1912498116

Chowdhury, C., Sinha, S., Chun, S., Yeates, T. O., & Bobik, T. A. (2014). Diverse Bacterial Microcompartment Organelles. *Microbiology and Molecular Biology Reviews*, *78*(3), 438–468. https://doi.org/10.1128/mmbr.00009-14

Clarke, T. A., Edwards, M. J., Gates, A. J., Hall, A., White, G. F., Bradley, J., Reardon, C. L., Shi, L., Beliaev, A. S., Marshall, M. J., Wang, Z., Watmough, N. J., Fredrickson, J. K., Zachara, J. M., Butt, J. N., & Richardson, D. J. (2011). Structure

of a bacterial cell surface decaheme electron conduit. *Proceedings of the National Academy of Sciences*, *108*(23), 9384–9389. https://doi.org/10.1073/pnas.1017200108

Coppi, M. V. (2005). The hydrogenases of Geobacter sulfurreducens: A comparative genomic perspective. *Microbiology*, *151*(4), 1239–1254. https://doi.org/10.1099/mic.0.27535-0

Cuellar-Bermudez, S. P., Romero-Ogawa, M. A., Vannela, R., Lai, Y. J. S., Rittmann, B. E., & Parra-Saldivar, R. (2015). Effects of light intensity and carbon dioxide on lipids and fatty acids produced by Synechocystis sp. PCC6803 during continuous flow. *Algal Research*, *12*, 10–16. https://doi.org/10.1016/j.algal.2015.07.018

Daly, M. J., Gaidamakova, E. K., Matrosova, V. Y., Vasilenko, A., Zhai, M., Venkateswaran, A., Hess, M., Omelchenko, M. V., Kostandarithes, H. M., Makarova, K. S., Wackett, L. P., Fredrickson, J. K., & Ghosal, D. (2004). Accumulation of Mn(II) in Deinococcus radiodurans Facilitates Gamma-Radiation Resistance. *Science*, *306*(5698), 1025–1028. https://doi.org/10.1126/science.1103185

Damoglou, A. P., & Dawes, E. A. (1968). Studies on the lipid content and phosphate requirement of glucose-and acetate-grown Escherichia coli. *The Biochemical Journal*, *110*(4), 775–781. https://doi.org/10.1042/bj1100775

Davies, S. L., & Whittenbury, R. (1970). Fine structure of methane and other hydrocarbon-utilizing bacteria. *Journal of General Microbiology*, *61*(2), 227–232. https://doi.org/10.1099/00221287-61-2-227

Ding, Y. H. R., Hixson, K. K., Aklujkar, M. A., Lipton, M. S., Smith, R. D., Lovley, D. R., & Mester, T. (2008). Proteome of Geobacter sulfurreducens grown with Fe(III) oxide or Fe(III) citrate as the electron acceptor. *Biochimica et Biophysica Acta - Proteins and Proteomics*, *1784*(12), 1935–1941. https://doi.org/10.1016/j.bbapap.2008.06.011

DuBois, M., Gilles, K. A., Hamilton, J. K., Rebers, P. A., & Smith, F. (1956). Colorimetric Method for Determination of Sugars and Related Substances. *Analytical Chemistry*, *28*(3), 350–356. https://doi.org/10.1021/ac60111a017

Ducret, A., Quardokus, E. M., & Brun, Y. V. (2016). MicrobeJ, a tool for high throughput bacterial cell detection and quantitative analysis. *Nature Microbiology*, *1*(7), 1–7. https://doi.org/10.1038/nmicrobiol.2016.77

Dulay, H., Tabares, M., Kashefi, K., & Reguera, G. (2020). Cobalt Resistance via Detoxification and Mineralization in the Iron-Reducing Bacterium Geobacter sulfurreducens. *Frontiers in Microbiology*, *11*(November), 1–17. https://doi.org/10.3389/fmicb.2020.600463

Esteve-Núñez, A., Núñez, C., & Lovley, D. R. (2004). Preferential Reduction of Fe(III) over Fumarate by Geobacter sulfurreducens. *Journal of Bacteriology*, *186*(9), 2897–2899. https://doi.org/10.1128/JB.186.9.2897-2899.2004

Estevez-Canales, M., Kuzume, A., Borjas, Z., Füeg, M., Lovley, D., Wandlowski, T., & Esteve-Núñez, A. (2015). A severe reduction in the cytochrome C content of Geobacter sulfurreducens eliminates its capacity for extracellular electron transfer. *Environmental Microbiology Reports*, *7*(2), 219–226. https://doi.org/10.1111/1758-2229.12230

Fagan, R. P., & Fairweather, N. F. (2014). Biogenesis and functions of bacterial S-layers. *Nature Reviews Microbiology*, *12*(3), 211–222. https://doi.org/10.1038/nrmicro3213

Fassel, T. A., Buchholz, L. A., Collins, M. L. P., & Remsen, C. C. (1992). Localization of methanol dehydrogenase in two strains of methylotrophic bacteria detected by immunogold labeling. *Applied and Environmental Microbiology*, *58*(7), 2302–2307. https://doi.org/10.1128/aem.58.7.2302-2307.1992

Faustino, M. M., Fonseca, B. M., Costa, N. L., Lousa, D., Louro, R. O., & Paquete, C. M. (2021). Crossing the wall: Characterization of the multiheme cytochromes involved in the extracellular electron transfer pathway of Thermincola ferriacetica. *Microorganisms*, *9*(2), 1–14. https://doi.org/10.3390/microorganisms9020293

Fiencke, C., & Bock, E. (2006). Immunocytochemical localization of membrane-bound ammonia monooxygenase in cells of ammonia oxidizing bacteria. *Archives of Microbiology*, *185*(2), 99–106. https://doi.org/10.1007/s00203-005-0074-4

Folch, J., Lees, M., & Sloane Stanley, G. H. (1957). A simple method for the isolation and purification of total lipides from animal tissues. *The Journal of Biological Chemistry*, *226*(1), 497–509. https://doi.org/10.1016/s0021-9258(18)64849-5

Gao, Y., Sun, D., Wang, H., Lu, L., Ma, H., Wang, L., Ren, Z. J., Liang, P., Zhang, X., Chen, X., & Huang, X. (2018). Urine-powered synergy of nutrient recovery and urine purification in a microbial electrochemical system. *Environmental Science: Water Research and Technology*, *4*(10), 1427–1438. https://doi.org/10.1039/c8ew00306h

Gong, Y., Werth, C. J., He, Y., Su, Y., Zhang, Y., & Zhou, X. (2018). Intracellular versus extracellular accumulation of Hexavalent chromium reduction products by Geobacter sulfurreducens PCA. *Environmental Pollution*, *240*, 485–492. https://doi.org/10.1016/j.envpol.2018.04.046

Greening, C., & Lithgow, T. (2020). Formation and function of bacterial organelles. *Nature Reviews Microbiology*, *18*(12), 677–689. https://doi.org/10.1038/s41579-020-0413-0

Greenspan, P., Mayer, E. P., & Fowler, S. D. (1985). Nile red: A selective fluorescent

stain for intracellular lipid droplets. *Journal of Cell Biology*, *100*(3), 965–973. https://doi.org/10.1083/jcb.100.3.965

Hagen, W. J. H., Wan, W., & Briggs, J. A. G. (2017). Implementation of a cryo-electron tomography tilt-scheme optimized for high resolution subtomogram averaging. *Journal of Structural Biology*, *197*(2), 191–198. https://doi.org/10.1016/j.jsb.2016.06.007

Hartmann, A., & Braun, V. (1981). Iron uptake and iron limited growth of Escherichia coli K-12. *Archives of Microbiology*, *130*(5), 353–356. https://doi.org/10.1007/BF00414599

He, X., Chadwick, G., Jiménez Otero, F., Orphan, V., & Meile, C. (2021). Spatially Resolved Electron Transport through Anode-Respiring Geobacter sulfurreducens Biofilms: Controls and Constraints. *ChemElectroChem*, 1–13. https://doi.org/10.1002/celc.202100111

Hernández-Eligio, A., Pat-Espadas, A. M., Vega-Alvarado, L., Huerta-Amparán, M., Cervantes, F. J., & Juárez, K. (2020). Global transcriptional analysis of Geobacter sulfurreducens under palladium reducing conditions reveals new key cytochromes involved. *Applied Microbiology and Biotechnology*, *104*(9), 4059–4069. https://doi.org/10.1007/s00253-020-10502-5

Holmes, D. E., Chaudhuri, S. K., Nevin, K. P., Mehta, T., Methé, B. A., Liu, A., Ward, J. E., Woodard, T. L., Webster, J., & Lovley, D. R. (2006). Microarray and genetic analysis of electron transfer to electrodes in Geobacter sulfurreducens. *Environmental Microbiology*, *8*(10), 1805–1815. https://doi.org/10.1111/j.1462-2920.2006.01065.x

Holmes, D. E., Mester, T., O'Neil, R. A., Perpetua, L. A., Larrahondo, M. J., Glaven, R., Sharma, M. L., Ward, J. E., Nevin, K. P., & Lovley, D. R. (2008). Genes for two multicopper proteins required for Fe(III) oxide reduction in Geobacter sulfurreducens have different expression patterns both in the subsurface and on energy-harvesting electrodes. *Microbiology*, *154*(5), 1422–1435. https://doi.org/10.1099/mic.0.2007/014365-0

Howley, E., Ki, D., Krajmalnik-brown, R., & Torres, C. I. (2022). Geobacter sulfurreducens ' unique metabolism results in cells with a high iron and lipid content. *BioarXiv*, *2*, 1–28.

Howley, E., Krajmalnik-Brown, R., & Torres, C. I. (2022). Cytochrome expression shifts in Geobacter sulfurreducens to maximize energy conservation in response to changes in redox conditions. *BioarXiv*, 1–34.

Inoue, K., Qian, X., Morgado, L., Kim, B., Izallalen, M., Salgueiro, C. A., & Lovley, D. R. (2010). *Purification and Characterization of OmcZ , an Outer-Surface , Octaheme c -Type Cytochrome Essential for Optimal Current Production by*

Geobacter sulfurreducens □ *†*. *76*(12), 3999–4007. https://doi.org/10.1128/AEM.00027-10

Jiménez Otero, F., Chadwick, G. L., Yates, M. D., Mickol, R. L., Saunders, S. H., Glaven, S. M., Gralnick, J. A., Newman, D. K., Tender, L. M., Orphan, V. J., & Bond, D. R. (2021). Evidence of a Streamlined Extracellular Electron Transfer Pathway from Biofilm Structure, Metabolic Stratification, and Long-Range Electron Transfer Parameters. *Applied and Environmental Microbiology*, *87*(17). https://doi.org/10.1128/aem.00706-21

Joshi, K., Chan, C. H., & Bond, D. R. (2021). Geobacter sulfurreducens inner membrane cytochrome CbcBA controls electron transfer and growth yield near the energetic limit of respiration. *Molecular Microbiology*, *116*(4), 1124–1139. https://doi.org/https://doi.org/10.1111/mmi.14801

Kassner, R. J., & Kamen, M. D. (1968). Trace Metal Composition of Photosynthetic Bacteria. *Biochimica et Biophysica Acta*, *153*, 270–278.

Kato Marcus, A., Torres, C. I., Rittmann, B. E., & Andrew Kato Marcus, Cesar I. Torres, B. E. R. (2007). Conduction-based modeling of the biofilm anode of a microbial fuel cell. *Biotechnology and Bioengineering*, *98*(6), 1171–1182. https://doi.org/10.1002/bit.21533

Kim, B. C., Leang, C., Ding, Y. H. R., Glaven, R. H., Coppi, M. V., & Lovley, D. R. (2005). OmcF , a Putative c -Type Monoheme Outer Membrane Cytochrome Required for the Expression of Other Outer Membrane Cytochromes in Geobacter sulfurreducens. *Journal of Bacteriology*, *187*(13), 4505–4513. https://doi.org/10.1128/JB.187.13.4505

Kimber, R. L., Bagshaw, H., Smith, K., Buchanan, D. M., Coker, V. S., Cavet, J. S., & Lloyd, J. R. (2020). Biomineralization of Cu2S Nanoparticles by Geobacter sulfurreducens. *Applied and Environmental Microbiology*, *86*(18), 1–11.

Lancaster, W. A., Menon, A. L., Scott, I., Poole, F. L., Vaccaro, B. J., Thorgersen, M. P., Geller, J., Hazen, T. C., Hurt, R. A., Brown, S. D., Elias, D. A., & Adams, M. W. W. (2014). Metallomics of two microorganisms relevant to heavy metal bioremediation reveal fundamental differences in metal assimilation and utilization. *Metallomics*, *6*(5), 1004–1013. https://doi.org/10.1039/c4mt00050a

Langmead, B., & Salzberg, S. L. (2012). Fast gapped-read alignment with Bowtie 2. *Nature Methods*, *9*(4), 357–359. https://doi.org/10.1038/nmeth.1923

Leang, C., Adams, L. A., Chin, K. J., Nevin, K. P., Methé, B. A., Webster, J., Sharma, M. L., & Lovley, D. R. (2005). Adaptation to disruption of the electron transfer pathway for Fe(III) reduction in Geobacter sulfurreducens. *Journal of Bacteriology*, *187*(17), 5918–5926. https://doi.org/10.1128/JB.187.17.5918-5926.2005

Lee, S., Jeon, E., Yun, H. S., & Lee, J. (2011). Improvement of fatty acid biosynthesis by engineered recombinant Escherichia coli. *Biotechnology and Bioprocess Engineering*, *16*(4), 706–713. https://doi.org/10.1007/s12257-011-0034-6

Levar, C. E., Chan, C. H., Mehta-kolte, M. G., & Bond, D. R. (2014). An Inner Membrane Cytochrome Required Only for Reduction of. *MBio*, *5*(6), 02034–14. https://doi.org/10.1128/mBio.02034-14.Editor

Levar, C. E., Chan, C. H., Mehta-Kolte, M. G., & Bond, D. R. (2014). An inner membrane cytochrome required only for reduction of high redox potential extracellular electron acceptors. *MBio*, *5*(6), 1–9. https://doi.org/10.1128/mBio.02034-14

Levar, C. E., Hoffman, C. L., Dunshee, A. J., Toner, B. M., & Bond, D. R. (2017). *Redox potential as a master variable controlling pathways of metal reduction by Geobacter sulfurreducens*. *11*(3), 741–752. https://doi.org/10.1038/ismej.2016.146

Li, H., Handsaker, B., Wysoker, A., Fennell, T., Ruan, J., Homer, N., Marth, G., Abecasis, G., & Durbin, R. (2009). The Sequence Alignment/Map format and SAMtools. *Bioinformatics*, *25*(16), 2078–2079. https://doi.org/10.1093/bioinformatics/btp352

Liu, Y., Fredrickson, J. K., Zachara, J. M., & Shi, L. (2015). Direct involvement of ombB, omaB, and omcB genes in extracellular reduction of Fe(III) by Geobacter sulfurreducens PCA. *Frontiers in Microbiology*, *6*(OCT), 1–8. https://doi.org/10.3389/fmicb.2015.01075

Lloyd, J. R., Leang, C., Hodges Myerson, A. L., Coppi, M. V., Cuifo, S., Methe, B., Sandler, S. J., & Lovley, D. R. (2003). Biochemical and genetic characterization of PpcA, a periplasmic c-type cytochrome in Geobacter sulfurreducens. *Biochemical Journal*, *369*(1), 153–161. https://doi.org/10.1042/BJ20020597

Loferer-Krößbacher, M., Klima, J., & Psenner, R. (1998). Determination of Bacterial Cell Dry Mass by Transmission Electron Microscopy and Densitometric Image Analysis. *Applied and Environmental Microbiology*, *64*(2), 688–694. https://doi.org/10.1128/AEM.64.2.688-694.1998

Love, M. I., Huber, W., & Anders, S. (2014). Moderated estimation of fold change and dispersion for RNA-seq data with DESeq2. *Genome Biology*, *15*(12), 1–21. https://doi.org/10.1186/s13059-014-0550-8

Lovley, D. R., Ueki, T., Zhang, T., Malvankar, N. S., Shrestha, P. M., Flanagan, K. A., Aklujkar, M., Butler, J. E., Giloteaux, L., Rotaru, A. E., Holmes, D. E., Franks, A. E., Orellana, R., Risso, C., & Nevin, K. P. (2011). Geobacter. The Microbe Electric's Physiology, Ecology, and Practical Applications. In *Advances in Microbial Physiology* (1st ed., Vol. 59). Elsevier Ltd. https://doi.org/10.1016/B978-0-12-387661-4.00004-5

Geobacter Protein Nanowires, 10 Frontiers in Microbiology (2019). https://doi.org/10.3389/fmicb.2019.02078

Lusk, B. G., Peraza, I., Albal, G., Marcus, A. K., Popat, S. C., & Torres, C. I. (2018). PH Dependency in Anode Biofilms of Thermincola ferriacetica Suggests a Proton-Dependent Electrochemical Response. *Journal of the American Chemical Society*, *140*(16), 5527–5534. https://doi.org/10.1021/jacs.8b01734

Ma, C., Wen, H., Xing, D., Pei, X., Zhu, J., Ren, N., & Liu, B. (2017). Molasses wastewater treatment and lipid production at low temperature conditions by a microalgal mutant Scenedesmus sp. Z-4. *Biotechnology for Biofuels*, *10*(1), 1–13. https://doi.org/10.1186/s13068-017-0797-x

Ma, J. F., Ochsner, U. A., Klotz, M. G., Nanayakkara, V. K., Howell, M. L., Johnson, Z., Posey, J. E., Vasil, M. L., Monaco, J. J., & Hassett, D. J. (1999). Bacterioferritin A modulates catalase A (KatA) activity and resistance to hydrogen peroxide in Pseudomonas aeruginosa. *Journal of Bacteriology*, *181*(12), 3730–3742. https://doi.org/10.1128/jb.181.12.3730-3742.1999

Mahadevan, R., Bond, D. R., Butler, J. E., & Coppi, M. V. (2006). Characterization of Metabolism in the Fe (III) -Reducing Organism Geobacter sulfurreducens by Constraint-Based Modeling. *Applied and Environmental Microbiology*, *72*(2), 1558–1568. https://doi.org/10.1128/AEM.72.2.1558

Malvankar, N. S., Vargas, M., Nevin, K. P., Franks, A. E., Leang, C., Kim, B. C., Inoue, K., Mester, T., Covalla, S. F., Johnson, J. P., Rotello, V. M., Tuominen, M. T., & Lovley, D. R. (2011). Tunable metallic-like conductivity in microbial nanowire networks. *Nature Nanotechnology*, *6*(9), 573–579. https://doi.org/10.1038/nnano.2011.119

Mastronarde, D. N., & Held, S. R. (2017). Automated tilt series alignment and tomographic reconstruction in IMOD. *Journal of Structural Biology*, *197*(2), 102–113. https://doi.org/10.1016/j.jsb.2016.07.011

McCarty, P. L., & Rittmann, B. E. (2001). *Environmental biotechnology: principles and applications* [Book]. McGraw-Hill.

Mehta, T., Coppi, M. V., Childers, S. E., & Lovley, D. R. (2005). Outer Membrane c-Type Cytochromes Required for Fe(III) and Mn(IV) Oxide Reduction in Geobacter sulfurreducens. *Microbiology*, *71*(12), 8634–8641. https://doi.org/10.1128/AEM.71.12.8634

Morgado, L., Brulx, M., Pessanha, M., Londer, Y. Y., & Salgueiro, C. A. (2010). Thermodynamic characterization of a triheme cytochrome family From Geobacter sulfurreducens reveals mechanistic And functional diversity. *Biophysical Journal*, *99*(1), 293–301. https://doi.org/10.1016/j.bpj.2010.04.017

Murray, R. G., & Watson, S. W. (1965). Structure of Nitrosocystis Oceanus and Comparison With Nitrosomonas and Nitrobacter. *Journal of Bacteriology*, *89*(6), 1594–1609. https://doi.org/10.1128/jb.89.6.1594-1609.1965

Neidhart, F. C., Ingraham, J. L., & Schaechter, M. (1990). *Physiology of the Bacterial Cell: A Molecular Approach*. Sinauer Associates.

Nevin, K. P., Kim, B. C., Glaven, R. H., Johnson, J. P., Woodward, T. L., Methé, B. A., Didonato, R. J., Covalla, S. F., Franks, A. E., Liu, A., & Lovley, D. R. (2009). Anode biofilm transcriptomics reveals outer surface components essential for high density current production in Geobacter sulfurreducens fuel cells. *PLoS ONE*, *4*(5). https://doi.org/10.1371/journal.pone.0005628

Orsetti, S., Laskov, C., & Haderlein, S. B. (2013). Electron transfer between iron minerals and quinones: Estimating the reduction potential of the Fe(II)-goethite surface from AQDS speciation. *Environmental Science and Technology*, *47*(24), 14161–14168. https://doi.org/10.1021/es403658g

Otero, F. J., Chadwick, G. L., Yates, M. D., Mickol, R. L., Saunders, S. H., Glaven, S. M., Gralnick, J. A., Newman, D. K., Tender, L. M., Orphan, V. J., Bond, D. R., Jiménez Otero, F., Chadwick, G. L., Yates, M. D., Mickol, R. L., Saunders, S. H., Glaven, S. M., Gralnick, J. A., Newman, D. K., … Bond, D. R. (2021). Evidence of a Streamlined Extracellular Electron Transfer Pathway from Biofilm Structure, Metabolic Stratification, and Long-Range Electron Transfer Parameters. *Applied and Environmental Microbiology*, *87*(17), 1–16. https://doi.org/10.1128/AEM.00706-21

Otero, F. J., Chi Ho Chan, D. R. B., Jiménez Otero, F., Chan, C. H., & Bond, D. R. (2018). Identification of Different Putative Outer Membrane Electron Conduits Necessary for Fe(III) Citrate, Fe(III) Oxide, Mn(IV) Oxide, or Electrode Reduction by Geobacter sulfurreducens. *Journal of Bacteriology*, *200*(19), 1–20. https://doi.org/10.1128/JB.00347-18

Parameswaran, P., Bry, T., Popat, S. C., Lusk, B. G., Rittmann, B. E., & Torres, C. I. (2013). Kinetic, electrochemical, and microscopic characterization of the thermophilic, anode-respiring bacterium Thermincola ferriacetica. *Environmental Science and Technology*, *47*(9), 4934–4940. https://doi.org/10.1021/es400321c

Pat-Espadas, A. M., Razo-Flores, E., Rangel-Mendez, J. R., & Cervantes, F. J. (2013). Reduction of palladium and production of nano-catalyst by Geobacter sulfurreducens. *Applied Microbiology and Biotechnology*, *97*(21), 9553–9560. https://doi.org/10.1007/s00253-012-4640-9

Patt, T. E., & Hanson, R. S. (1978). Intracytoplasmic membrane, phospholipid, and sterol content of Methylobacterium organophilum cells grown under different conditions. *Journal of Bacteriology*, *134*(2), 636–644. https://doi.org/10.1128/jb.134.2.636-644.1978

Peng, L., Zhang, X., Yin, J., Xu, S., Zhang, Y., & Xie, D. (2016). Geobacter sulfurreducens adapts to low electrode potential for extracellular electron transfer. *Electrochimica Acta*, *191*, 743–749. https://doi.org/10.1016/j.electacta.2016.01.033

Peng, L., & Zhang, Y. (2017). Cytochrome OmcZ is essential for the current generation by Geobacter sulfurreducens under low electrode potential. *Electrochimica Acta*, *228*, 447–452. https://doi.org/10.1016/j.electacta.2017.01.091

Pessanha, M., Morgado, L., Louro, R. O., Londer, Y. Y., Pokkuluri, P. R., Schiffer, M., & Salgueiro, C. A. (2006). Thermodynamic Characterization of Triheme Cytochrome PpcA from Geobacter sulfurreducens : Evidence for a Role Played in e - / H + Energy Transduction. *Biochemistry*, *45*, 13910–13917.

Pettersen, E. F., Goddard, T. D., Huang, C. C., Meng, E. C., Couch, G. S., Croll, T. I., Morris, J. H., & Ferrin, T. E. (2021). UCSF ChimeraX: Structure visualization for researchers, educators, and developers. *Protein Science*, *30*(1), 70–82. https://doi.org/10.1002/pro.3943

Piligaev, A. V., Sorokina, K. N., Shashkov, M. V., & Parmon, V. N. (2018). Screening and comparative metabolic profiling of high lipid content microalgae strains for application in wastewater treatment. *Bioresource Technology*, *250*(November 2017), 538–547. https://doi.org/10.1016/j.biortech.2017.11.063

Pinchuk, G. E., Hill, E. A., Geydebrekht, O. V., de Ingeniis, J., Zhang, X., Osterman, A., Scott, J. H., Reed, S. B., Romine, M. F., Konopka, A. E., Beliaev, A. S., Fredrickson, J. K., & Reed, J. L. (2010). Constraint-based model of Shewanella oneidensis MR-1 metabolism: A tool for data analysis and hypothesis generation. *PLoS Computational Biology*, *6*(6), 1–8. https://doi.org/10.1371/journal.pcbi.1000822

Pirbadian, S., Barchinger, S. E., Leung, K. M., Byun, H. S., Jangir, Y., Bouhenni, R. A., Reed, S. B., Romine, M. F., Saffarini, D. A., Shi, L., Gorby, Y. A., Golbeck, J. H., & El-Naggar, M. Y. (2014). Shewanella oneidensis MR-1 nanowires are outer membrane and periplasmic extensions of the extracellular electron transport components. *Proceedings of the National Academy of Sciences of the United States of America*, *111*(35), 12883–12888. https://doi.org/10.1073/pnas.1410551111

Pokkuluri, P. R., Londer, Y. Y., Duke, N. E. C., Pessanha, M., Yang, X., Orshonsky, V., Orshonsky, L., Erickson, J., Zagyanskiy, Y., Salgueiro, C. A., & Schiffer, M. (2011). Structure of a novel dodecaheme cytochrome c from Geobacter sulfurreducens reveals an extended 12nm protein with interacting hemes. *Journal of Structural Biology*, *174*(1), 223–233. https://doi.org/10.1016/j.jsb.2010.11.022

Popat, S. C., & Torres, C. I. (2016). Critical transport rates that limit the performance of microbial electrochemistry technologies. *Bioresource Technology*, *215*, 265–273. https://doi.org/10.1016/j.biortech.2016.04.136

Ragsdale, S. W., & Pierce, E. (2008). Acetogenesis and the Wood–Ljungdahl pathway of CO2 fixation. *Biochimica et Biophysica Acta (BBA) - Proteins and Proteomics*, *1784*(12), 1873–1898. https://doi.org/10.1016/j.bbapap.2008.08.012

Reguera, G., Nevin, K. P., Nicoll, J. S., Covalla, S. F., Woodard, T. L., & Lovley, D. R. (2006). Biofilm and nanowire production leads to increased current in Geobacter sulfurreducens fuel cells. *Applied and Environmental Microbiology*, *72*(11), 7345–7348. https://doi.org/10.1128/AEM.01444-06

Richter, H., Nevin, K. P., Jia, H., Lowy, D. A., Lovley, D. R., & Tender, L. M. (2009). Cyclic voltammetry of biofilms of wild type and mutant Geobacter sulfurreducens on fuel cell anodes indicates possible roles of OmcB, OmcZ, type IV pili, and protons in extracellular electron transfer. *Energy and Environmental Science*, *2*(5), 506–516. https://doi.org/10.1039/b816647a

Rollefson, J. B., Stephen, C. S., Tien, M., & Bond, D. R. (2011). Identification of an extracellular polysaccharide network essential for cytochrome anchoring and biofilm formation in Geobacter sulfurreducens. *Journal of Bacteriology*, *193*(5), 1023–1033. https://doi.org/10.1128/JB.01092-10

Rouf, M. A. (1964). Spectrochemical Analysis of Inorganic Elements in Bacteria. *Journal of Bacteriology*, *88*(1963), 1545–1549. https://doi.org/10.1128/jb.88.6.1545-1549.1964

Salgueiro, C. A., Morgado, L., Silva, M. A., Ferreira, M. R., Fernandes, T. M., & Portela, P. C. (2022). From iron to bacterial electroconductive filaments: Exploring cytochrome diversity using Geobacter bacteria. *Coordination Chemistry Reviews*, *452*, 214284. https://doi.org/10.1016/j.ccr.2021.214284

Santos, T. C., Silva, M. A., Morgado, L., Dantas, J. M., & Salgueiro, C. A. (2015). Diving into the redox properties of Geobacter sulfurreducens cytochromes: A model for extracellular electron transfer. *Dalton Transactions*, *44*(20), 9335–9344. https://doi.org/10.1039/c5dt00556f

Schmidt, I., Zart, D., & Bock, E. (2001). Effects of gaseous NO2 on cells of Nitrosomonas eutropha previously incapable of using ammonia as an energy source. *Antonie van Leeuwenhoek, International Journal of General and Molecular Microbiology*, *79*(1), 39–47. https://doi.org/10.1023/A:1010269331350

Seufferheld, M., Vieira, M. C. F., Ruiz, F. A., Rodrigues, C. O., Moreno, S. N. J., & Docampo, R. (2003). Identification of organelles in bacteria similar to acidocalcisomes of unicellular eukaryotes. *Journal of Biological Chemistry*, *278*(32), 29971–29978. https://doi.org/10.1074/jbc.M304548200

Shelobolina, E. S., Coppi, M. V., Korenevsky, A. A., DiDonato, L. N., Sullivan, S. A., Konishi, H., Xu, H., Leang, C., Butler, J. E., Kim, B. C., & Lovley, D. R. (2007). Importance of c-type cytochromes for U(VI) reduction by Geobacter sulfurreducens.

BMC Microbiology, *7*(Vi), 1–15. https://doi.org/10.1186/1471-2180-7-16

Shively, J. M. (2006). *Complex Intracellular Structures in Prokaryotes* (1st ed.). Springer Berlin Heidelberg. https://doi.org/https://doi.org/10.1007/11497158

Shively, J. M., Ball, F. L., & Kline, B. W. (1973). Electron microscopy of the carboxysomes (polyhedral bodies) of Thiobacillus neapolitanus. *Journal of Bacteriology*, *116*(3), 1405–1411. https://doi.org/10.1128/jb.116.3.1405-1411.1973

Silva, M. A., Portela, P. C., & Salgueiro, C. A. (2021). Rational design of electron/proton transfer mechanisms in the exoelectrogenic bacteria Geobacter sulfurreducens. *Biochemical Journal*, *478*(14), 2871–2887. https://doi.org/10.1042/BCJ20210365

Sluiter, A., Hames, B., Ruiz, R., Scarlata, C., Sluiter, J., Templeton, D., & Crocker, D. (2008). Determination of structural carbohydrates and lignin in Biomass. *National Renewable Energy Laboratory*, *April 2008*, 17. http://www.nrel.gov/docs/gen/fy13/42618.pdf

Snider, R. M., Strycharz-Glaven, S. M., Tsoi, S. D., Erickson, J. S., & Tender, L. M. (2012). Long-range electron transport in Geobacter sulfurreducens biofilms is redox gradient-driven. *Proceedings of the National Academy of Sciences*, *109*(38), 15467–15472. https://doi.org/10.1073/pnas.1209829109

Staehelin, L. A., Golecki, J. R., & Drews, G. (1980). SUPRAMOLECULAR ORGANIZATION OF CHLOROSOMES (CHLOROBIUM VESICLES) AND OF THEIR MEMBRANE ATTACHMENT SITES IN CHLOROBIUM LIMICOLA. *Biochimica et Biophysica Acta*, *589*, 30–45.

Stöckl, M., Teubner, N. C., Holtmann, D., Mangold, K. M., & Sand, W. (2019). Extracellular Polymeric Substances from Geobacter sulfurreducens Biofilms in Microbial Fuel Cells. *ACS Applied Materials and Interfaces*, *11*(9), 8961–8968. https://doi.org/10.1021/acsami.8b14340

Strous, M., Planet, E., Mechanics, T., America, M., Appl, P., Island, A., Islands, A., Init, O. D. P., Rica, C., Fuerst, J. A., Kramer, E. H. M., Logemann, S., Muyzer, G., van de Pas-Schoonen, K. T., Webb, R., Kuenen, J. G., & Jetten, M. S. M. (1999). Missing lithotroph identified as new planctomycete. *Nature*, *400*(July), 446. https://doi.org/10.1038/22749%0Ahttp://10.0.4.14/22749

Strycharz-Glaven, S. M., Snider, R. M., Guiseppi-Elie, A., & Tender, L. M. (2011). On the electrical conductivity of microbial nanowires and biofilms. *Energy and Environmental Science*, *4*(11), 4366–4379. https://doi.org/10.1039/c1ee01753e

Subramanian, P., Pirbadian, S., El-Naggar, M. Y., & Jensen, G. J. (2018). Ultrastructure of *Shewanella oneidensis* MR-1 nanowires revealed by electron cryotomography. *Proceedings of the National Academy of Sciences*, 201718810. https://doi.org/10.1073/pnas.1718810115

Torres, C. I. (2014). On the importance of identifying, characterizing, and predicting fundamental phenomena towards microbial electrochemistry applications. *Current Opinion in Biotechnology*, *27*, 107–114. https://doi.org/10.1016/j.copbio.2013.12.008

Torres, C. I. C. I., Marcus, A. K., & Rittmann, B. E. (2008). Proton transport inside the biofilm limits electrical current generation by anode-respiring bacteria. *Biotechnology and Bioengineering*, *100*(5), 872–881. https://doi.org/10.1002/bit.21821

Torres, C. I., Marcus, A. K., Lee, H. S., Parameswaran, P., Krajmalnik-Brown, R., & Rittmann, B. E. (2010). A kinetic perspective on extracellular electron transfer by anode-respiring bacteria. *FEMS Microbiology Reviews*, *34*(1), 3–17. https://doi.org/10.1111/j.1574-6976.2009.00191.x

Torres, C. I., Marcus, A. K., Parameswaram, P., & Rittmann, B. E. (2008). Kinetic Experiments for Evaluating the Nernst-Monod Model for Anode-Respiring Bacteria (ARB) in a Biofilm Anode. *Environmental Science & Technology*, *42*(17), 6593–6597. 10.1021/es800970w

Tremblay, P. L., & Lovley, D. R. (2012). Role of the NiFe hydrogenase hya in oxidative stress defense in Geobacter sulfurreducens. *Journal of Bacteriology*, *194*(9), 2248–2253. https://doi.org/10.1128/JB.00044-12

Tucker, J. D., Siebert, C. A., Escalante, M., Adams, P. G., Olsen, J. D., Otto, C., Stokes, D. L., & Hunter, C. N. (2010). Membrane invagination in Rhodobacter sphaeroides is initiated at curved regions of the cytoplasmic membrane, then forms both budded and fully detached spherical vesicles. *Molecular Microbiology*, *76*(4), 833–847. https://doi.org/10.1111/j.1365-2958.2010.07153.x

Ueki, T., & Lovley, D. R. (2009). Genome-wide gene regulation of biosynthesis and energy generation by a novel transcriptional repressor in Geobacter species. *Nucleic Acids Research*, *38*(3), 810–821. https://doi.org/10.1093/nar/gkp1085

von Meyenburg, K., Jørgensen, B. B., & van Deurs, B. (1984). Physiological and morphological effects of overproduction of membrane-bound ATP synthase in Escherichia coli K-12. *The EMBO Journal*, *3*(8), 1791–1797. https://doi.org/10.1002/j.1460-2075.1984.tb02047.x

Wahidin, S., Idris, A., & Shaleh, S. R. M. (2013). The influence of light intensity and photoperiod on the growth and lipid content of microalgae Nannochloropsis sp. *Bioresource Technology*, *129*, 7–11. https://doi.org/10.1016/j.biortech.2012.11.032

Wang, F., Coureuil, M., Osinski, T., Orlova, A., Altindal, T., Gesbert, G., Nassif, X., Egelman, E. H., & Craig, L. (2017). Cryoelectron Microscopy Reconstructions of the Pseudomonas aeruginosa and Neisseria gonorrhoeae Type IV Pili at Sub-nanometer Resolution. *Structure*, *25*(9), 1423-1435.e4.

https://doi.org/10.1016/j.str.2017.07.016

Wang, F., Gu, Y., O'Brien, J. P., Yi, S. M., Yalcin, S. E., Srikanth, V., Shen, C., Vu, D., Ing, N. L., Hochbaum, A. I., Egelman, E. H., Malvankar, N. S., O'Brien, J. P., Yi, S. M., Yalcin, S. E., Srikanth, V., Shen, C., Vu, D., Ing, N. L., … Malvankar, N. S. (2019). Structure of Microbial Nanowires Reveals Stacked Hemes that Transport Electrons over Micrometers. *Cell*, *177*(2), 361-369.e10. https://doi.org/10.1016/j.cell.2019.03.029

Wang, Q., Jones, A.-A. D., Gralnick, J. A., Lin, L., & Buie, C. R. (2019). Microfluidic dielectrophoresis illuminates the relationship between microbial cell envelope polarizability and electrochemical activity. *Science Advances*, *5*(1). https://doi.org/10.1126/sciadv.aat5664

Watson, S. (1971). Taxonomic Considerations of the Family Nitrobacteraceae Buchanan. *International Journal of Systematic Bacteriology*, *21*(3), 254–270. http://ijs.sgmjournals.org/content/21/3/254.full.pdf+html

Wei, J., Liang, P., Cao, X., & Huang, X. (2010). A new insight into potential regulation on growth and power generation of geobacter sulfurreducens in microbial fuel cells based on energy viewpoint. *Environmental Science and Technology*, *44*(8), 3187–3191. https://doi.org/10.1021/es903758m

Weiner, J. H., & Lemire, B. D. (1984). Overproduction of Fumarate Reductase in Escherichia. *Microbiology*, *158*(2), 590–596.

Whiddon, K. T., Gudneppanavar, R., Hammer, T. J., West, D. A., & Konopka, M. C. (2019). Fluorescence-based analysis of the intracytoplasmic membranes of type I methanotrophs. *Microbial Biotechnology*, *12*(5), 1024–1033. https://doi.org/10.1111/1751-7915.13458

WOLIN, E. A., WOLIN, M. J., & WOLFE, R. S. (1963). Formation of Methane By Bacterial Extracts. *The Journal of Biological Chemistry*, *238*(8), 2882–2886. https://doi.org/10.1016/s0021-9258(18)67912-8

Woronowicz, K., Harrold, J. W., Kay, J. M., & Niederman, R. A. (2013). Structural and functional proteomics of intracytoplasmic membrane assembly in Rhodobacter sphaeroides. *Journal of Molecular Microbiology and Biotechnology*, *23*(1–2), 48–62. https://doi.org/10.1159/000346520

Wrighton, K. C., Thrash, J. C., Melnyk, R. A., Bigi, J. P., Byrne-Bailey, K. G., Remis, J. P., Schichnes, D., Auer, M., Chang, C. J., & Coates, J. D. (2011). Evidence for direct electron transfer by a gram-positive bacterium isolated from a microbial fuel cell. *Applied and Environmental Microbiology*, *77*(21), 7633–7639. https://doi.org/10.1128/AEM.05365-11

Yalcin, S. E., O'Brien, J. P., Gu, Y., Reiss, K., Yi, S. M., Jain, R., Srikanth, V., Dahl, P.

J., Huynh, W., Vu, D., Acharya, A., Chaudhuri, S., Varga, T., Batista, V. S., & Malvankar, N. S. (2020). Electric field stimulates production of highly conductive microbial OmcZ nanowires. *Nature Chemical Biology*, *16*(10), 1136–1142. https://doi.org/10.1038/s41589-020-0623-9

Yan, J., Ritalahti, K. M., Wagner, D. D., & Löffler, F. E. (2012). Unexpected specificity of interspecies cobamide transfer from geobacter spp. to organohalide-respiring dehalococcoides mccartyi strains. *Applied and Environmental Microbiology*, *78*(18), 6630–6636. https://doi.org/10.1128/AEM.01535-12

Yates, M. D., Kiely, P. D., Call, D. F., Rismani-Yazdi, H., Bibby, K., Peccia, J., Regan, J. M., & Logan, B. E. (2012). Convergent development of anodic bacterial communities in microbial fuel cells. *ISME Journal*, *6*(11), 2002–2013. https://doi.org/10.1038/ismej.2012.42

Yates, M. D., Strycharz-Glaven, S. M., Golden, J. P., Roy, J., Tsoi, S., Erickson, J. S., El-Naggar, M. Y., Barton, S. C., & Tender, L. M. (2016). Measuring conductivity of living geobacter sulfurreducens biofilms. *Nature Nanotechnology*, *11*(11), 910–913. https://doi.org/10.1038/nnano.2016.186

Yoho, R. A., Popat, S. C., & Torres, C. I. (2014). Dynamic potential-dependent electron transport pathway shifts in anode biofilms of Geobacter sulfurreducens. *ChemSusChem*, *7*(12), 3413–3419. https://doi.org/10.1002/cssc.201402589

Zacharoff, L., Chan, C. H., & Bond, D. R. (2016). Reduction of low potential electron acceptors requires the CbcL inner membrane cytochrome of Geobacter sulfurreducens. *Bioelectrochemistry*, *107*, 7–13. https://doi.org/10.1016/j.bioelechem.2015.08.003

Zavarzina, D. G., Sokolova, T. G., Tourova, T. P., Chernyh, N. A., Kostrikina, N. A., & Bonch-Osmolovskaya, E. A. (2007). Thermincola ferriacetica sp. nov., a new anaerobic, thermophilic, facultatively chemolithoautotrophic bacterium capable of dissimilatory Fe(III) reduction. In *Extremophiles* (Vol. 11, Issue 1, pp. 1–7). https://doi.org/10.1007/s00792-006-0004-7

Zheng, S. Q., Palovcak, E., Armache, J.-P., Verba, K. A., Cheng, Y., & Agard, D. A. (2017). MotionCor2: anisotropic correction of beam-induced motion for improved cryo-electron microscopy. *Nature Methods*, *14*(4), 331–332. https://doi.org/10.1038/nmeth.4193

Zhu, X., Yates, M. D., & Logan, B. E. (2012). Set potential regulation reveals additional oxidation peaks of Geobacter sulfurreducens anodic biofilms. *Electrochemistry Communications*, *22*(1), 116–119. https://doi.org/10.1016/j.elecom.2012.06.013

APPENDIX A

SUPPLEMENTAL FIGURES AND TABLES

Table A.1 Multiheme cytochromes with significant differential expression and electrochemical data suggesting an association to one of the three eet pathways. These associations were inferred from the differential expression comparisons in Figure 2.3, and the electrochemical modeling in Table 2.1. I assume the fumarate samples exhibit primarily the high pathway due to the relatively high redox potential of the fumarate/succinate couple. ExtJ is not a multiheme c-type cytochrome, but I include it here due to its presence in the extHIJK cluster.

Gene		*Pathway*	*Location*	*Comparisons*
ppcB	*GSU0364*	*Low*	*Periplasmic*[c]	*Fig. 2.3D*
GSU1538	*GSU1538*	*Low*	*Periplasmic*[a]	*Fig. 2.3E, Fig. 2.3F*
ppcE	*GSU1760*	*Low*	*Periplasmic*[c]	*Fig. 2.3F*
GSU1996	*GSU1996*	*Low*	*Periplasmic*[b]	*Fig. 2.3D, Fig. 2.3F*
OmcM	*GSU2294*	*Low*	*unknown*	*Fig. 2.3B, Fig. 2.3F*
extC	*GSU2643*	*Low*	*Outer Membrane*[e]	*Fig. 2.3E, Fig. 2.3F*
extA	*GSU2645*	*Low*	*Periplasmic*[a]*/ OM*[e]	*Fig. 2.3E, Fig. 2.3F*
dhc1	*GSU2767*	*Low*	*Inner membrane*[a]	*Fig. 2.3D, Fig. 2.3F*
GSU2808	*GSU2808*	*Low*	*unknown*	*Fig. 2.3B, Fig. 2.3D, Fig. 2.3E, Fig. 2.3F*
GSU2887	*GSU2887*	*Low*	*Extracellular*[a]	*Fig. 2.3E, Fig. 2.3F*
GSU3615	*GSU3615*	*Low*	*Extracellular*[a]	*Fig. 2.3E, Fig. 2.3F*
cbcL	*GSU0274*	*Medium*	*inner membrane*[f]	*Fig. 2.3B, Fig. 2.3C*
omcQ	*GSU0592*	*Medium*	*Cytoplasmic*[a]	*Fig. 2.3E*

ppcA	*GSU0612*	*Medium*	*Periplasmic*[a]	*Fig. 2.3D*
omcX	*GSU0670*	*Medium*	*Periplasmic*[a]	*Fig. 2.3B, Fig. 2.3D, Fig. 2.3E*
omcJ	*GSU0701*	*Medium*	*unknown*	*Fig. 2.3E*
GSU0702	*GSU0702*	*Medium*	*Extracellular*[a]	*Fig. 2.3E, Fig. 2.3F*
frdC	*GSU1176*	*Medium*	*inner membrane*[a]	*Fig. 2.3B, Fig. 2.3D, Fig. 2.3E*
omcZ	*GSU2076*	*Medium*	*Extracellular*[d]	*Fig. 2.3D, Fig. 2.3E*
omcK	*GSU2203*	*Medium*	*Periplasmic*[a]	*Fig. 2.3E*
GSU2299	*GSU2299*	*Medium*	*Periplasmic*[a]	*Fig. 2.3B, Fig. 2.3E*
omcB	*GSU2737*	*Medium*	*unknown*	*Fig. 2.3B, Fig. 2.3C, Fig. 2.3D*
omcN	*GSU2898*	*Medium*	*Periplasmic*[a]	*Fig. 2.3B, Fig. 2.3C, Fig. 2.3D*
GSU2899	*GSU2899*	*Medium*	*Extracellular*[a]	*Fig. 2.3B, Fig. 2.3C*
extK	*GSU2937*	*Medium*	*Outer Membrane*[e]	*Fig. 2.3D, Fig. 2.3E*
extJ	*GSU2938*	*Medium*	*Outer Membrane*[e]	*Fig. 2.3D, Fig. 2.3E (not labeled)*
nrfA	*GSU3154*	*Medium*	*Periplasmic*[a]	*Fig. 2.3B, Fig. 2.3D, Fig. 2.3E*
nrfH	*GSU3155*	*Medium*	*Periplasmic*[a]	*Fig. 2.3B, Fig. 2.3D*
GSU3214	*GSU3214*	*Medium*	*unknown*	*Fig. 2.3D*

GSU3218	*GSU3218*	*Medium*	*Periplasmic*[a]	*Fig. 2.3A, Fig. 2.3D, Fig. 2.3E*
GSU3221	*GSU3221*	*Medium*	*unknown*	*Fig. 2.3E*
GSU3226	*GSU3226*	*Medium*	*unknown*	*Fig. 2.3E*
GSU3228	*GSU3228*	*Medium*	*unknown*	*Fig. 2.3B, Fig. 2.3D, Fig. 2.3E*
GSU3233	*GSU3233*	*Medium*	*Periplasmic*[a]	*Fig. 2.3E*
GSU702	*GSU702*	*Medium*	*Extracellular*[a]	*Fig. 2.3D, Fig. 2.3E Fig. 2.3F*
omcS	*GSU2504*	*High, Fumarate*	*Extracellular*[g]	*Fig. 2.3A, Fig. 2.3B, Fig. 2.3E, Fig. 2.3F*
omcT	*GSU2503*	*High, Fumarate*	*Periplasmic*[a]	*Fig. 2.3B, Fig. 2.3E, Fig. 2.3F*
GSU2501	*GSU2501*	*Fumarate*	*Periplasmic*[a]	*Fig. 2.3E, Fig. 2.3F*
extG	*GSU2724*	*Fumarate*	*Periplasmic*[e]	*Fig. 2.3E, Fig. 2.3F*
extF	*GSU2725*	*Fumarate*	*Outer Membrane*[e]	*Fig. 2.3F*

a: PSORTb v3.0, b: (Pokkuluri et al., 2011), c: (Morgado et al., 2010), d: (Inoue et al., 2010), e: (Jiménez Otero et al., 2021), f: (Zacharoff et al., 2016), g: (F. Wang et al., 2019)

Table A.2 Chemicals in Ringer's solution per L of medium used. One fourth strength of Ringer's solution was used for washing cells.

Chemical	Amount (g)	Concentration (mM)	¼ Strength Ringer's solution Conc. (mM)
NaCl	6.5	111	27.8
KCl	0.42	5.6	1.41
CaCl2	0.25	2.3	0.56
NaHCO3	0.2	2.4	0.6

Table A.3 Metal content in dry cell mass of *Geobacter sulfurreducens* PCA and *Escherichia coli* K-12 (unit: milligram of each metal per gram of dried bacterial cell, mg/gdw).

	G. sulfurreducens		***E. coli***	
	Anode	Fumarate	M9 medium	*Geobacter* medium
Ag	0.098 (± 0.073)	0.106 (± 0.034)	ND	ND
Ba	0.028 (± 0.002)	0.025 (± 0.003)	0.021 (± 0.005)	0.027 (± 0.003)
Co	0.028 (± 0.005)	0.021 (± 0.029)	ND	0.003 (± 0.002)
Cr	0.081 (± 0.016)	0.086 (± 0.014)	0.006 (± 0.003)	0.003 (± 0.000)
Cu	0.224 (± 0.086)	0.471 (± 0.107)	0.017 (± 0.005)	0.048 (± 0.010)
Fe	1.970 (± 0.226)	1.96 (± 0.229)	0.134 (± 0.053)	0.428(± 0.089)
Li	0.047 (± 0.030)	0.017 (± 0.001)	0.040 (± 0.003)	0.047 (± 0.006)
Mg	0.67 (± 0.27)	0.54 (± 0.11)	2.07 (± 0.75)	1.79 (± 0.38)
Mn	0.583 (± 0.076)	0.324 (± 0.067)	0.023 (± 0.021)	0.570 (± 0.122)
Ni	0.069 (± 0.012)	0.076 (± 0.012)	0.002 (± 0.003)	ND
Pb	0.036 (± 0.015)	0.023 (± 0.003)	0.018 (± 0.011)	0.016 (± 0.010)
Se	0.104 (± 0.058)	0.177 (± 0.112)	0.012 (± 0.005)	0.101 (± 0.016)
Sr	0.008 (± 0.002)	0.017 (± 0.006)	0.005 (± 0.003)	0.003 (± 0.001)
V	0.002 (± 0.001)	0.003 (± 0.002)	0.035 (± 0.006)	0.045 (± 0.005)
Zn	3.5 (± 1.9)	10.0 (± 2.4)	0.135 (± 0.034)	0.176 (± 0.024)

Table A.4 Estimated growth of *G. sulfurreducens* per L of medium at an anode based on the available mineral concentrations in Geobacter medium.

Metal	*Geobacter* Medium [mg element/L]	Average *G. sulfurreducens* content (mg element/g cell)	Estimated growth (g cells/L)
Mg	2.958	0.67	4.42
Mn	1.625	0.583	2.79
Fe	0.201	1.97	0.10
Co	0.248	0.028	8.80
Zn	0.624	3.5	0.18
Cu	0.025	0.224	0.11
Ni	0.059	0.069	0.86

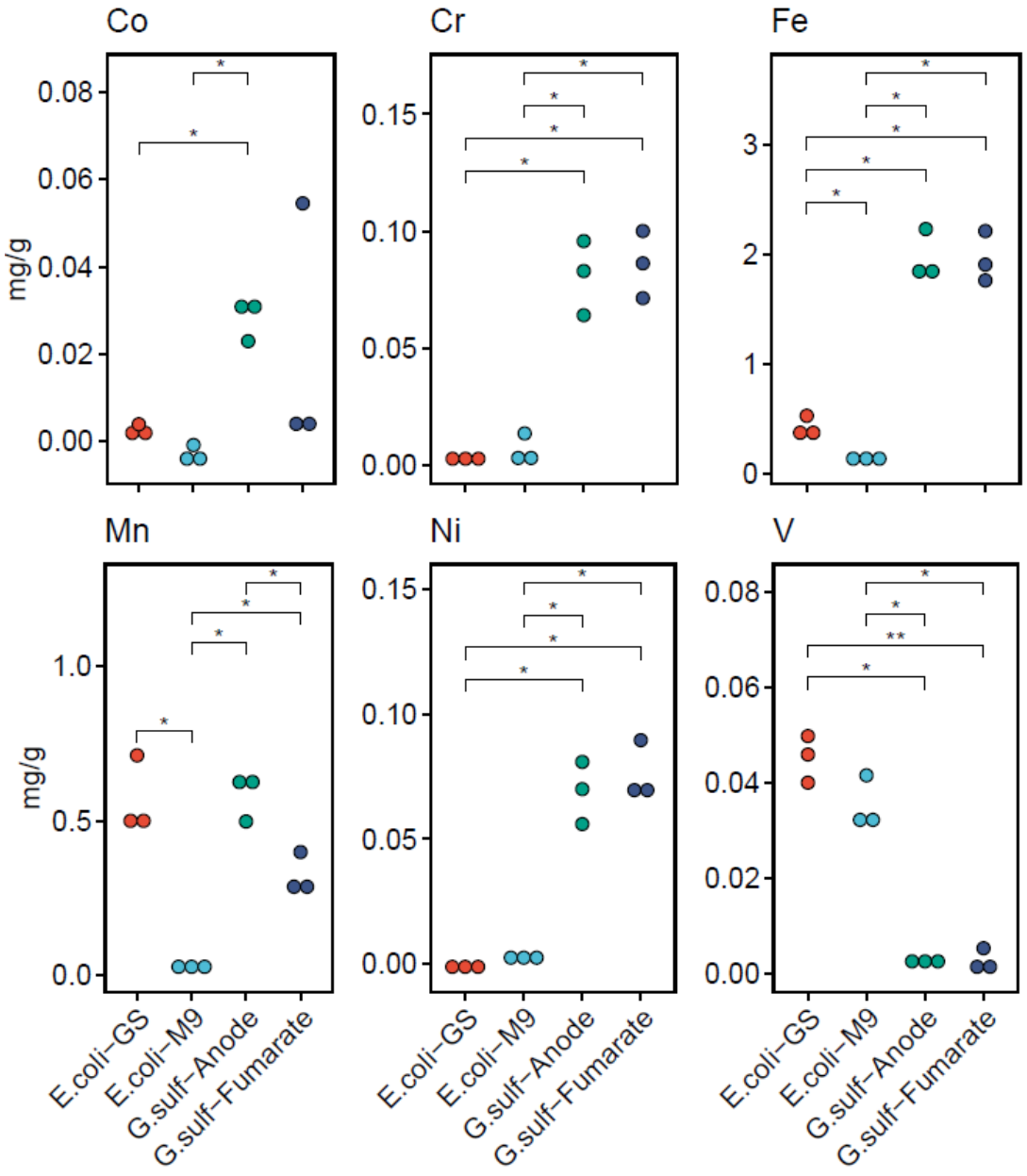

Figure A.1 Statistically significant differences in metal concentrations between *E. coli*-GS (Geobacter medium), *E. coli*-M9 (M9 medium), *G. sulf*-Anode (biofilm grown on an electrode), and *G. sulf*-Fumarate (planktonic cells using fumarate as the electron acceptor). *(p<0.05), **(p<0.001), pairwise t-test with multiple comparison correction performed with the Benjamini-Hochberg method. We chose to omit alkali metals from this figure, but Lithium did have significant differences as well (Table A.2).

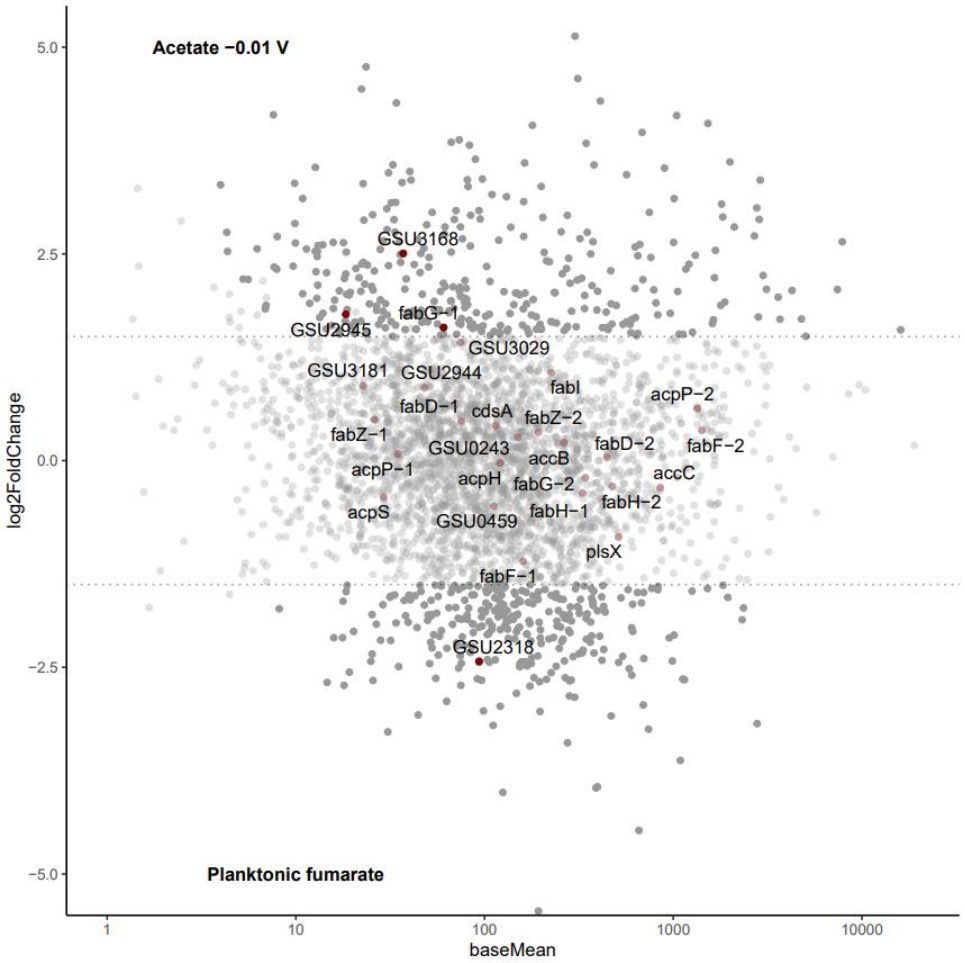

Figure A.2 MA plot with lipid synthesis pathway genes annotated. Dotted lines indicate $\log_2$ fold change of 1.5, and solid dots indicate an adjusted p value under 0.05.

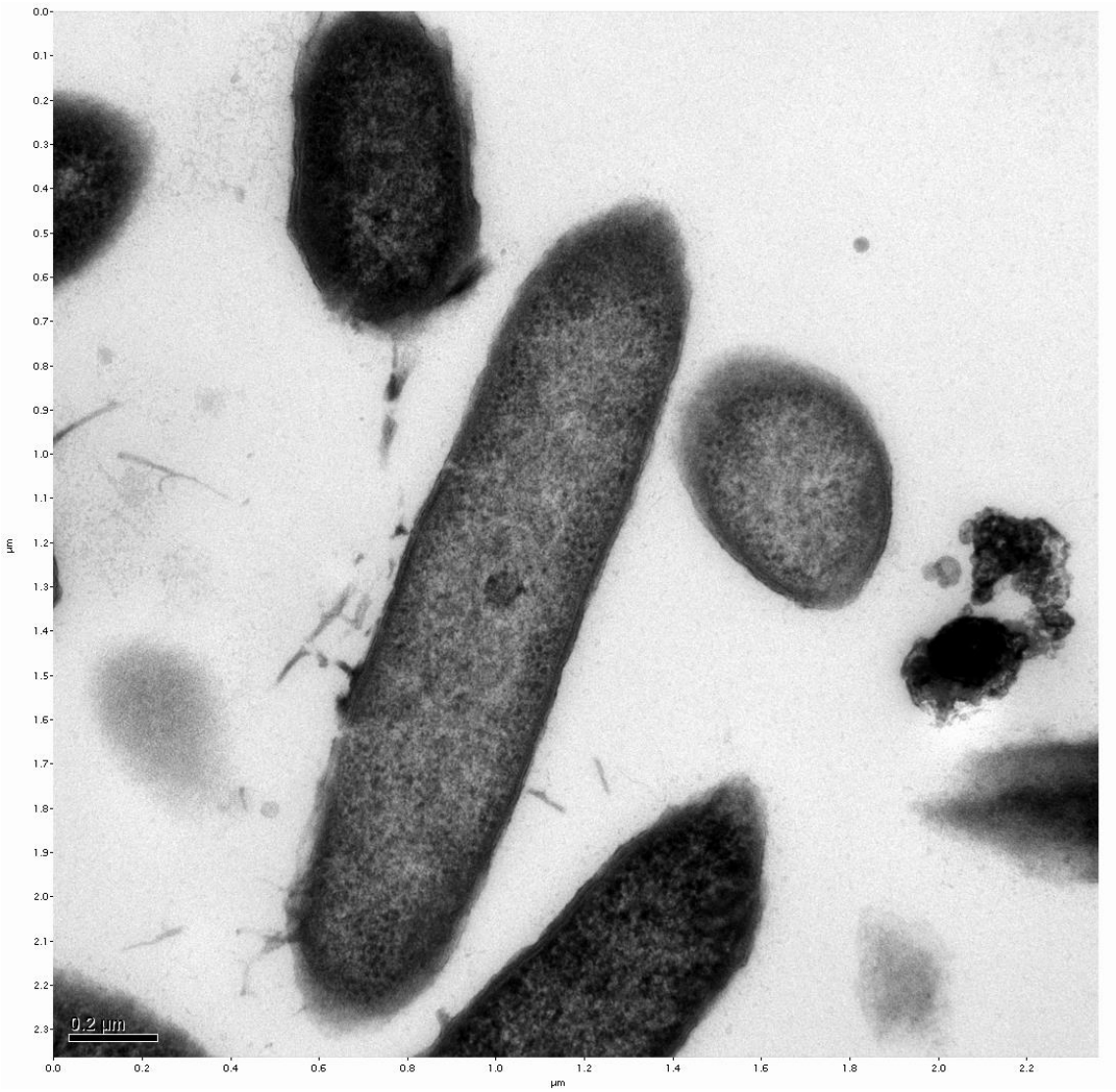

Figure A.3 Conventional thin section TEM micrograph of *G. sulfurreducens* cells grown using fumarate as the electron acceptor. No ICM was observed.

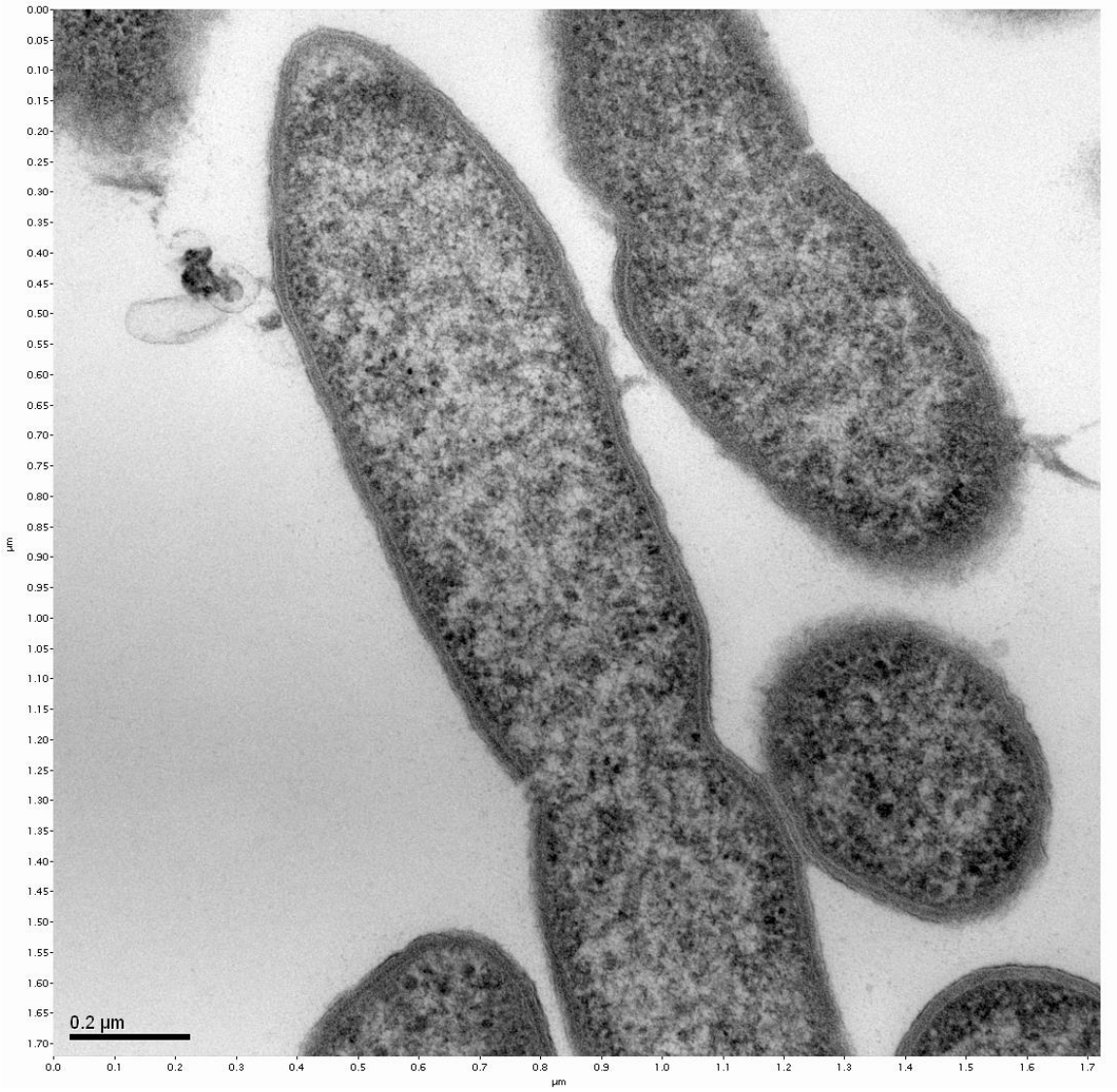

Figure A.4 Conventional thin section TEM micrograph of *G. sulfurreducens* cells grown using fumarate as the electron acceptor. No ICM was observed.

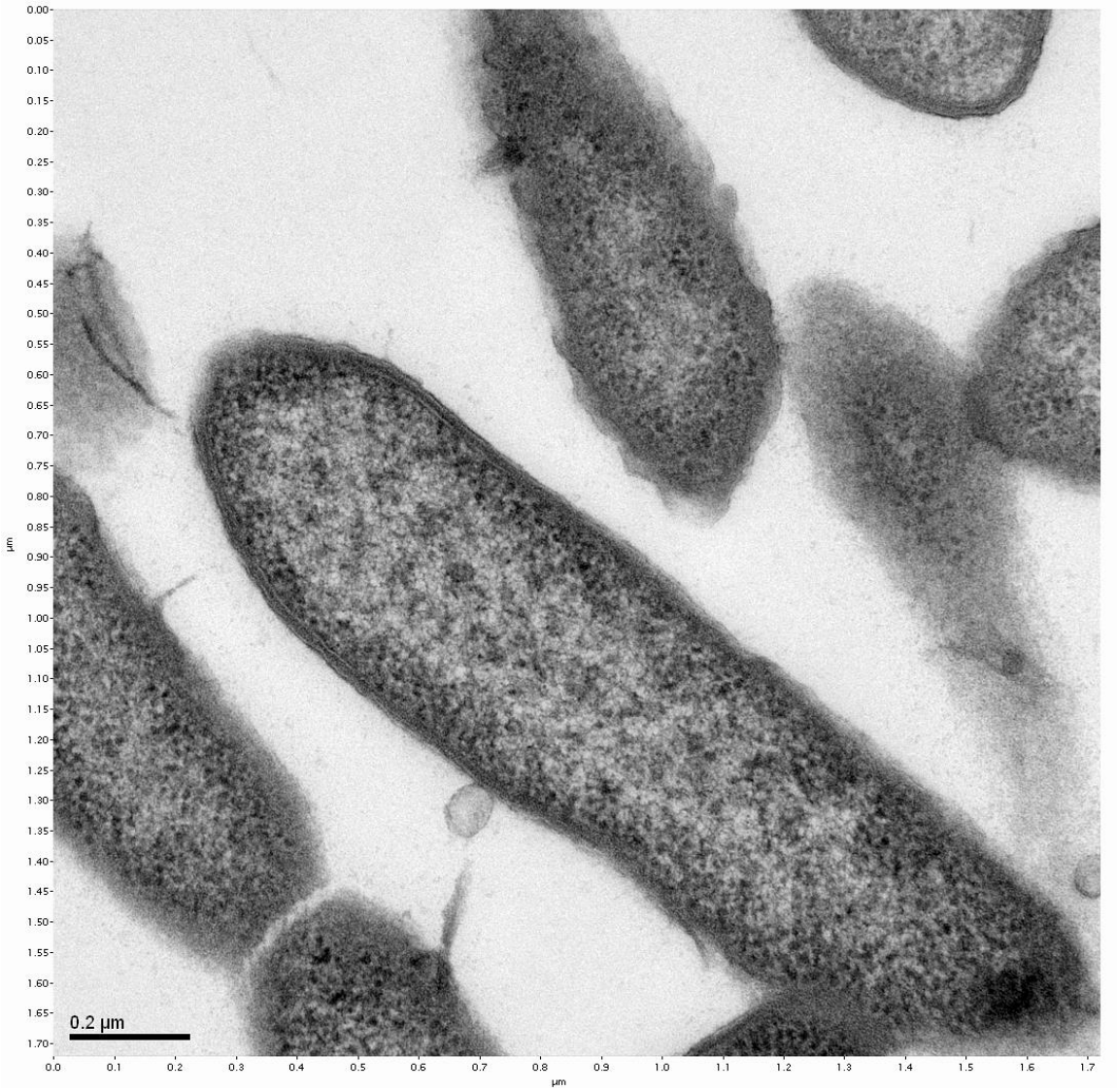

Figure A.5 Conventional thin section TEM micrograph of *G. sulfurreducens* cells grown using fumarate as the electron acceptor. No ICM was observed.

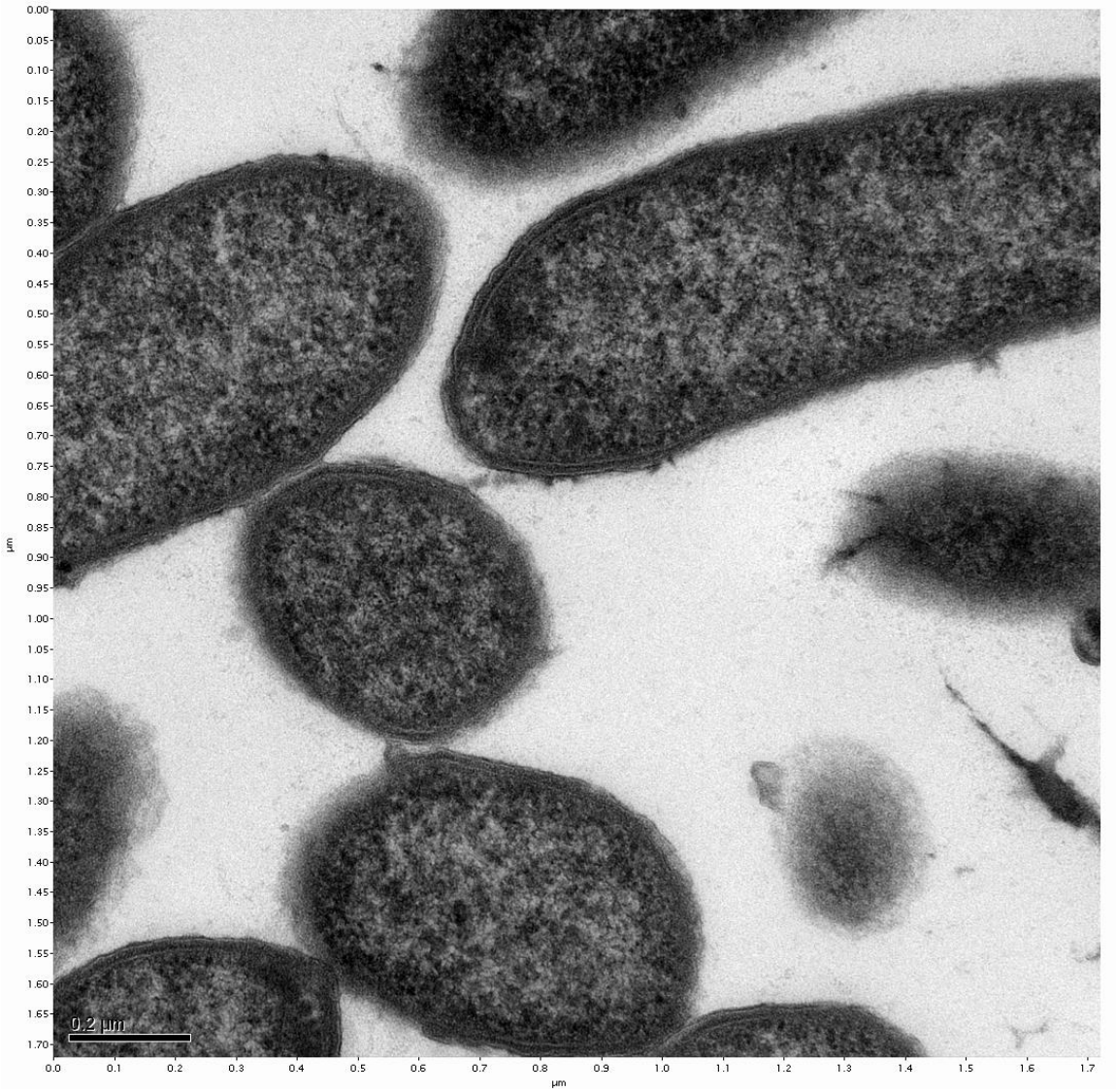

Figure A.6 Conventional thin section TEM micrograph of *G. sulfurreducens* cells grown using fumarate as the electron acceptor. No ICM was observed.

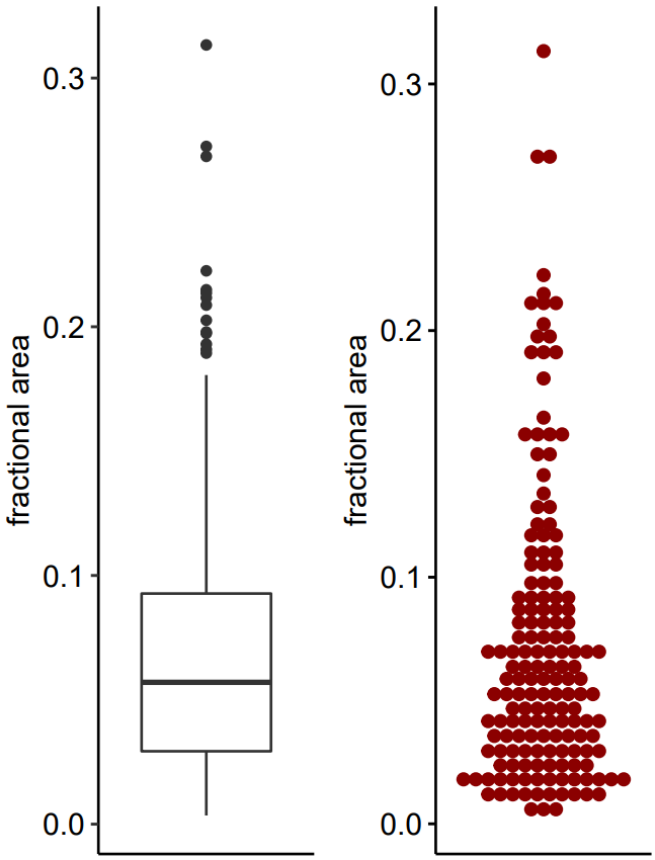

Figure A.7 Fractional cell area occupied by ICM in sum projections of confocal z-stacks collected using Nile red, a lipid stain. Each dot represents a cell (n=164). Every cell represented here came from an electrode biofilm poised at -0.07 V vs. SHE. ICM area and cell area were calculated by MicrobeJ as described in the methods. (Left) box plot, (right) dot plot. Box plot quartile breaks are at 0.029, 0.057, and 0.093.

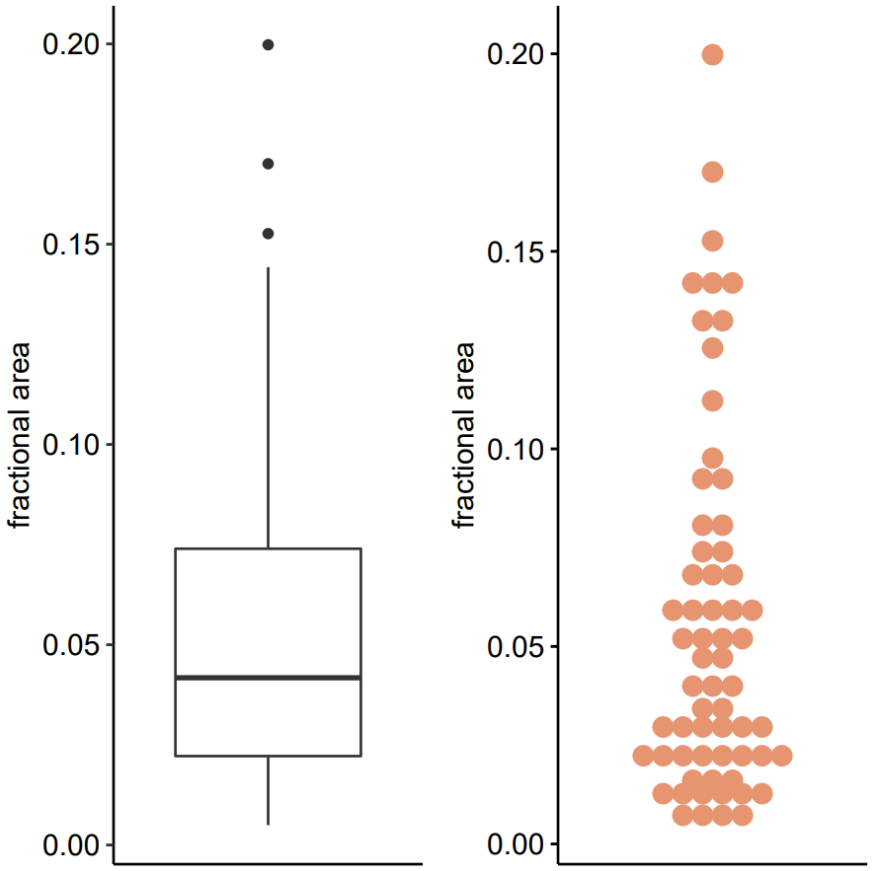

Figure A.7 Fractional area of cell area occupied by ICM in sum projections of confocal z-stacks collected using Nile red, a lipid stain. Each dot represents a cell (n=63). Every cell represented here came from planktonic cultures grown with 50 mM fumarate as the electron acceptor. ICM area and cell area were calculated by MicrobeJ as described in the methods. (Left) box plot, (right) dot plot. Box plot quartile breaks are at 0.022, 0.042, and 0.074.

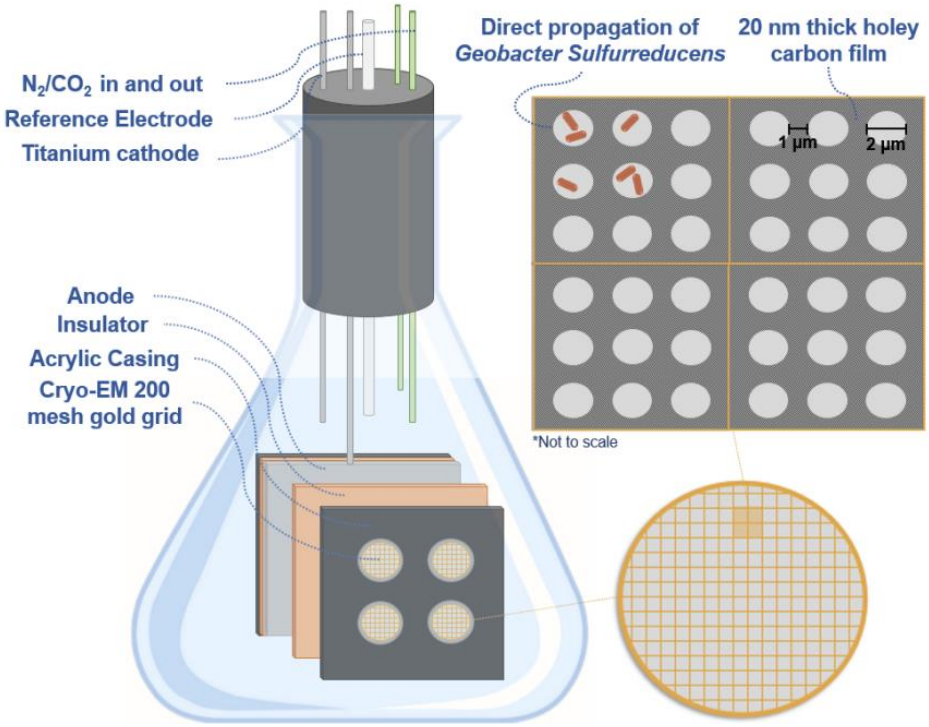

Figure A.8 Cartoon depicting the design elements of the bioreactor grid holder that is poised as an anode to capture cells in an active state for cryoET. The cartoon is not to scale, and a picture of the actual holder is in Figure A.9

Figure A.9 Photograph of the grid holder used in a microbial electrochemical cell to grow *G. sulfurreducens* directly on EM grids for cryoET preparation.

Table A.5 Summary of the number of cells detected and the fraction of those cells that had detectable ICM in all the images used to create Figure 4.4a. Cell and local maxima detection were performed with MicrobeJ in ImageJ.

Image Name	No. cells detected	type	No. of cells with ICM	Fraction with ICM
1-3-004	46	Electrode -0.07V	32	0.696
1-3-006	52	Electrode -0.07V	22	0.423
1-3-010	77	Electrode -0.07V	50	0.649
1-12-001	223	Electrode -0.07V	87	0.390
1-12-002	217	Electrode -0.07V	88	0.406
3-30-001	86	Electrode -0.07V	51	0.593
3-30-002	70	Electrode -0.07V	36	0.514
3-30-003	68	Electrode -0.07V	45	0.662
3-30-004	69	Electrode -0.07V	44	0.638
3-30-005	81	Electrode -0.07V	41	0.506
3-30-006	82	Electrode -0.07V	37	0.451
3-30-007	90	Electrode -0.07V	53	0.589
3-30-008	100	Electrode -0.07V	54	0.540
3-30-009	93	Electrode -0.07V	60	0.645
3-30-010	66	Electrode -0.07V	34	0.515
3-30-011	66	Electrode -0.07V	37	0.561
1-21-008a	67	Fumarate 50mM	24	0.358
1-21-009	37	Fumarate 50mM	1	0.027
1-24-011	56	Fumarate 50mM	10	0.179

1-24-014	227	Fumarate 50mM	37	0.163
1-26-001	188	Fumarate 50mM	29	0.154
1-26-002	63	Fumarate 50mM	8	0.127
1-26-005	47	Fumarate 50mM	5	0.106
3-4-006	67	Fumarate 50mM	0	0.000
3-4-001	14	Fumarate 50mM	2	0.143
3-18-006	119	Electrode -0.17V	56	0.504
3-30-001	75	Electrode -0.17V	36	0.560
3-30-002	69	Electrode -0.17V	43	0.710
3-30-003	88	Electrode -0.17V	39	0.545
3-30-004	102	Electrode -0.17V	51	0.569
5-9-003	234	Electrode -0.03V	107	0.457
5-9-004	182	Electrode -0.03V	75	0.412
5-9-006	122	Electrode -0.03V	58	0.475
5-9-007	168	Electrode -0.03V	70	0.417
5-9-008	282	Electrode -0.03V	99	0.351
5-9-009	259	Electrode -0.03V	98	0.378
5-9-010	141	Electrode -0.03V	56	0.397
5-9-011	215	Electrode -0.03V	80	0.372

Table A.6 Top 30 most abundant gene transcripts in anode biofilm samples of *T. ferriacetica*

locus_tag	product	baseMean	gene name
Tfer_RS15470	S-layer homology domain-containing protein	29518	Tfer_3268
Tfer_RS10235	cytochrome c3 family protein	25303	Tfer_2153
Tfer_RS00375	cytochrome c3 family protein	18660	Tfer_0075
Tfer_RS00385	hypothetical cytochrome c7	18068	Tfer_0077
Tfer_RS06145	Peptidase_C39_2 domain-containing protein	10994	Tfer_1280
Tfer_RS06155	S8 family peptidase	7986	NA
Tfer_RS00565	CO dehydrogenase/CO-methylating acetyl-CoA synthase complex subunit beta	5828	Tfer_0114
Tfer_RS00560	anaerobic carbon-monoxide dehydrogenase catalytic subunit	5109	Tfer_0113
Tfer_RS14555	S8 family peptidase	3622	NA
Tfer_RS15985	formate dehydrogenase subunit alpha	3600	NA
Tfer_RS11895	formate--tetrahydrofolate ligase	3154	Tfer_2491
Tfer_RS08925	hypothetical multiheme cytochrome c	3029	Tfer_1887
Tfer_RS05970	flagellin	2921	Tfer_1242
Tfer_RS15570	YkuD domain-containing protein	2766	Tfer_3289
Tfer_RS00570	acetyl-CoA decarbonylase/synthase complex subunit gamma	2727	Tfer_0115
Tfer_RS00580	methyltetrahydrofolate cobalamin methyltransferase	2375	Tfer_0117
Tfer_RS00575	acetyl-CoA decarbonylase/synthase complex subunit delta	2327	Tfer_0116
Tfer_RS15095	ammonia-forming cytochrome c nitrite reductase subunit c552	2244	Tfer_3193
Tfer_RS06685	sodium-translocating pyrophosphatase	2202	Tfer_1390
Tfer_RS11285	chaperonin GroEL	2158	Tfer_2368
Tfer_RS07265	NADH-quinone oxidoreductase subunit NuoF	2149	Tfer_1512
Tfer_RS14510	methyltransferase domain-containing protein	1921	Tfer_3075
Tfer_RS09795	hypothetical protein	1853	Tfer_2063
Tfer_RS14375	F0F1 ATP synthase subunit alpha	1786	Tfer_3048
Tfer_RS15565	S8 family serine peptidase	1783	NA
Tfer_RS05460	CoB--CoM heterodisulfide reductase iron-sulfur subunit A family protein	1757	Tfer_1140
Tfer_RS14525	B12 lower ligand biosynthesis ThiC-like protein BzaB	1721	Tfer_3078
Tfer_RS03510	hypothetical protein	1643	Tfer_0722
Tfer_RS10600	hypothetical protein	1602	Tfer_2224
Tfer_RS14530	phosphomethylpyrimidine synthase ThiC	1599	Tfer_3079

APPENDIX B

AUTHORSHIP AND COPYRIGHT

Chapters 2 through 5 are adapted from publishable works where I am the first author and there were co-authors who contributed. The other contributing authors have given their consent to their work being used in this format. At the time of writing this, none of the chapters are officially published. Chapters 2 through 4 have been posted as preprints or open access publications on BioarXiv citations listed below. The preprints are released with a CC-BY copyright that allows free use for any purpose with citation:

Howley E, Krajmalnik-Brown R, Torres CI. 2022. Cytochrome expression shifts in *Geobacter sulfurreducens* to maximize energy conservation in response to changes in redox conditions. BioarXiv 1–34. doi.org/10.1101/2022.05.22.492868

Howley, E., Ki, D., Krajmalnik-Brown, R., & Torres, C. I. (2022). Geobacter sulfurreducens' unique metabolism results in cells with a high iron and lipid content. Microbiology Spectrum, 2, 1–6.

Howley E, Mangus A, Williams D, Torres CI. 2022. Intracytoplasmic membranes develop in *Geobacter sulfurreducens* under thermodynamically limiting conditions. BioarXiv https://doi.org/https://doi.org/10.1101/2022.08.05.502997.